



Durham E-Theses

The spatial characteristics of muons in large cosmic ray showers

Gibson, A.I.

How to cite:

Gibson, A.I. (1976) *The spatial characteristics of muons in large cosmic ray showers*, Durham theses, Durham University. Available at Durham E-Theses Online: <http://etheses.dur.ac.uk/9017/>

Use policy

The full-text may be used and/or reproduced, and given to third parties in any format or medium, without prior permission or charge, for personal research or study, educational, or not-for-profit purposes provided that:

- a full bibliographic reference is made to the original source
- a [link](#) is made to the metadata record in Durham E-Theses
- the full-text is not changed in any way

The full-text must not be sold in any format or medium without the formal permission of the copyright holders.

Please consult the [full Durham E-Theses policy](#) for further details.

The copyright of this thesis rests with the author.
No quotation from it should be published without
his prior written consent and information derived
from it should be acknowledged.

THE SPATIAL CHARACTERISTICS OF MUONS IN
LARGE COSMIC RAY SHOWERS

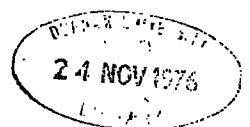
by

A.I. Gibson, B.Sc.

A Thesis submitted to the University of Durham in
accordance with the Regulations for Admittance
to the Degree of Master of Science

Department of Physics
University of Durham.

August 1976



Abstract.

Early experimental work on the heights of origin of muons in Extensive Air Showers, particularly that of Earnshaw et al (1973) is described in detail and the relative merits of the experimental techniques used are considered. As an extension of the work, an extensive series of computer simulations was performed both as an aid to interpretation of experimental data and to indicate measurable parameters for future experiments. Both the temporal and spatial characteristics were simulated and a large amount of data is presented and compared where possible with available experimental results. Recent work using a different model for shower cascade development is described and compared with the earlier simulations.

A design for a new experiment which has evolved from this work and is now nearing completion is fully described. The experiment consists of two widely separated (250m), heavily shielded spatial angle detectors (employing neon flash tubes) with a particle track resolution better than half a degree. Methods of data extraction and interpretation are described and the likely modes of operation discussed.

Preface.

This thesis gives an account of work performed in Durham and at the British Universities Air Shower Array at Haverah Park during the period 1973 to June 1976.

Experimental work on the heights of origin of muons by Earnshaw et al is described in detail. A subsequent series of rigorous computer simulations made by Dr. K. E. Turver and Mr. W. Stephenson on the spatial and temporal properties of muons in Extensive Air Showers, to aid in the interpretation of experimental data and to act as a basis for the design of a new experiment are described. More recently, new simulations have been made employing the same techniques as Stephenson and Turver to investigate the effects on the muon component's temporal and spatial properties when using a different model for the nucleon cascade. Preliminary results of this latter work are presented.

A new experiment (designed on the basis of the early simulation data) to investigate the spatial properties of muons in large EAS is now nearing completion and is described in detail together with an outline of likely running conditions. The design and construction of the new instrument has been the sole responsibility of the author together with the analysis of the new simulation results.

Contents.

	<u>Page</u>
<u>Abstract</u>	i
<u>Preface</u>	ii
<u>Contents</u>	iii
<u>Chapter One: Introduction</u>	
1-1 The Cosmic Rays at the Highest Energies	1
1-2 The Extensive Air Shower	1
1-3 The Longitudinal Development of Large Air Showers	4
1-3.1 The Electron Photon Cascade	5
1-3.2 The Muon Component	5
1-4 The Primary Composition and Energy Spectrum of the Cosmic Radiation	6
1-5 The Stage III Muon Experiment at Haverah Park	7
<u>Chapter Two: The Muon Component and Shower Cascade Development.</u>	
2-1 Introduction	9
2-2 Experimental Method Employed by Earnshaw et al	10
2-3 The Mean Heights of Origin of Muons Derived Experimentally from Investigating the Charge Ratio Distortion Resulting from Interactions with the Geomagnetic Field	10
2-3.1 Theoretical Considerations	10
2-3.2 Validity of the Calculations	12
2-3.3 The Mean Heights of Origin of EAS Muons Derived from Geomagnetic Effects	13
2-4 The Mean Heights of Origin of Muons Derived	

Experimentally by a Trigonometric Method	14
2-4.1 Theoretical Considerations	14
2-4.2 Errors and Effects Arising from Main Array Geometry	15
2-4.3 Experimental Results	17
2-5 Comparison of Results with Data from Other Experiments	18
2-5.1 Results from Other Experiments	18
2-6 Simulation Predictions of the Distortion in Charge Ratio and the Distribution in Muon Angles with respect to the Shower Core	19
2-6.1 Comparison between Simulation Predictions and the $(\Psi_p - \Psi_o)$ Distribution as a test of Validity for Shower Models	19
2-6.2 Comparison of the Observed Muon Charge Ratio with Predictions from Various Shower Models	20

Chapter Three: Computer Simulations of the Spatial
and Temporal Characteristics of Muons
in Large Air Showers.

3-1 Introduction	22
3-2 Computational Procedure	23
3-3 Spatial Characteristics	25
3-3.1 Comparison of Simulations with Experiment	26
3-4 Temporal Characteristics	27
3-4.1 Comparison of Simulation Data with Experiment	28
3-5 Sensitivity of the Simulations to the Parameters	

of Showers and Shower Models	29
3-5.1 Sensitivity to Changes in the Propagation Model	29
3-5.2 Sensitivity to the Model of High Energy Interactions	30
3-5.3 Sensitivity to the Atomic Mass Number of the Primary Particles	30
<u>Chapter Four: The Experiment.</u>	
4-1 Introduction	32
4-2 The Requirements of the Measurement	32
4-3 The Haverah Park Experimental Array	34
4-4 The Instrument	35
4-4.1 The Neon Flash Tube Detector	35
4-4.2 The Flash Tube Mountings and Common Constructional Details	36
4-4.3 Detector A	37
4-4.4 Detector B	39
4-5 Electronics and Pulsing System	40
4-6 The Optics and Photographic Recording System	41
4-7 Extraction of Data for Analysis	42
<u>Chapter Five: Recent Computer Simulations and an Outline of Likely Running Conditions for the New Experiment.</u>	
5-1 Introduction	44
5-2 The Recent Simulations	44
5-3 The Spatial Characteristics of Muons in EAS as Indicated by the New Simulations	46

5-4	The Temporal Effects According to the New Simulations	47
5-5	Implications of the Recent Simulations for the New Experiment	48
5-6	An Outline of Likely Running Conditions for the New Experiment	50
5-7	Future Work and Prospects	52
	<u>References</u>	54
	Acknowledgements	57

Chapter One.Introduction1-1 The Cosmic Rays at the Highest Energies.

The presence of the cosmic radiation was first detected in the year 1900 when C.T.R. Wilson observed that a thoroughly insulated gold leaf electroscope slowly lost charge. This phenomenon was originally ascribed to ionizing radiations emanating from rocks in the earth's crust. When the experiments were repeated at sea no change in the rate of charge loss was observed which led to suggestions that the radiation was extra-terrestrial in origin. This was confirmed in 1912 when Hess and colleagues made several balloon ascents and found a steady increase in the radiation with altitude (Hess 1912) The cosmic radiation (as it became known) has been responsible for many important and exciting discoveries in both Nuclear Physics and Astronomy (for example, many of the now well known fundamental particles were first observed in cosmic rays). Subsequent research both above and at the bottom of the atmosphere has shown the existence of a wide range of radiation of energies ranging from soft X rays through to 10^{20} eV particles. Some of the most interesting particles are those of energy greater than 10^{18} eV which are possibly of extra-galactic origin but the direct observation of which is difficult due to their scarcity (rate of arrival of $> 10^{18}$ eV particles $\approx 1\text{m}^{-2}/3000$ years). Fortunately there exist techniques to study secondary radiation which offset the above difficulties and make possible the indirect study of these energetic primaries.

1-2 The Extensive Air Shower.

Up to an energy of $\approx 10^{14}$ eV the primary flux is of sufficient strength to permit direct observations to be made at high altitudes (balloons or orbital observation platforms) with useful observation periods being as short as a few days. Above this energy however, direct observation becomes increasingly difficult and at the higher energies indirect methods must be employed.

When a highly energetic cosmic ray primary impinges on the earth's atmosphere it is presented with approximately 1030gcm^{-2} of material to traverse before reaching sea level. Laboratory studies have shown the proton to have an interaction length of approximately 80gcm^{-2} in air (the mean free path for a heavy nucleus is correspondingly shorter). Thus a primary is likely to interact catastrophically with an air nucleus producing a shower of secondaries. Accelerator and other experimental data indicate that the secondaries are pions, strange particles and heavy mesons. With a sufficiently energetic primary the secondaries carry off sufficient energy to initiate further interactions with air nuclei. This atmospheric cascade is repeated until the secondaries decay, are no longer energetic enough to initiate further interactions with air nuclei or ground level is reached. The transverse momentum of the secondaries plus Coulomb scattering in the atmosphere causes a laterally developing extensive shower of particles covering many square kilometres at ground level (Extensive Air Shower [EAS]). A large array of detectors specifically designed to observe these showers offsets the low primary flux rate and makes possible the study of the most energetic cosmic rays.

Many different techniques are used to detect and study large showers. To date they have all relied on sampling various parameters of the secondary particles (relative arrival times, pulse profiles,

particle numbers/density, etc.) at widely spaced detectors and subsequently using computer analysis to reconstruct the shower in detail. Most of the world's air shower arrays use scintillation detectors (employing either liquid or plastic scintillator) as primary detectors. The British Universities Air Shower Array at Haverah Park however is unique in that an unusual and economic detection technique is employed based on the Čerenkov radiation emitted by the charged particles as they traverse 1.2m of clear water. The low cost of the method enables very large detector areas (34m^2) to be employed.

During recent years several different techniques have been suggested which may offer attractive alternative methods for the detection of the largest showers. They are:-

a) Radio Frequency Emission. Subsequent to the pioneer work of Jelley et al (1965) studies were made, particularly by Allan and co-workers at Haverah Park, of the radio emission from EAS as a function of various shower parameters. The initial hopes that the method would compete favourably with conventional arrays (particularly with respect to the detection of large distant showers) seem unlikely and most work on this topic has been terminated with the recognition of the poor signal to noise ratio.

b) Night Sky Optical Čerenkov Emission. In contrast to the radio work studies of the night sky Optical Čerenkov radiation are rapidly assuming increasing importance following consideration of the early work of Galbraith and Jelley (1953). Offering a simple, reliable, accurate and portable means of air shower study, Čerenkov light measurements contain valuable detail of the EAS development and make possible measurements at any site thus allowing cross calibration of the world's fixed particle detector arrays.

c) Atmospheric Scintillation. Greisen (1966a) suggested using the atmosphere as a scintillation medium to record the passage of very large distant air showers and to track their development. A sophisticated experiment to study the phenomenon is currently under development and is fully described by Bergeson et al (1975). The success of this experiment may suggest an exciting future for EAS studies.

1-3 The Longitudinal Development of Large Air Showers.

At ground level a shower consists of many millions of secondary particles moving in substantially the same direction as the primary particle. The particles in the region of the core are mainly electrons propagated by the electron photon cascade. The muon component comprises only a few percent of the total of charged particles at small core distances but, at the large distances normally considered in many extensive air showers they represent a significant proportion of the total and they dominate other components in the shower periphery.

Although the size of the secondary component of a shower at varying atmospheric depths has yet to be measured directly equivalent data have been obtained by cross relating results from the various high altitude experiments. This is of great importance as the mean height of maximum cascade development and individual fluctuations reflect the rate of shower development, nature of the primary particle and details of high energy interactions. The longitudinal development of showers arising from primary protons or light nuclei should fluctuate greatly (mainly due to the long mean free path of the primary) with the maximum shower size remaining constant but the depth of maximum varying considerably. In contrast, heavy nucleus primaries with a reduced mean free path for interaction with an air nucleus may

cause a small decrease in the depth of maximum but will lack large scale fluctuations.

1-3.1 The Electron Photon Cascade.

The electron component arises from the decay of uncharged pions from the hadron cascade to photons with subsequent pair production. The electron-positron pairs so produced then radiate bremsstrahlung photons leading to more pair production and a self perpetuating cascade of electrons, positrons and photons.

Early experimental investigation of the electron photon cascade quickly showed that the size of the electron shower was directly related to the primary energy. Difficulties arose in that accurate measurement of shower size is difficult due to the low particle densities at the greater distances from the shower core giving rise to the necessity for large detector areas. Recently this problem has been overcome by measuring a ground parameter in showers which is dependant on the primary energy but which shows small fluctuations and may be well measured (Hillas et al [1971]).

1-3.2 The Muon Component.

The muon component of EAS arises from the decay of charged pions in the upper parts of the shower. The transverse momentum of the parent pions is transferred to the daughter muons causing the shower to spread laterally and the muons to dominate the outer regions.

Due to their small interaction cross section and long life, many of the muons survive to sea level. Scattering due to Coulomb effects and interactions with the geomagnetic field is modest and well understood; thus study of the muon component yields much information

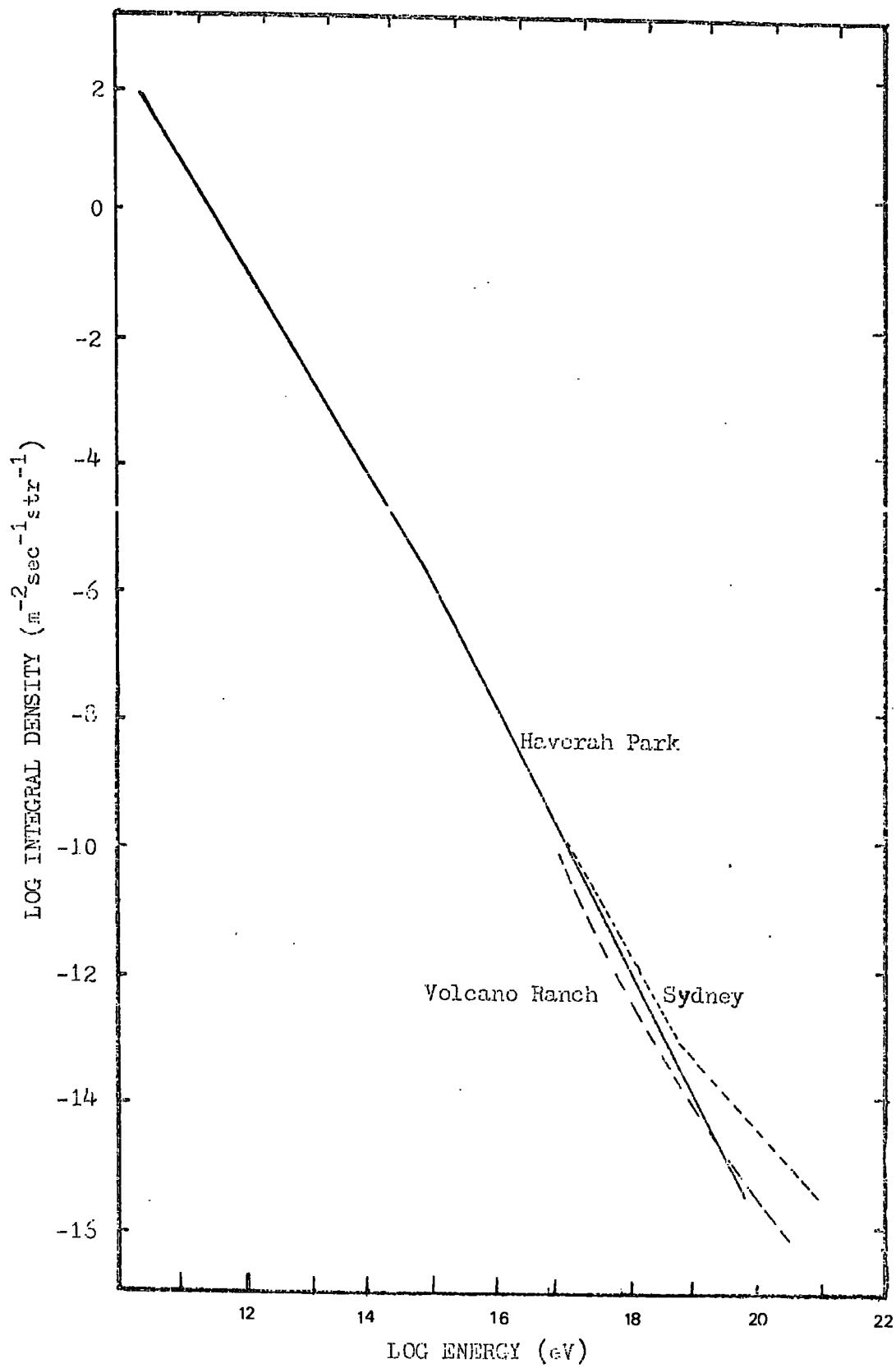
about shower development. In the past, work has been mainly concerned with the definitive measurement of the average momentum spectrum, arrival times etc., but current developments are tending towards a study of the muon components' origin and development in individual showers.

1-4 The Primary Composition and Energy Spectrum of the
Cosmic Radiation.

At energies where direct observation is possible the primary mass spectrum has been investigated by emulsion stacks flown in balloons and data from orbital satellites. Up to about 10^{13} eV it has been possible to identify the primaries confirming the presence of protons and heavier nuclei although the relative abundances remain undetermined at these energies.

In the air shower region of the energy spectrum the chemical composition of the primaries is still largely unknown and the identification of the mass spectrum in these regions is one of the major quests of current research. In the foreseeable future it is unlikely that much direct or detailed data will become available on the primary composition, but it may well be possible to determine the ratio of protons to heavy nuclei at these energies. A review of the available data in the energy range 10^{10} - 10^{19} eV has been made by Sreekantan (1972) which demonstrates the present inconclusive position.

The shape of the primary energy spectrum has posed a problem over many regions and current data indicates a slope equivalent to an exponent of 2.2 in the integral energy spectrum for energies between 10^{16} eV and 10^{19} eV. In contradiction to earlier indications a flattening in the spectrum is again suggested at higher energies.



Greisen (1966b) suggested the existence of a cut-off at the highest energies ($>10^{19}$ eV) arising from the interaction between high energy protons and the low energy photons of the 3°K background radiation. Extragalactic protons with a path length greater than the characteristic distance for the $p - \gamma$ interaction should be removed from the primary flux, investigation to date has been hampered by the scarcity of such high energy primaries although no evidence for a cut-off has yet been observed.

1-5 The Stage III Muon Experiment at Haverah Park.

In the work of Earnshaw et al (1973), reviewed in detail in Chapter Two, attempts were made to investigate the heights of origin of muons by two different methods, firstly by investigating the muon charge ratio distortion due to interactions of the muons with the geomagnetic field and secondly by means of a direct trigonometric method. The experimental limitations imposed by the small sensitive area of the Haverah Park Spectrograph restricted the work to obtaining mean heights of origin for muons in a number of showers. The trigonometric method proved to be superior in both experimental simplicity and in the quality of the results which were in good agreement with the model simulation data. Consequently, a series of in depth computer simulations were commenced to pursue the matter further and act as a design study for a new experiment to measure the height of origin of muons in individual showers.

The simulations were made for vertical showers initiated by 10^{17} and 10^{18} eV proton primaries with varying heights of maximum. The computations followed the development of the shower muons in a small segment of the shower until they either decayed, reached sea

level or struck a hypothetical array of detectors at varying core distances. These detectors were assumed to be track delineating and particle timing devices of high precision beneath varying thicknesses of absorber. The simulations allowed fully for the problem of 'sampling' the sparse muon flux with detectors of finite area. The results confirmed the sensitivity of the muon heights of origin to cascade development and confirmed the viability of the experiment as a possible indicator of the atomic mass number of the primaries.

Two large area muon detectors at the Haverah Park Array are now nearing completion and should become fully operational by September 1976. Designed on the basis of the simulation results the detectors are capable of high accuracy track delineation ($<0.5^\circ$) and of recording at least 15 - 30 muons in 10^{18} eV showers at core distances in excess of 300m.

Chapter Two.

The Muon Component and Shower Cascade Development.

2-1 Introduction.

Muons were one of the earliest and most studied components of air showers as, due to their long lifetime, low interaction cross section and small Geomagnetic effects they carry information from all parts of a shower. Muons may be expected to reveal much information about the shower cascade development. In this context several attempts have been made during the last 15 years to study the muon's spatial angles with respect to each other and the shower core direction (de Beer et al [1962,1970], Earnshaw et al [1968]).

Somogyi (1966) suggested and Orford et al (1968) showed that it was practical to estimate the muon heights of origin from the charge distortion of the ratio induced by the Earth's magnetic field. Khristiansen (1957), Clark et al (1958), Oren (1959) and Kamiya et al (1962) estimated the interactions of muons with the Geomagnetic field in relation to the possible broadening of the muon lateral distribution, rather than in studies of the heights of origin. The experiments to date have only confirmed the general properties of muons' origin in EAS and have been restricted by several factors including a lack of precision in EAS and muon data, poor statistics and over-simplified analysis methods.

The situation was further considered by Earnshaw et al (1973) who obtained improved data and used a more refined analysis technique to obtain the mean values for height of origin for muons of various momenta recorded at different core distances. In view of the relevance of this work to the new experiment a detailed review is given in this

chapter.

2-2 Experimental Method Employed by Earnshaw et al.

All measurements were made at Haverah Park Air Shower Array using the Mk II Magnet Spectrograph which has been described by Machin (1973) and Pickersgill (1973). The Spectrograph flash tubes were triggered on command from the main shower array whenever it detected a shower initiated by a primary of energy about 10^{17} eV. The quantities measured for each muon were charge, momentum, and arrival direction. Muons in the momentum band 1-30 GeV/c and at core distance 150-600m were studied.

2-3 The Mean Heights of Origin of Muons Derived Experimentally from Investigating the Charge Ratio Distortion Resulting from Interactions with the Geomagnetic Field.

Superimposed on all individual particle studies is a deflection due to Coulomb Scattering, allowance for which must be made in all cases where the arrival direction of particles is important. If large numbers of particles are considered deflections due to geomagnetic effects are superimposed on all their paths regardless of Coulomb Scattering and if angular deviation due to the latter is small the geomagnetic deflection in the bulk of muons is directly related to their heights of origin. This can be measured by study of the distortion in charge ratio brought about by lateral shifts in opposing directions of oppositely charged particles.

2-3.1 Theoretical Considerations.

(a) Muon deflections in the geomagnetic field.

The deflection in the geomagnetic field was evaluated for muons of varying heights of production and momentum for an initial primary direction specified by zenith angle θ and azimuth angle ϕ . The values of the sea level momentum chosen included an allowance for energy loss by ionization, the deflection being evaluated as the mean of production and sea level momenta. The resulting mean deflection weighted by the observed Haverah Park zenith angle distribution was obtained for a range of azimuth, thus enabling the projected component of the mean deflection into each of the three sensitive lobes of the array (see Figure 2-1) to be derived.

(b) Charge ratio distortion by the geomagnetic field.

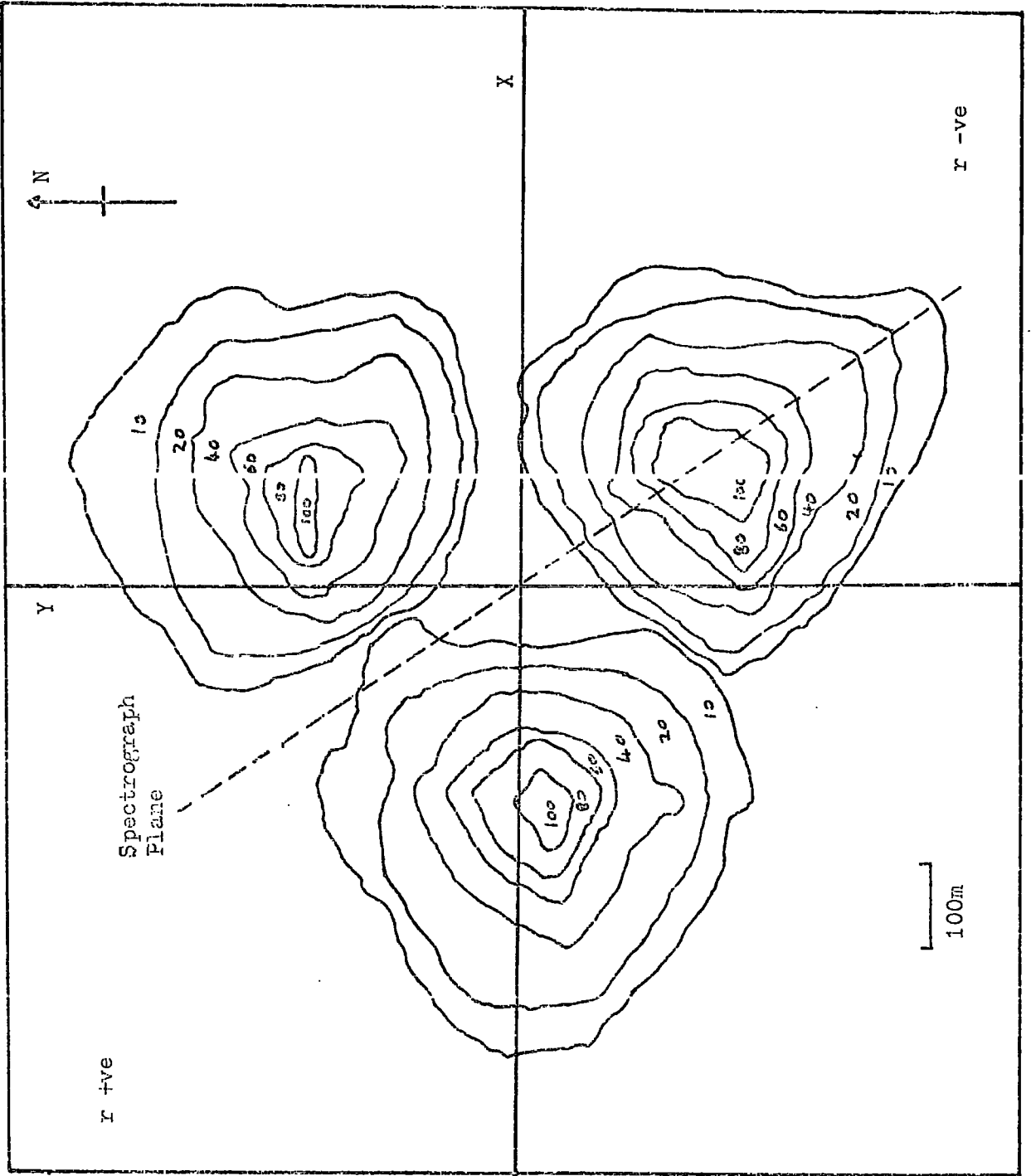
To derive the muon charge ratio appropriate to showers landing in each of the lobes shown in Figure 2-1 three assumptions were made:-

1) The lateral distributions for positive and negative muons are identical in the absence of any geomagnetic field.

2) In the presence of the geomagnetic field oppositely charged particles undergo the same geomagnetic effects but in opposite senses. Thus the lateral distributions of negative and positive muons are separated by twice the mean deflection.

3) At a given core distance the ratio of the ordinates of the lateral distributions appropriate to positive and negative muons indicates the expected muon charge ratios.

To determine the mean height of origin an experimental lateral distribution appropriate to the mean considered momenta was used. The number of events investigated was small, restricting the possibility of investigating the phenomena at several core distances. As a result, studies were constrained to a single distance interval of



150-600m corresponding to the predicted charge ratio for the median distance interval of $300 \pm 10m$.

The calculated values for geomagnetic deflections of positive muons originating at a height H above sea level, with zenith and azimuthal angles θ and ϕ respectively and two momentum values are presented in table 2-1. Other values may be obtained by interpolation. It is still possible however for the height of production or the charge ratio distortion to be obscured by other factors, both experimentally and theoretically. The following possible sources of uncertainty were considered and in all cases shown to be insignificant:-

- 1) Variations in the geomagnetic field with altitude.
- 2) Deflections in muon trajectory induced by the earth's electric field.
- 3) Errors in core location.
- 4) The acceptance probability by the Spectrograph of a muon deflected in the geomagnetic field.
- 5) The mean momentum ascribed to events of known deflection in the Spectrograph's magnetic field.

2-3.2 Validity of the Calculations.

The validity of the calculations was checked by predicting the variation of charge ratio recorded in each sensitive lobe for various azimuth angles at all momenta greater than 1GeV/c and a mean height of origin of 5km. These results were compared with the appropriate experimental lateral distribution function for the X^+Y^+ lobe (see Figure 2-1). This was found to be the same as X^+Y^- but with a reversed azimuth angle, thus, to improve the statistics the events in the two regions were summed. The other regions (X^+Y^- , X^-Y^- etc.) received

S.L. NOM.(GEV/C)= 2.0

HEIGHT(KMS)= 2.5

THETA(DEG)= 0.
PHI(DEG) EAST(N) NORTH(M)
0. 5.7 0.0

THETA(DEG)= 10.
PHI(DEG) EAST(N) NORTH(M)
0. 9.8 0.0
45. 9.0 -2.0
90. 7.0 -3.0
135. 4.7 -2.2
180. 3.7 0.0
225. 4.7 2.4
270. 6.9 3.3
315. 8.9 2.3

THETA(DEG)= 20.
PHI(DEG) EAST(N) NORTH(M)
0. 13.5 0.1
45. 12.1 -4.1
90. 8.0 -6.5
135. 2.9 -5.0
180. 0.5 0.0
225. 2.7 5.2
270. 7.8 0.7
315. 12.0 4.5

THETA(DEG)= 30.
PHI(DEG) EAST(N) NORTH(M)
0. 18.6 0.1
45. 16.5 -6.5
90. 10.1 -11.0
135. 1.0 -9.1
180. -3.5 -0.0
225. 0.7 9.1
270. 9.9 11.3
315. 16.5 7.0

THETA(DEG)= 40.
PHI(DEG) EAST(N) NORTH(M)
0. 26.2 0.1
45. 23.9 -9.5
90. 14.3 -17.7
135. -1.2 -15.5
180. -7.5 -0.1
225. -1.7 15.5
270. 13.7 18.1
315. 23.5 10.1

S.L. NOM.(GEV/C)= 2.0

HEIGHT(KMS)= 15.0

THETA(DEG)= 0.
PHI(DEG) EAST(N) NORTH(M)
0. 187.8 0.0

THETA(DEG)= 10.
PHI(DEG) EAST(N) NORTH(M)
0. 276.6 5.5
45. 253.1 -51.9
90. 195.5 -80.5
135. 133.5 -59.9
180. 104.8 2.4
225. 131.6 66.3
270. 194.5 89.6
315. 252.2 62.7

THETA(DEG)= 20.
PHI(DEG) EAST(N) NORTH(M)
0. 376.6 7.1
45. 336.9 -107.8
90. 223.5 -174.9
135. 83.4 -130.2
180. 14.9 0.4
225. 78.0 143.5
270. 219.5 187.2
315. 339.1 122.6

THETA(DEG)= 30.
PHI(DEG) EAST(N) NORTH(M)
0. 509.1 9.2
45. 453.9 -169.5
90. 277.8 -293.1
135. 32.3 -245.7
180. -96.0 -2.8
225. 21.0 250.8
270. 272.2 312.5
315. 455.5 190.4

THETA(DEG)= 40.
PHI(DEG) EAST(N) NORTH(M)
0. 698.3 11.8
45. 632.8 -242.5
90. 382.2 -457.9
135. -23.6 -410.3
180. -751.7 -8.5
225. -46.1 417.7
270. 376.7 493.0
315. 661.9 273.5

S.L. NOM.(GEV/C)= 5.0

HEIGHT(KMS)= 5.0

THETA(DEG)= 0.
PHI(DEG) EAST(N) NORTH(M)
0. 11.2 0.0

THETA(DEG)= 10.
PHI(DEG) EAST(N) NORTH(M)
0. 16.4 0.1
45. 15.1 -3.3
90. 11.7 -5.5
135. 7.3 -3.7
180. 6.3 0.0
225. 7.7 4.1
270. 11.4 5.6
315. 14.9 4.1

THETA(DEG)= 20.
PHI(DEG) EAST(N) NORTH(M)
0. 22.7 0.1
45. 20.3 -6.9
90. 13.4 -10.8
135. 4.9 -8.5
180. 0.9 0.0
225. 4.5 8.7
270. 12.9 11.4
315. 20.0 7.7

THETA(DEG)= 30.
PHI(DEG) EAST(N) NORTH(M)
0. 31.3 0.1
45. 28.0 -10.9
90. 17.2 -18.5
135. 1.7 -15.2
180. -5.9 -0.0
225. 1.1 15.3
270. 15.3 19.1
315. 27.5 11.9

THETA(DEG)= 40.
PHI(DEG) EAST(N) NORTH(M)
0. 44.3 0.1
45. 40.4 -16.1
90. 24.1 -29.9
135. -2.0 -26.2
180. -16.0 -0.1
225. -3.0 26.1
270. 23.2 30.7
315. 40.0 17.2

S.L. NOM.(GEV/C)= 10.0

HEIGHT(KMS)= 15.0

THETA(DEG)= 0.
PHI(DEG) EAST(N) NORTH(M)
0. 42.5 0.0

THETA(DEG)= 10.
PHI(DEG) EAST(N) NORTH(M)
0. 62.3 0.4
45. 57.4 -12.6
90. 44.5 -18.9
135. 30.2 -14.1
180. 23.8 0.2
225. 29.9 14.9
270. 44.1 20.1
315. 57.2 14.0

THETA(DEG)= 20.
PHI(DEG) EAST(N) NORTH(M)
0. 86.2 0.6
45. 77.1 -25.8
90. 55.9 -43.9
135. 18.7 -37.0
180. 3.4 0.0
225. 18.0 32.6
270. 50.1 42.4
315. 76.7 27.6

THETA(DEG)= 30.
PHI(DEG) EAST(N) NORTH(M)
0. 118.4 0.7
45. 105.7 -40.4
90. 64.3 -69.6
135. 6.7 -57.6
180. -22.4 -6.2
225. 5.3 57.9
270. 63.1 71.6
315. 105.5 43.4

THETA(DEG)= 40.
PHI(DEG) EAST(N) NORTH(M)
0. 168.5 1.2
45. 151.6 -60.1
90. 90.8 -111.8
135. -7.3 -98.5
180. -60.1 -0.7
225. -9.9 98.9
270. 69.5 115.2
315. 151.9 63.5

S.L. NOM.(GEV/C)= 15.0

HEIGHT(KMS)= 5.0

THETA(DEG)= 0.
PHI(DEG) EAST(N) NORTH(M)
0. 4.0 0.0

THETA(DEG)= 10.
PHI(DEG) EAST(N) NORTH(M)
0. 5.8 0.0
45. 5.4 -1.2
90. 4.2 -1.8
135. 2.8 -1.3
180. 2.2 0.0
225. 2.4 2.3
270. 3.6 3.2
315. 5.0 2.9

THETA(DEG)= 20.
PHI(DEG) EAST(N) NORTH(M)
0. 8.1 0.0
45. 7.3 -2.5
90. 4.8 -3.9
135. 1.7 -3.0
180. 0.3 0.0
225. 0.8 3.5
270. 3.6 5.2
315. 6.5 4.4

THETA(DEG)= 30.
PHI(DEG) EAST(N) NORTH(M)
0. 11.3 0.0
45. 10.1 -4.0
90. 6.1 -6.7
135. 0.6 -5.5
180. -2.1 -0.0
225. -3.8 5.4
270. 4.3 7.9
315. 9.0 6.0

THETA(DEG)= 40.
PHI(DEG) EAST(N) NORTH(M)
0. 16.1 0.0
45. 14.7 -5.9
90. 8.8 -10.9
135. -0.6 -9.5
180. -5.8 -0.0
225. -2.8 8.9
270. 6.5 12.0
315. 13.5 8.0

S.L. NOM.(GEV/C)= 15.0

HEIGHT(KMS)= 7.5

THETA(DEG)= 0.
PHI(DEG) EAST(N) NORTH(M)
0. 8.9 0.0

THETA(DEG)= 10.
PHI(DEG) EAST(N) NORTH(M)
0. 13.0 0.0
45. 12.0 -2.7
90. 9.3 -4.0
135. 6.3 -3.0
180. 5.0 0.0
225. 5.8 4.0
270. 8.6 5.4
315. 11.6 4.4

THETA(DEG)= 20.
PHI(DEG) EAST(N) NORTH(M)
0. 18.1 0.0
45. 16.2 -5.5
90. 10.7 -8.7
135. 3.9 -6.8
180. 0.7 0.0
225. 2.9 7.3
270. 9.4 10.0
315. 15.4 7.5

THETA(DEG)= 30.
PHI(DEG) EAST(N) NORTH(M)
0. 25.1 0.0
45. 22.4 -8.8
90. 13.6 -14.8
135. 1.4 -12.2
180. -4.7 -0.0
225. -0.2 12.2
270. 11.8 16.1
315. 21.3 10.9

THETA(DEG)= 40.
PHI(DEG) EAST(N) NORTH(M)
0. 35.7 0.1
45. 32.6 -13.1
90. 19.5 -24.2
135. -1.7 -21.2
180. -12.9 -0.0
225. -3.0 20.0
270. 17.1 29.5
315. 31.4 15.3

S.L. NOM.(GEV/C)= 50.0

HEIGHT(KMS)= 7.5

THETA(DEG)= 0.
PHI(DEG) EAST(N) NORTH(M)
0. 2.7 0.0

THETA(DEG)= 10.
PHI(DEG) EAST(N) NORTH(M)
0. 4.0 0.0
45. 3.7 -0.8
90. 2.9 -1.2
135. 1.9 -0.9
180. 1.5 0.0
225. 0.5 4.1
270. 0.9 5.6
315. 2.4 6.3

THETA(DEG)= 20.
PHI(DEG) EAST(N) NORTH(M)
0. 5.6 0.0
45. 5.0 -1.7
90. 3.3 -2.7
135. 1.2 -2.1
180. 0.2 0.0
225. -1.8 3.7
270. -0.6 6.9
315. 2.5 8.0

THETA(DEG)= 30.
PHI(DEG) EAST(N) NORTH(M)
0. 7.8 0.0
45. 7.0 -2.7
90. 4.2 -4.6
135. 0.4 -3.8
180. -1.5 -0.0
225. -4.3 3.6
270. -1.5 0.5
315. 3.6 9.4

THETA(DEG)= 40.
PHI(DEG) EAST(N) NORTH(M)
0. 11.2 0.0
45. 10.2 -4.1
90. 6.1 -7.6
135. -0.5 -6.6
180. -4.0 -0.0
225. -6.9 4.5
270. -1.3 11.0
315. 6.2 10.7

S.L. NOM.(GEV/C)= 50.0

HEIGHT(KMS)= 15.0

THETA(DEG)= 0.
PHI(DEG) EAST(N) NORTH(M)
0. 10.9 0.0

THETA(DEG)= 10.
PHI(DEG) EAST(N) NORTH(M)
0. 16.1 0.0
45. 14.8 -3.3
90. 11.4 -4.9
135. 7.8 -3.7
180. 6.1 0.0
225. 6.3 6.9
270. 9.4 9.4
315. 13.4 8.9

THETA(DEG)= 20.
PHI(DEG) EAST(N) NORTH(M)
0. 22.3 0.0
45. 20.0 -6.8
90. 13.2 -10.7
135. 4.8 -8.3
180. 0.9 0.0
225. 1.7 10.0
270. 9.2 15.0
315. 17.5 13.1

THETA(DEG)= 30.
PHI(DEG) EAST(N) NORTH(M)
0. 31.0 0.0
45. 27.7 -10.9
90. 16.8 -18.4
135. 1.7 -15.1
180. -5.9 -0.0
225. -3.1 14.9
270. 11.0 22.3
315. 26.3 17.6

THETA(DEG)= 40.
PHI(DEG) EAST(N) NORTH(M)
0. 44.4 0.0
45. 40.4 -16.3
90. 24.2 -30.1
135. -2.1 -26.3
180. -16.0 -0.0
225. -8.7 24.2
270. 15.7 33.7
315. 36.5 23.1

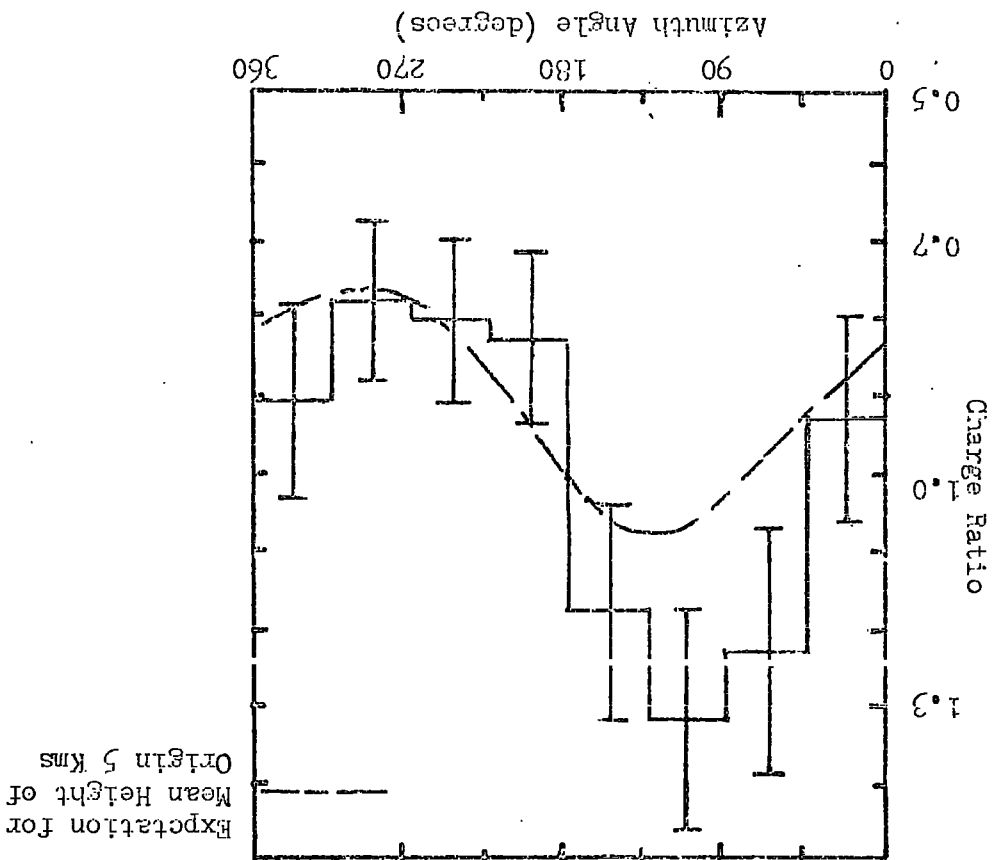
similar treatment. The resulting charge variation is presented in Figure 2-2 and it will be seen that good agreement exists between observations and predictions. In a similar manner the X^-Y^\pm region is symmetrical about an azimuth of 180° and is presented in Figure 2-3. Once again good agreement is evident indicating the overall validity of the calculations.

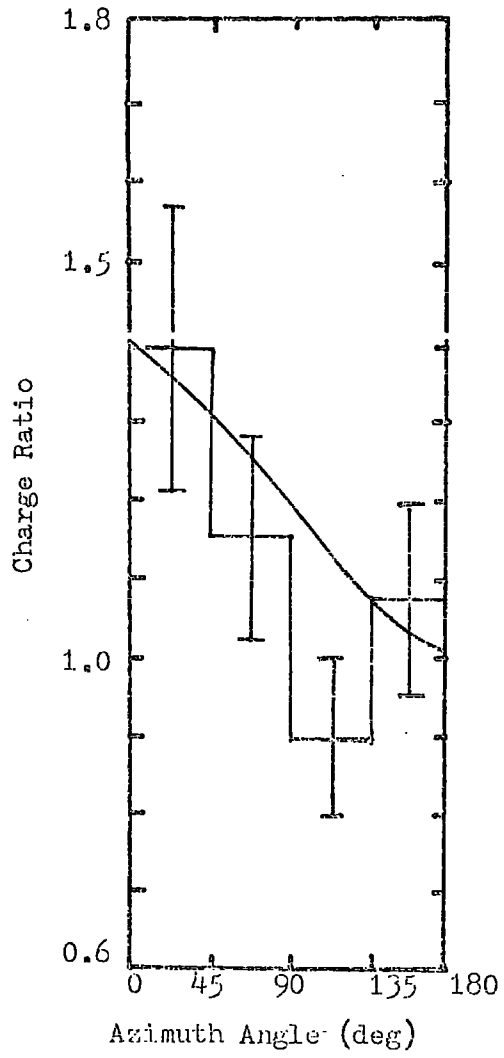
2-3.3 The Mean Heights of Origin of E.A.S. Muons Derived from Geomagnetic Effects.

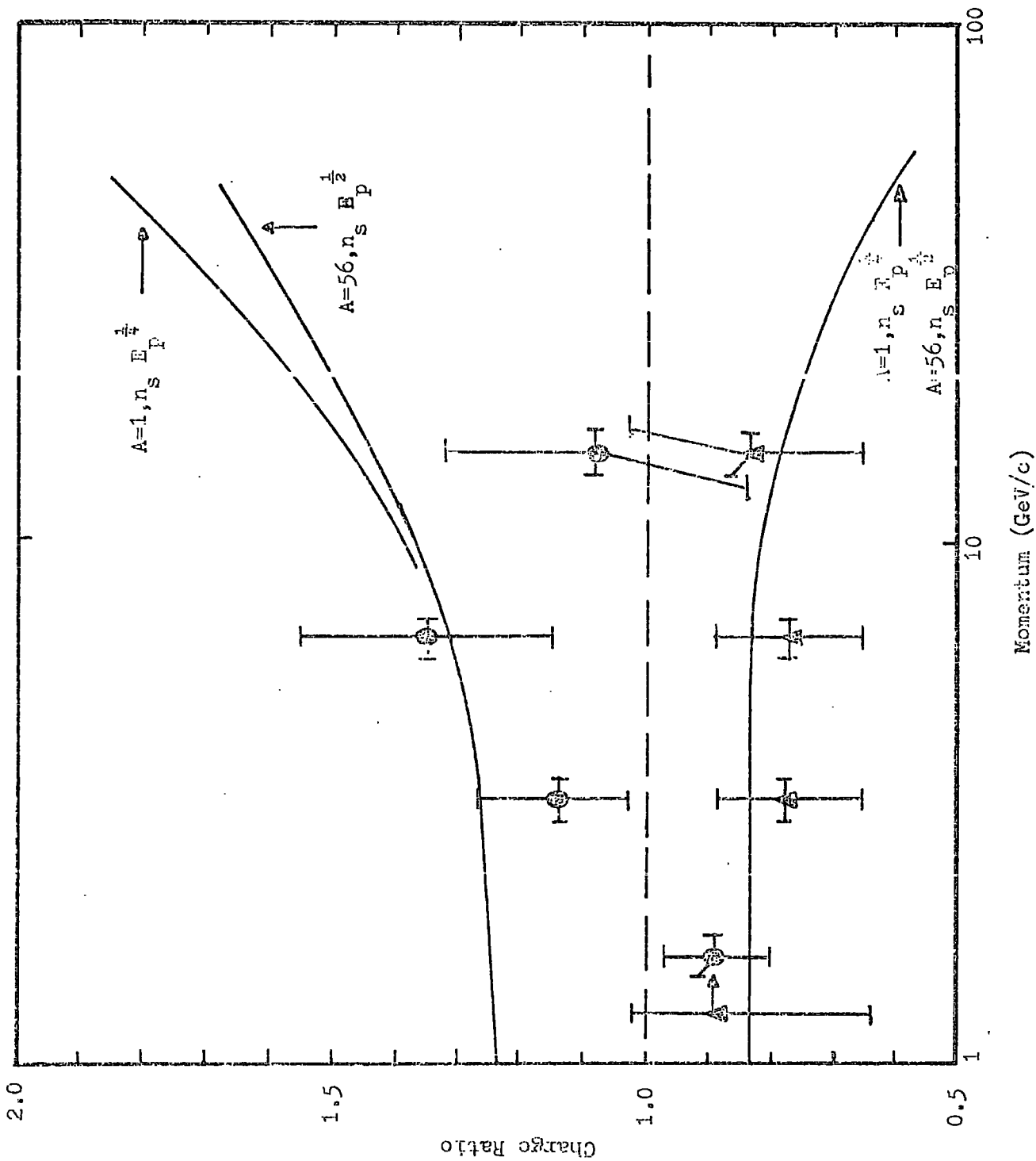
An estimate of the muons' height of origin was obtained by comparing experimentally observed charge ratios with predicted variations for muons of given momentum and heights of origin.

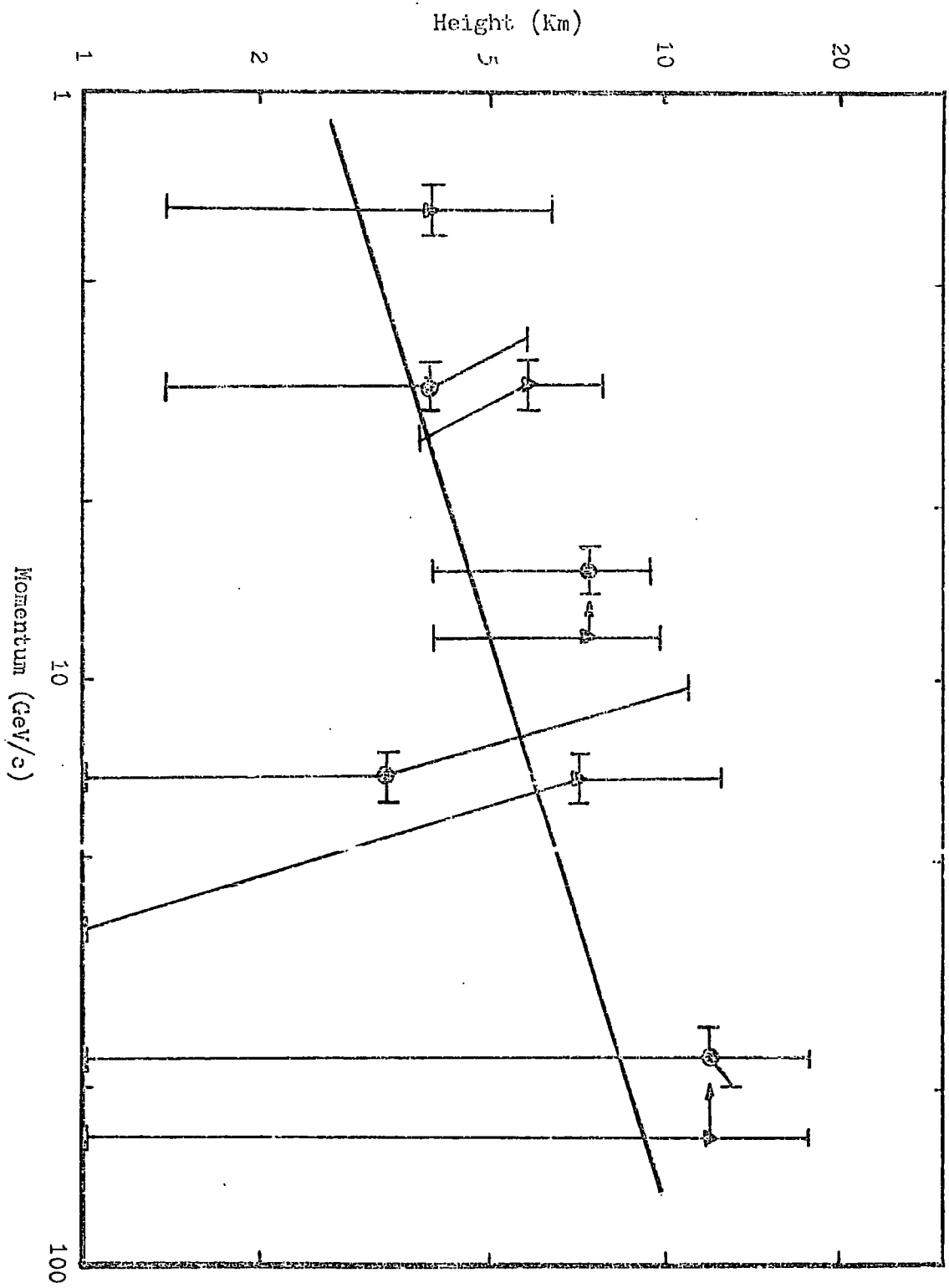
In an attempt to improve statistics the data were combined as described above and the mean charge ratio ($N[\mu^+]/N[\mu^-]$) found. The range of azimuth angle was restricted to include ratios which were either greater than or less than one but not both. In the X^-Y^\pm region limitations were not imposed as the predicted charge ratio was greater than unity over the entire range $0-360^\circ$. In the combined area X^+Y^\pm the range taken ($180^\circ-360^\circ-45^\circ$) caused the predicted charge ratio to be less than unity.

Hence two estimates for the height of origin were obtained for each momentum band, one for the X^-Y^\pm region where the charge ratio is greater than one and the X^+Y^\pm region with a charge ratio less than unity. The variation of these two observed mean charged ratios with sea level momentum are shown in Figure 2-4 and the estimated muon heights of origin are shown in Figure 2-5. The vertical error bars indicate the one standard deviation limits due to Poissonian errors and the uncertainty in the experimental lateral distribution function,









a 10% uncertainty in momentum is represented by the horizontal error bars. Also shown are the predicted mean heights of origin expected from showers initiated by primary protons.

2-4 The Mean Heights of Origin of Muons Derived Experimentally by a Trigonometric Method.

2-4.1 Theoretical Considerations.

The height of origin of a muon can be derived from elementary dynamics and is represented in Figure 2-6. An energetic muon of momentum P (and transverse momentum P_t) originating from a height H landing a distance r from the shower core must obey:-

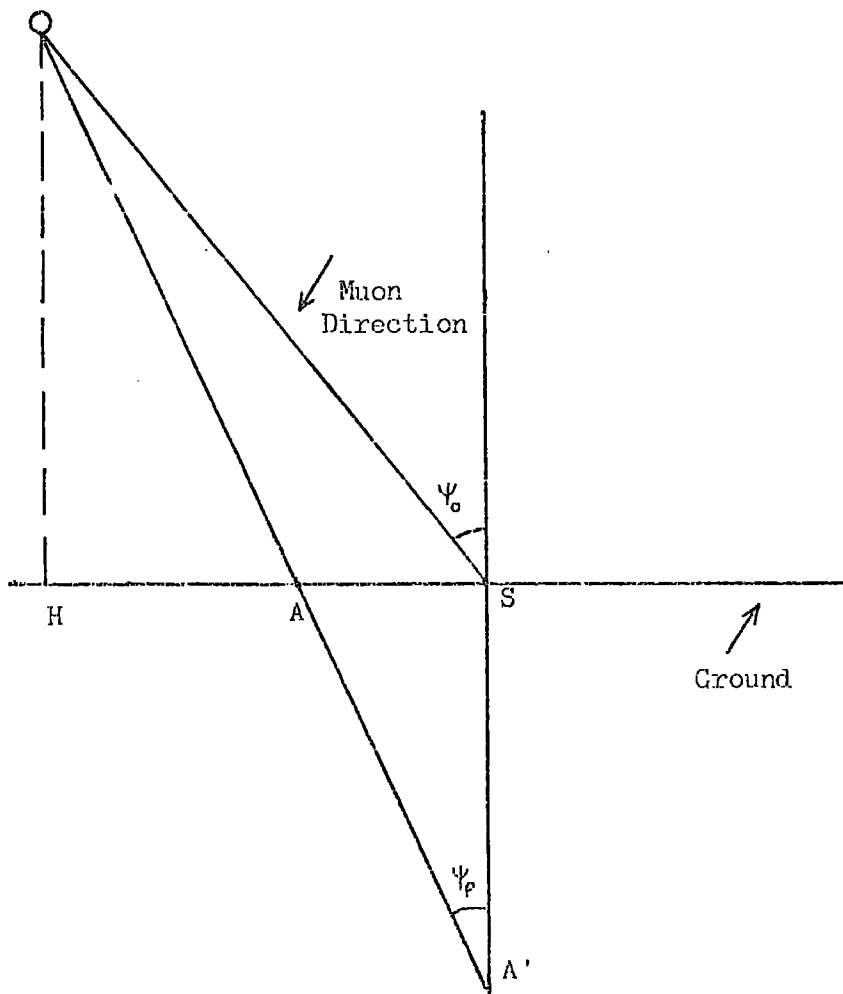
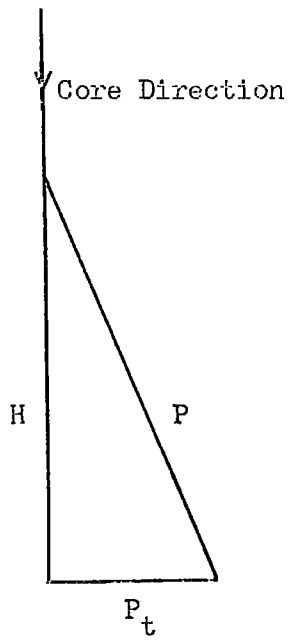
$$\frac{P_t}{P} = \frac{r}{H} \quad (1)$$

Scattering effects (Coulomb and Geomagnetic) on particles below a momentum of 10GeV/c cause deviation from this relation, but it is still broadly correct. The transverse momentum distribution postulated by Cocconi, Koester and Perkins (1961) (The CKP Distribution) was adopted for P_t which led to good agreement with experiment.

The experimental work was constrained by the geometry of the Spectrograph as the instrument was originally designed as a momentum analyser and the muon deflection only needed to be measured in one plane. Thus, as the muons' angles of incidence in this plane were known, all other measurements were transferred to this plane. The angle to the zenith made by the shower core in the Spectrograph's measuring plane (ψ_p) is given by:-

$$\tan(\psi_p) = \tan(\theta) \cdot \cos(\phi+E) \quad (2)$$

where:- θ , ϕ are zenith and azimuthal angles



respectively measured
by the main array and
E arises from orientation
of the Spectrograph
recording plane wrt the
main array.

From the rotation of axes the core distance r_{\perp} from the Spectrograph is given by:-

$$r_{\perp} = Y \cos(E) - X \sin(E) \quad (3)$$

where X, Y are core
coordinates.

Study of Figure 2-6(b) enables the following relationship to be derived:-

$$H = \frac{r_{\perp} \cos(\psi_p) \cos(\psi_o)}{\sin(\psi_p - \psi_o)} \quad (4)$$

$$\text{or } \frac{r_{\perp}}{H} = \tan(\psi_p) - \tan(\psi_o) \quad (5)$$

Simulations and experimentally obtained data have shown that the angle between the muon and core directions ($\psi_p - \psi_o$) is usually small (10° or less), thus errors in heights of origin are mainly dependant on errors in ($\psi_p - \psi_o$). Errors arising in r_{\perp} are less important but care was exercised and cases where r_{\perp} was less than 10m were excluded from the analyses.

2-4.2 Errors and Effects Arising from Main Array Geometry.

a) Core distance r_{\perp} .

The array triggering requirements and geometry (Tennent [1967]) define the smaller showers to fall in the regions between the lines connecting detectors (Figure 2-1). The Spectrograph plane rotation

of 34.5° with respect to the coordinate system causes more showers to be seen in the r_\perp positive region than r_\perp negative with a ratio of about 1.5 : 1. However, the mean value of (r_\perp negative) is larger than the mean value of (r_\perp positive) which tends to compensate in the analysis.

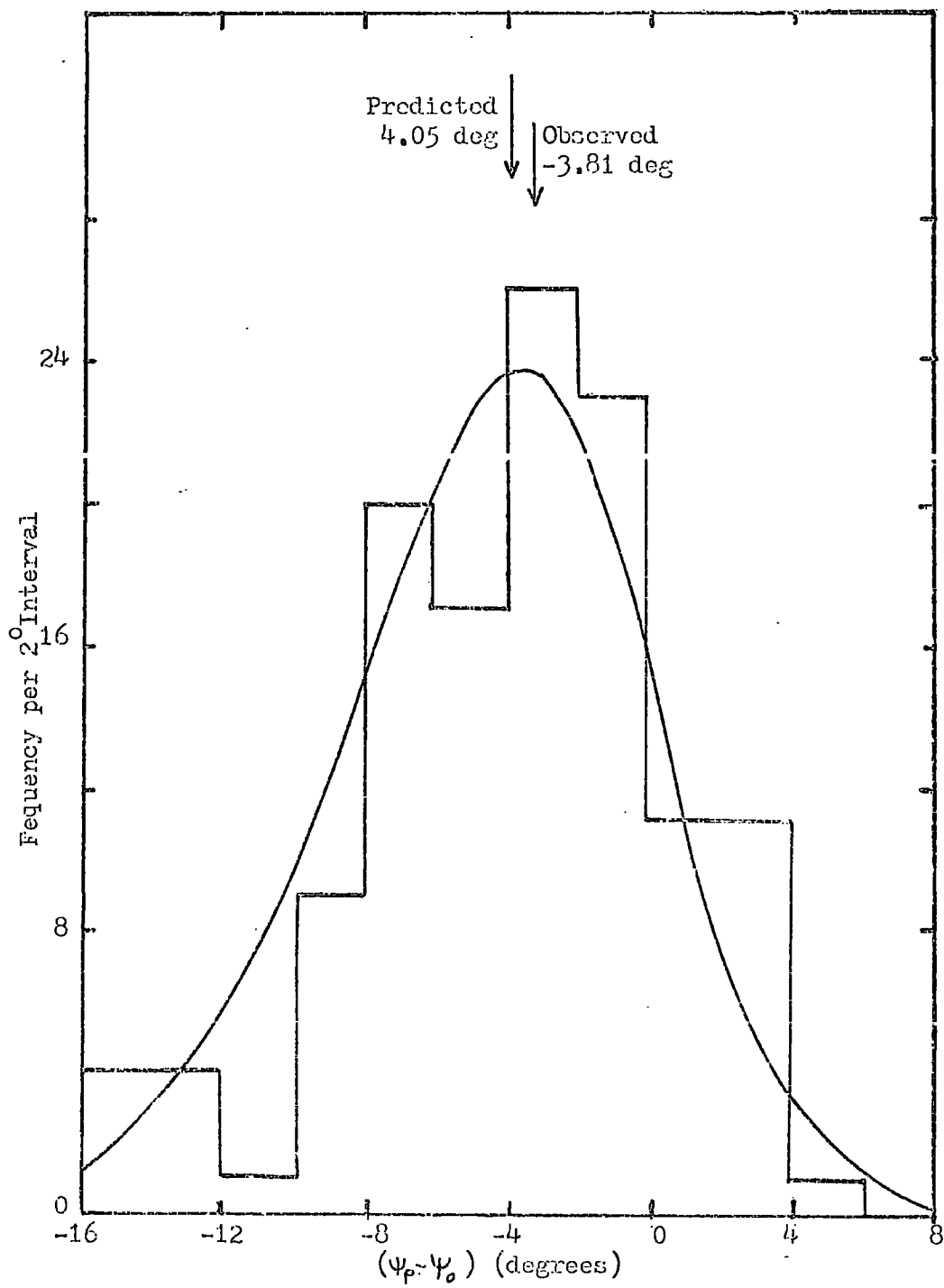
b) Effects on observed angle $(\psi_p - \psi_o)$.

From equation 4 it can be seen that if ψ_p and ψ_o have the same sign (differences can only be expected in near vertical showers), then their difference $(\psi_p - \psi_o)$ must have the same sign as r_\perp to give a positive value for H. From Figure 2-1 it can clearly be seen that two populations of r_\perp and thus $(\psi_p - \psi_o)$ exist each predominantly positive or negative. Figure 2-7 shows the generally negative tendency of $(\psi_p - \psi_o)$ for (r_\perp negative) events.

c) Measurement error on $(\psi_p - \psi_o)$.

Hollows (1969) estimated the overall measurement errors in zenith and azimuthal angles at the Haverah Park Array as about $\pm 2.2^\circ$ and $\pm 7^\circ$ respectively. When transformed into the Spectrograph plane this gave an error in core direction of about $\pm 2.5^\circ$, the error in the muon arrival direction ψ_o measured in the spectrograph plane was some 0.3° . Thus the greatest contribution to the overall error in $(\psi_p - \psi_o)$ occurs in θ and ϕ which are determined by the fast timing techniques used by the particle detector array.

Applying equation 1 to muons of momentum greater than $30\text{GeV}/c$, with height of origin of 10Km recorded at a typical core distance of 300m gives the angle $(\psi_p - \psi_o)$ arising from the transverse momentum of the parent pion as less than 1° . An estimate of the uncertainty in the angular measurement for high momentum muons from the distribution in $(\psi_p - \psi_o)$ is thus possible. This distribution was obtained using



values of ψ_p based on measurements of azimuth and zenith angles corrected for shower front curvature (Suri [1966]), giving good agreement between r.m.s. expected angular uncertainty and the observed values.

2-4.3 Experimental Results.

By direct application of equation 4 the mean reciprocal height of origin was determined for 16 intervals of momentum and core distance, viz:-

momentum	1-3	3-8	8-15	15-30 GcV/c
core distance	150-250,	250-350,	350-450,	450-600 m

The heights of production were obtained from the mean value and standard deviation of $1/H$ and are shown in figure 2-8. Also shown are typical simulation predictions for both a proton and iron nucleus primary. Figure 2-9 shows the heights of origin as a function of core distance for different momentum bands.

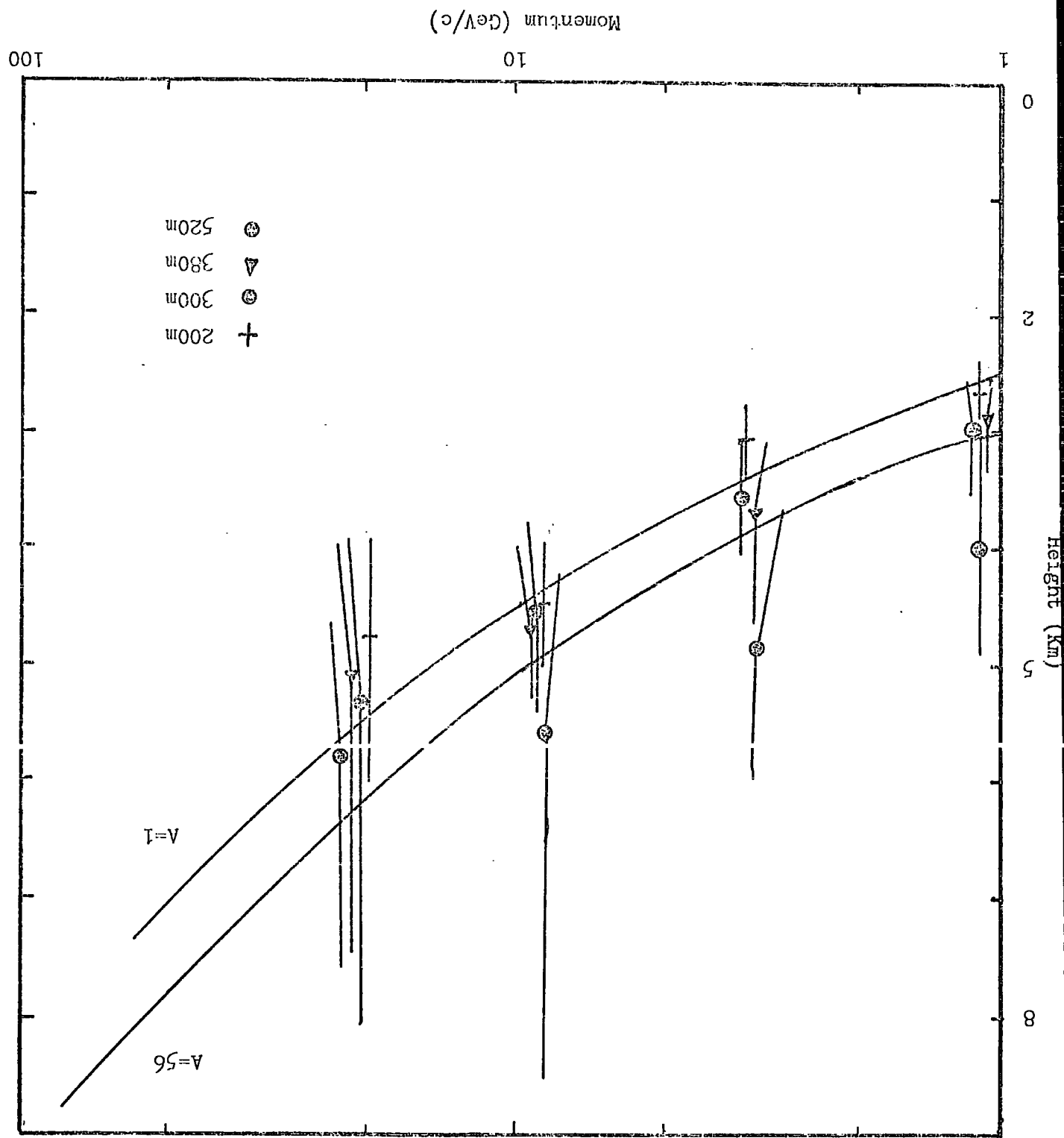
To allow direct comparison with other work a simple relation was fitted to the results. The data were assumed to be a linear function of core distance, so Figure 2-9 can be represented by straight parallel lines. Least squares fits were made and the slope determined from the mean and standard error. Comparison with the momentum dependence of production height enabled the constant terms to be resolved into a constant and a $\log_{10}P$ term giving a relation of the form:-

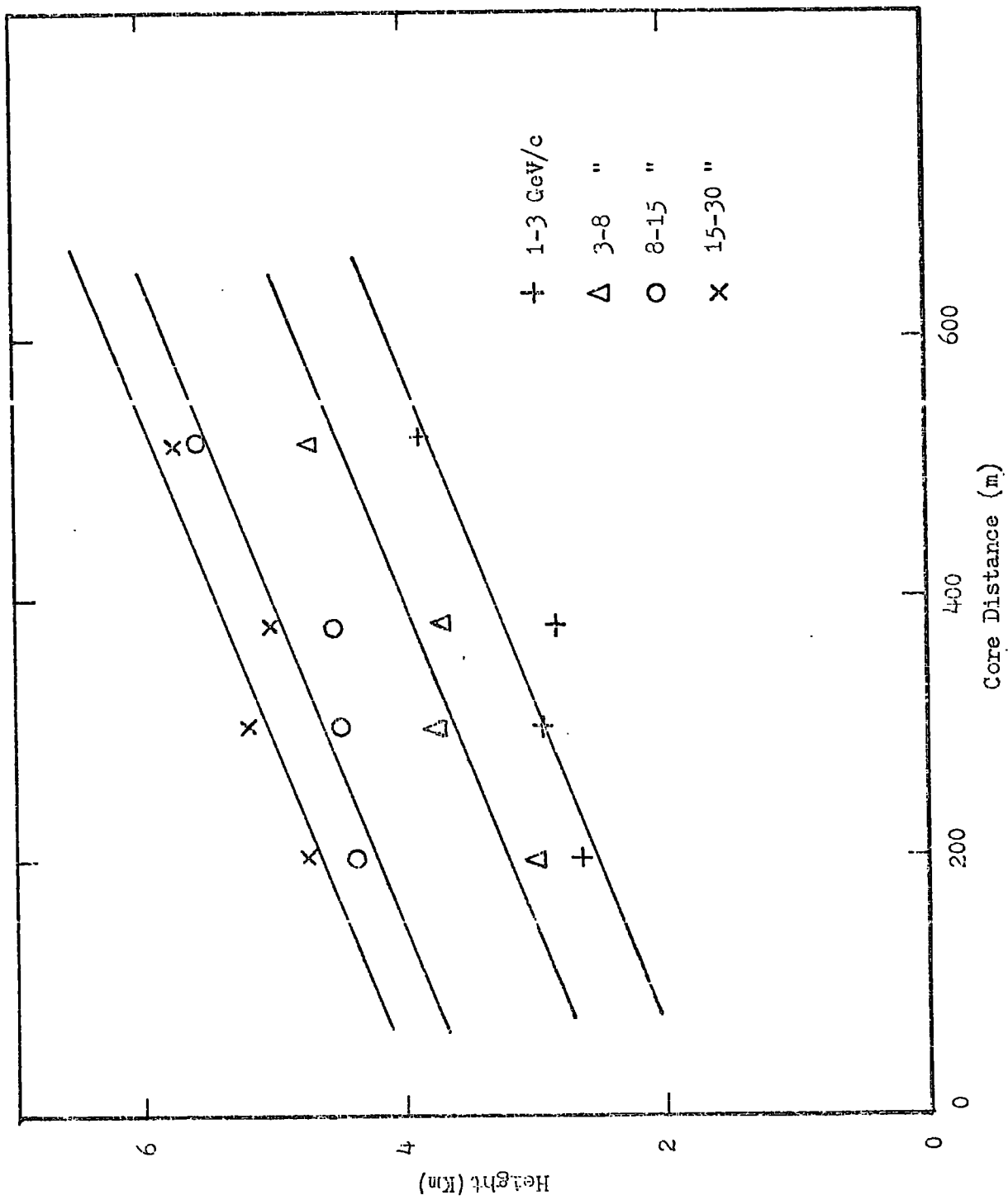
$$H(P,r) = H_0 + \alpha \log_{10}P + \frac{r}{\beta}$$

$$\text{where:- } H_0 = 1.68 \pm 0.15 \text{ Km}$$

$$\alpha = 1.74 \pm 0.020$$

$$\beta = 263 \pm 33 \text{ m}$$





which represents the production height of muons reasonably well in the momentum and core ranges studied.

2-5 Comparison of Results with Data from Other Experiments.

The production height of muons with momentum $>1\text{GeV}/c$ at a given core distance was obtained from the calculated muon momentum spectrum and the relation below:-

The expectation value of an experiment to measure the muon height of Production in the momentum range $1-300\text{GeV}/c$ with no resolution in momentum

$$\langle H(r) \rangle = \frac{\int_1^{30} H(P,r) S(P) dP}{\int_1^{30} S(P) dP} \quad (6)$$

where:- $H(P,r)$ = height of origin
 $S(P) dP$ = momentum spectrum

The work described here was limited to muons with momenta $>1\text{GeV}/c$ whereas other workers used a low energy cut off of $0.3\text{GeV}/c$. Therefore to effect a comparison the Durham results had to be extrapolated downwards in momentum to a figure of $0.5\text{GeV}/c$, which was also taken as the mean of the momentum band $0.3-1\text{GeV}/c$. A weighted mean height of production for all muons $>0.3\text{GeV}/c$ was obtained from simulated showers for each distance interval. The data, adjusted for a low energy cut off, is shown in Figure 2-10.

2-5.1 The Results from Other Experiments.

de Beer et al (1962) used similar methods to predict the angular distribution of muons with momenta $>1\text{GeV}/c$ and confirmed the general results of their predictions using spark chamber telescopes. At Haverah Park, Suri (1966) measured the mean radius of the shower

front by fast timing techniques and Baxter (1967) measured the mean height of production from studies of the water tank pulse profiles. Linsley and Scarsi (1962) timed the arrival of individual muons with respect to the shower front at the Volcano Ranch Array. Points from all these experiments are shown in Figure 2-10 where the results of Linsley and Scarsi are corrected to sea level.

2-6 Simulation Predictions of the Distortion in Charge Ratio and the Distribution in Muon Angles with respect to the Shower Core.

2-6.1 Comparison between Simulation Predictions and the $(\psi_p - \psi_o)$ Distribution as a Test of Validity for Shower Models.

The form of equations 3 and 4 imply that there exist regions of θ , ϕ , X , and Y where small changes cause large changes in $1/H$, also the mean heights of production shown in Figures 2-8 and 2-9 indicate slow change with core distance and momentum. Thus a strong dependence on assumed primary mass or detail in the model simulations was deemed unlikely. Hence it was decided to predict the distribution in $(\psi_p - \psi_o)$ for various core distances and shower models to seek out parameters sensitive to the shower model.

The production momentum of a given muon was calculated by assuming a constant rate of energy loss ($2.2 \text{ MeV g}^{-1}\text{cm}^2$) enabling the parent pions' momentum and hence the $\pi - \mu$ decay angle to be determined. The major factor in deviation from the core is the pions' transverse momentum and the CKP distribution was used to determine the probability of observing a muon of momentum P in a chosen distance band arising from a height interval $H, H+dH$. This process was repeated for all

height intervals and the results weighted by the predicted muon height distribution to give a probability distribution of angular deviation from the core at sea level. This distribution was then projected into the Spectrograph's measuring plane, allowance being made for:- array effects, Coulomb scattering and measurement errors. The quantity found to reflect the model used was the mean of the two ($\psi_p - \psi_o$) distributions (one for r_i positive and one for r_i negative). Figure 2-11 presents the predictions of the difference between the two distributions with the appropriate experimental data. It is apparent that the curve shapes vary little with overall noise as the distributions in ($\psi_p - \psi_o$) are closely gaussian, and as such, the separation between the mean changes slowly with the value of the standard deviation of the gaussian distribution used.

2-6.2 Comparison of the Observed Muon Charge Ratio with Predictions from Various Shower Models.

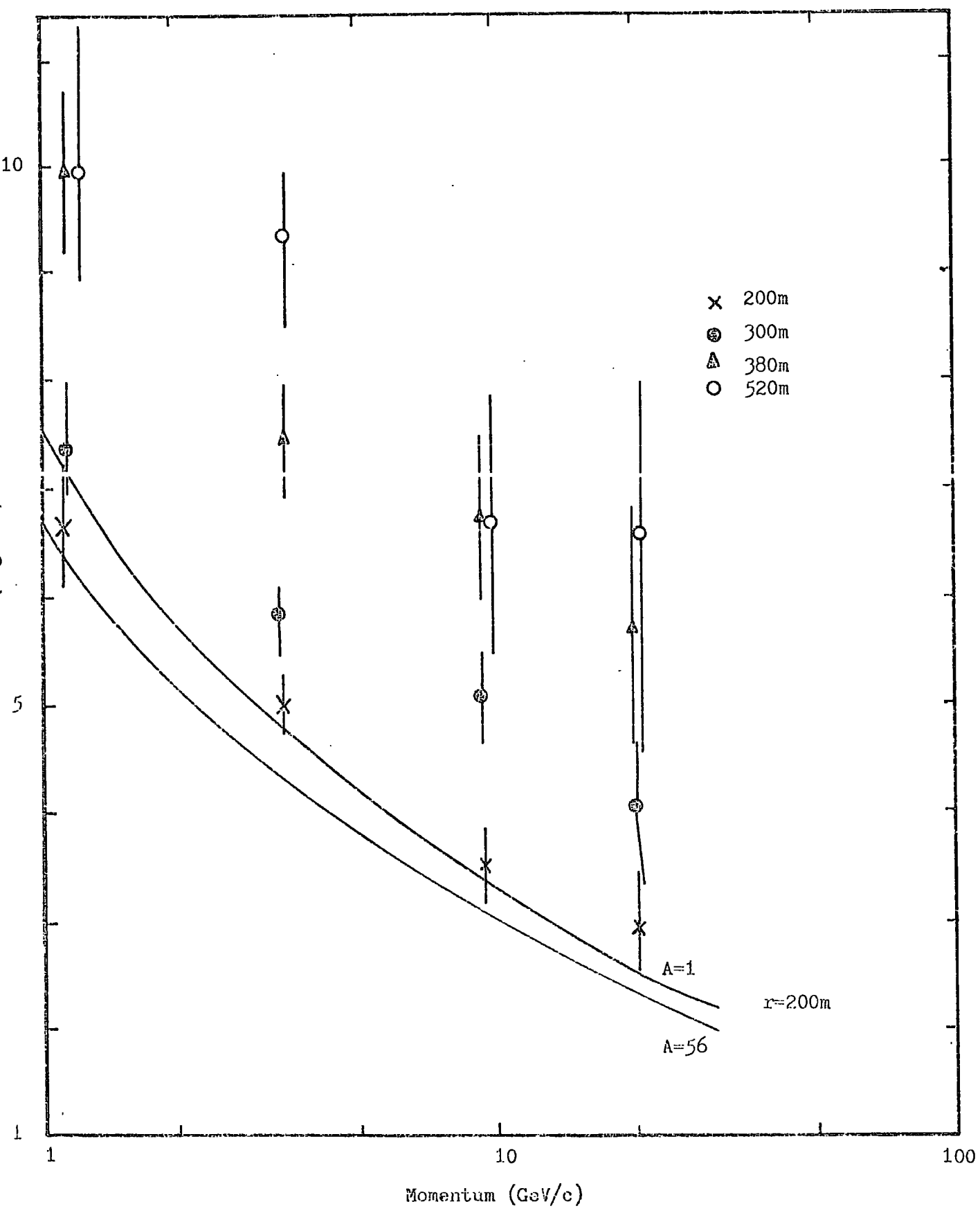
To compare the simulation models with observations, a weighting procedure was used:-

the fraction of positive muons P_i arriving at the point of observation from the i th height interval is

$$P_i = \frac{r_i W_i}{(1 + r_i)} \quad (7)$$

where:- W_i is predicted fraction of all μ of momentum P at sea level originating from the i th height interval.

r_i is the predicted geomagnetic charge ratio of these μ at the observation point.



Defining the total predicted charge ratio R as the total number of negative and positive muons originating from all height intervals arriving at the observation point is given by:-

$$R = \sum_{i=0}^{i=i_{\max}} \frac{P_i}{(W_i - P_i)} \quad (8)$$

The muon heights of origin are influenced by the multiplicity of secondary particles and the mass number of the primary particle. In relation to the heights of origin distributions the two extremes are represented by a proton induced shower with pion multiplicity varying as $E_p^{\frac{1}{4}}$ and an iron nucleus initiated shower following a multiplicity law varying as $E_p^{\frac{1}{2}}$. Using the models of Orford and Turver (1970) tests were made of the sensitivity of the expected muon charge ratio to the height of origin distribution, the charge ratios being predicted for the mean momentum appropriate to the experimental data. It should be noted that the lateral distribution for the proton induced shower is steeper than that for the iron nucleus primary despite their differences in multiplicity law. Therefore, although the heavy primary cascade develops earlier and is affected more by the geomagnetic field, the increased charge ratio deflection is not as great as it would have been if the lateral distribution had not also been flattened. Figure 2-4 shows the predicted charge ratios, and it is apparent that they are the same for all but the highest momenta.

In conclusion it may be deduced that the geomagnetic charge ratio distortion is not particularly sensitive to the chosen model of shower development owing to the fact that earlier developing cascades giving rise to a longer mean free path length in the geomagnetic field have a flatter lateral distribution at sea level.

Chapter Three.

Computer Simulations of the Spatial and Temporal Characteristics of Muons in Large Air Showers.

3-1 Introduction.

The experimental and simulation data reviewed in Chapter Two indicated that the temporal and spatial properties of the muon component contained much information pertinent to shower development and, by implication, to the nature of the primary particles. Before commencing work on a new experiment to extend the studies of Earnshaw et al on spatial characteristics, a programme of rigorous computer simulations to act both as an aid to design and the interpretation of experimental results was deemed necessary. A synopsis of the simulations was presented by Turver (1975) and a more detailed summary is presented in this chapter

Early work on the muon component in the late 1950s comprised ~~of~~ fundamental measurements of lateral distribution (e.g. Clark et al [1958]). This progressed to more recent measurements of charge and energy distributions pioneered by Bennett and Greisen (1961) which, in turn, was extended and consolidated by Dixon et al (1974). de Beer et al (1962) and Linsley and Scarsi (1962) made the first investigations and measurements of the spatial and temporal properties. This field was extended more recently by Armitage et al (1973) and Earnshaw et al (1973).

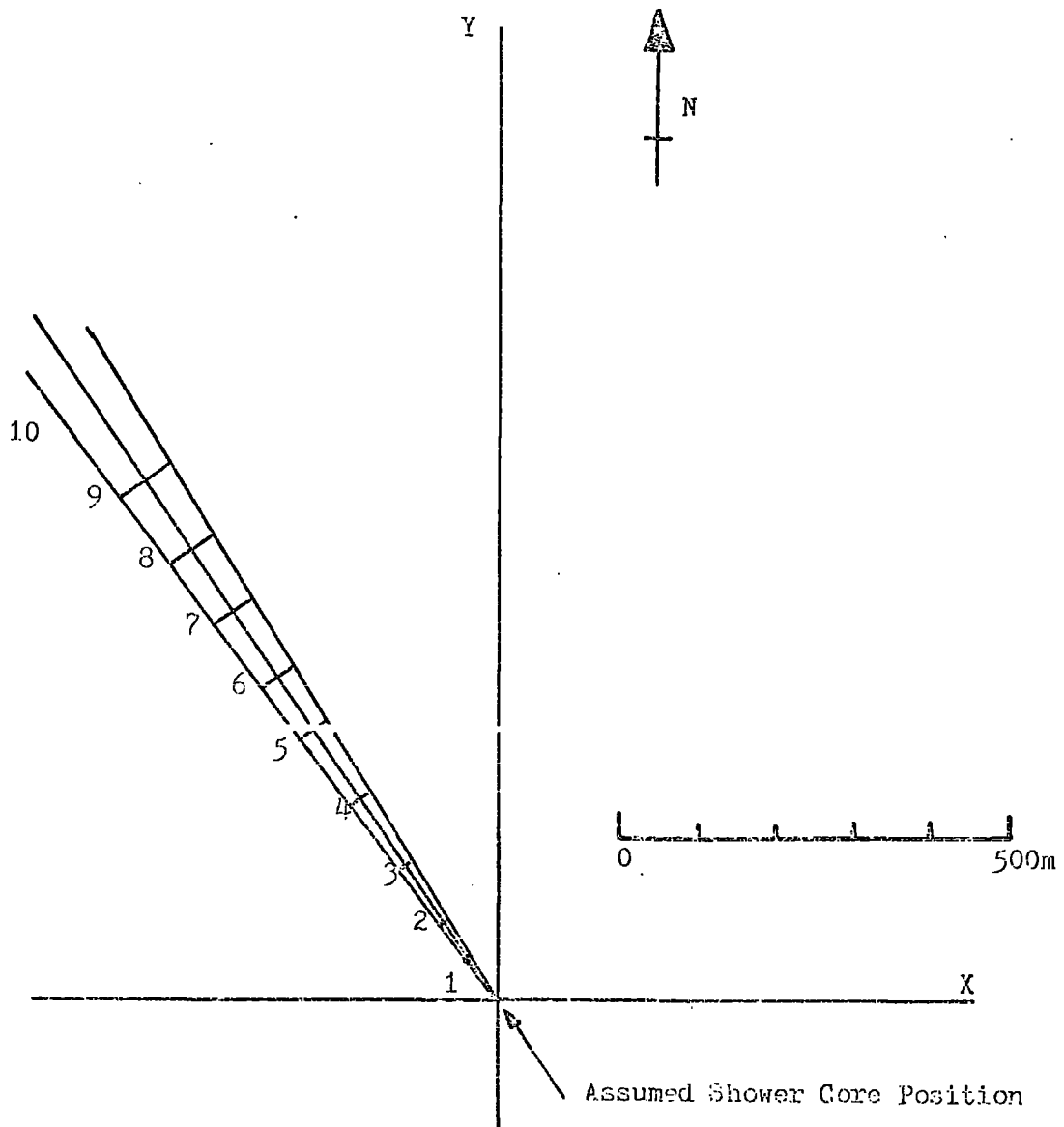
As an aid to understanding the measurements and to indicate the optimum measurable parameters for investigations of the atomic mass number of the primary particles, more thorough and extensive simulations were required. The work of de Beer et al (1966) and

Hillas (1966, 1971) gave a satisfactory over-all account of the muon energy and core distance measurements but did not explore the fine detail of the results. This chapter contains results of simulations which were specifically designed to investigate the spatial and temporal characteristics of muons, to act as a basis for experimental design and to form the basis for the interpretation of results.

The simulations were developed from a wide ranging programme executed at Durham which was reported by Dixon et al (1974 a and b) and Dixon and Turver (1974). The original simulations assumed that the transverse momentum of the parent pions was solely responsible for the muons' lateral development in both time and space. Certain effects such as geomagnetic interactions and Coulomb scattering which are non negligible were not initially considered; large area detectors were also assumed so as to compensate for the small number of muons in showers. The longitudinal development of showers was found to be well defined by the electron-photon cascade, particularly the depth of maximum, which is a direct consequence of the pion production spectrum in the nuclear cascade which, in turn, is dependent on the depth of the first interaction. Such pion spectra formed the starting point for the current study which relies on Monte Carlo techniques.

3-2 Computational Procedure.

As a means of rigorously simulating experiment and restricting the large amount of computer time needed for Monte Carlo type programs, the muons in a small segment in azimuth of each shower were considered (see Figure 3-1). The segment was divided to represent possible detectors each large enough to provide a sample of more than 20 muons in a 10^{18} eV proton induced shower.



Detector N ^o	Area (m ²)	Distance From Core (m)
1	0.5	20
2	1	50
3	3	100
4	8	200
5	20	300
6	30	400
7	30	500
8	30	600
9	30	700
10	30	800

In the simulation each pion produced in the shower of known energy and height of origin was considered. The pions' azimuth angles were chosen from a distribution ensuring symmetry and only those particles occurring in the narrow band defined above were considered further. The distribution due to Cocconi, Koester and Perkins (1961) was used to ascribe transverse momentum to the remaining particles. Pions which interacted or reached ground level before decaying, or moved outside the bin were neglected. The propagation through the atmosphere was then followed, due allowance being made for:-

- 1) energy loss of both pions and muons.
- 2) $\pi - \mu$ and $\mu - e$ decay processes.
- 3) atmospheric Coulomb scattering.
- 4) the velocity lag of particles.
- 5) geomagnetic effects on particle tracks. (The geomagnetic field used was appropriate to that at Haverah Park).

At ground level only those muons striking one of the hypothetical detectors were 'recorded'. The muon data available at this stage of the simulation were height of origin, energy, delay with respect to a reference time, angles made by muons to shower axis and details of the scattering processes undergone. The simulation continued to consider the effect on spatial characteristics as the muons passed through a 'detector' which comprised a sandwich of lead absorber (5cm thick) and track delineating devices of high accuracy.

All the simulations were made for vertical showers usually initiated by protons, although some iron primaries in the $10^{17} - 10^{18} \text{ eV}$

range were considered. Table 3-1 shows the core-axis distances at which the hypothetical detectors defined in Figure 3-1 lie together with typical samples from an average 10^{18} eV proton primary with depth of maximum 750gcm^{-2} . The mean energy, height of origin, spatial and temporal details are shown. It should also be noted that the data shown exhibits the effects of fluctuations arising from the 'sampling' of the shower.

Figure 3-2 presents detailed information for muon time delays and angles as might be recorded by a 30m^2 detector shielded by 5cm of lead at a core distance of 500m for a 10^{18} eV proton primary. The long delay between the arrival of low and high energy muons is clear.

3-3 Spatial Characteristics.

At least three possible methods of interpretation of the spatial properties of muons exist:-

a) By assuming that the only data available on particle directions are those from muon detectors. Such data are presented in Figure 3-3a from a single simulation of an 'average' shower.

b) Data from other sources (fast timing, particle density etc.) exist enabling the shower's axial direction and impact point to be determined. In this case the data in (a) above may be considered as angles with respect to shower core direction.

c) Finally, to consider the muon angular data in one detector and compare it with that recorded by another similar detector at a different core distance, such data are shown in Figure 3-3b, again for a single average shower.

With all considerations of spatial angles the detector energy

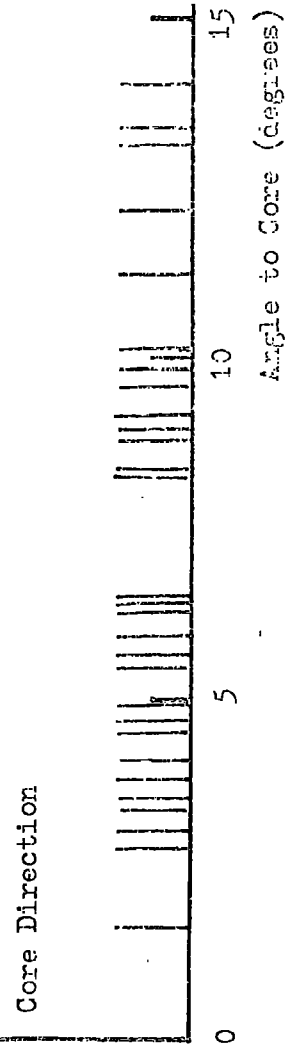
DETECTOR NUMBER	1	2	3	4	5	6	7	8	9	10
Core Distance (m)	20	50	100	200	300	400	500	600	700	800
Detector Area (m ²)	0.5	1	3	8	20	30	30	30	30	30
No. of Muons Detected ($E_{\mu} > 0$)	60	61	77	55	63	56	33	31	13	8
Mean Energy (GeV)	40.0	14.9	9.3	4.0	2.05	2.80	2.37	2.21	1.70	1.67
Mean Height of Origin (Km)	2.46	2.29	3.05	3.33	1.72	3.53	4.08	3.98	3.13	4.34
Mean Delay Time (nsec)	16.5	7.31	25.7	40.1	112.0	135.0	155.0	265.0	436.0	316.0
Mean Angle (No Lead) (deg)	-0.81	-1.89	-4.15	-3.46	-8.21	-8.79	-8.81	-12.7	-15.9	-14.0
Mean Angle (5 cm Lead) (deg)	-0.76	-1.80	-4.27	-3.58	-7.45	-8.10	-9.15	-13.0	-12.6	-13.4
Mean Angle (10 cm Lead) (deg)	-0.37	-1.84	-3.72	-3.66	-5.61	-8.78	-9.72	-12.8	-12.5	-12.3
Mean Angle (15 cm Lead) (deg)	-0.70	-1.85	-3.15	-3.90	-5.78	-7.30	-9.99	-11.2	-10.6	-10.6
Mean Angle (20 cm Lead) (deg)	-0.94	-1.92	-2.99	-3.66	-4.54	-7.47	-7.58	-11.3	-9.0	-12.7
Mean Angle (25 cm Lead) (deg)	-1.05	-1.68	-3.11	-3.59	-4.19	-6.34	-7.52	-8.92	-9.3	-12.7
Mean Angle (30 cm Lead) (deg)	-0.84	-1.57	-3.00	-3.95	-5.80	-6.50	-7.68	-8.6	-10.1	-13.3

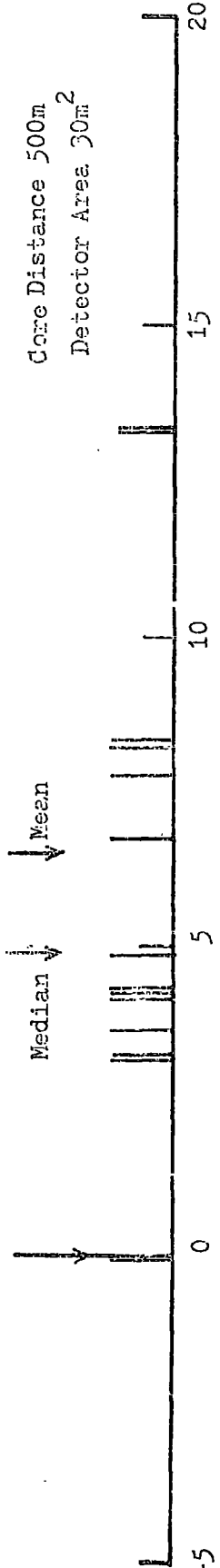
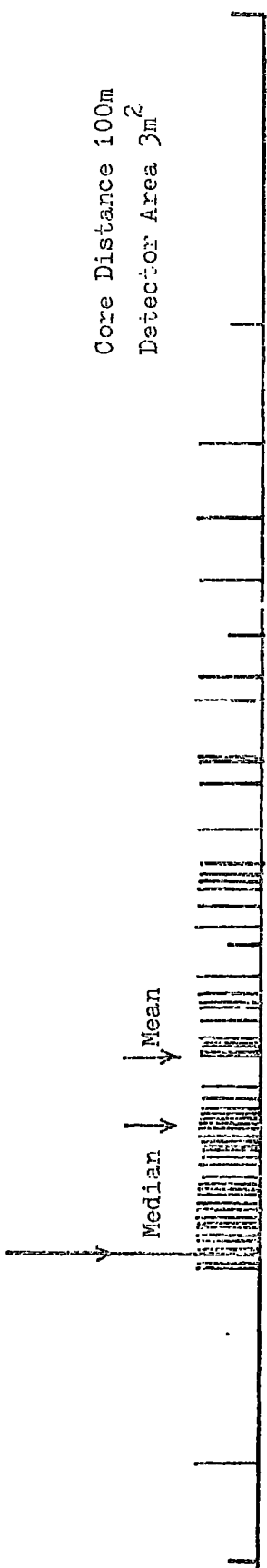
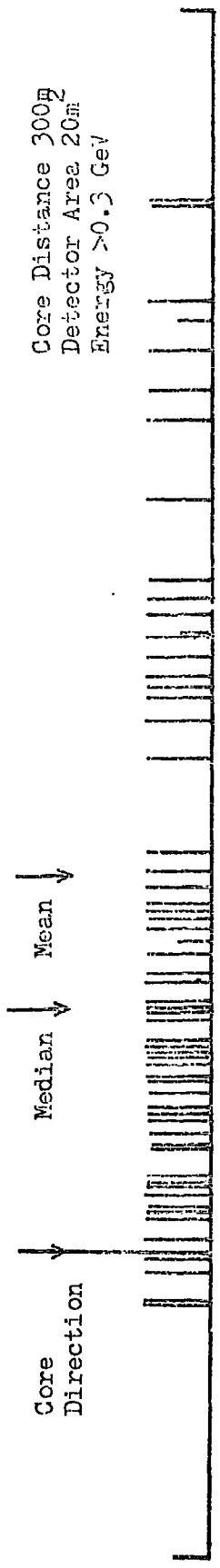
$E_{\mu} > 0.3 \text{ GeV}$
 $E_{\mu} < 0.3 \text{ GeV}$

Tangent Plane
 ↓ Zero Time
 Extreme Front
 ↓ Zero Reference Time



5cm Lead Absorber
 39.5
 29.0





Angle in Detector (deg)

threshold is of great importance (due to scattering processes in the shielding material) and expected distributions under various thicknesses of lead (0-30cm in 5cm steps) for a 10^{18} eV proton at 500m core distance are illustrated in Figure 3-4. The available data for vertical 10^{18} eV proton induced showers at various core distances and with an 'average' longitudinal development, together with an indication of the expected sampling fluctuations are given in Table 3-2. Figure 3-5 shows the heights of origin at various core distances with muon energies in excess of 0.3 and 1.0 GeV for a 10^{18} eV proton initiated shower.

3-3.1 Comparison of Simulation with Experiment.

Much of the available data on spatial angles at present originate from measurements made at Haverah Park. This has eliminated possible normalization problems which would have been necessary to accommodate data from widely differing experiments. The majority of the measurements used have provided data averaged over many showers, but data are now becoming available on individual large showers particularly of the fluctuations between them (e.g Watson and Wilson [1974]).

Comparison with the early spatial measurements of de Beer et al (1962) is not worthwhile. It is more useful to use the detailed unpublished work of Earnshaw et al (1973) who used data from the Haverah Park Magnet Spectrograph. This has been done in Figure 3-6 for data obtained at various core distances in showers with primaries of energy greater than 10^{17} eV.

The height of origin data in the primary energy range 10^{17} - 10^{18} eV is based on measurements made at Haverah Park by Suri (1966), Baxter (1967), Earnshaw et al (1973) and earlier data of Linsley and Scarsi

58 ↑

42 ↑

27 ↑



No Absorber

64 ↑

60 ↑

25 ↑

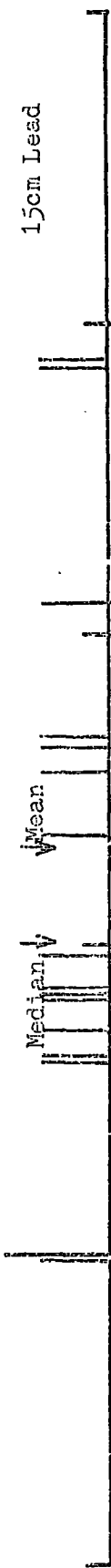
32 ↑



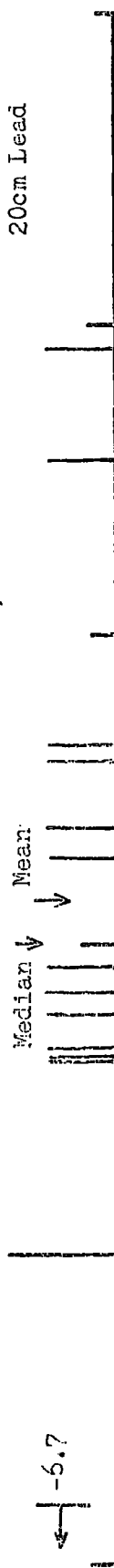
5cm Lead



10cm Lead



15cm Lead

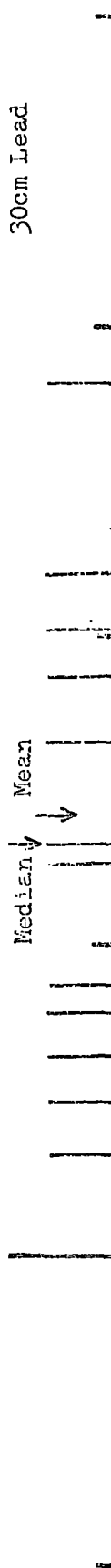


20cm Lead

-6.7



25cm Lead

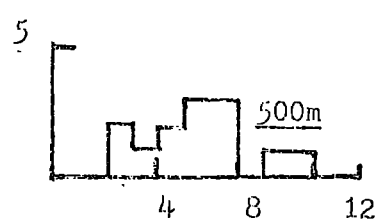
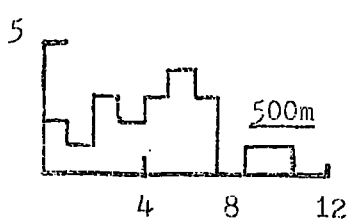
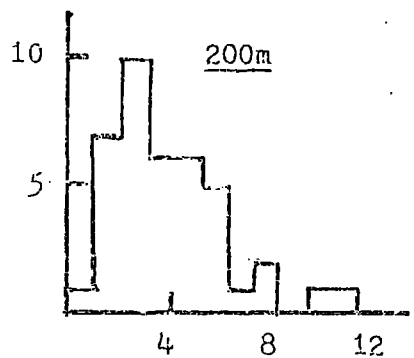
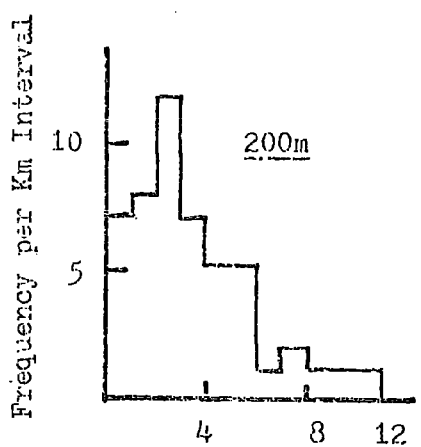
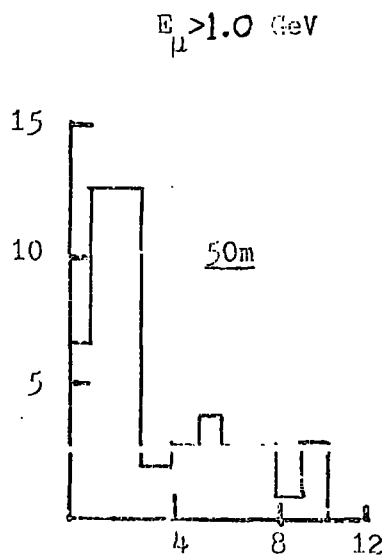
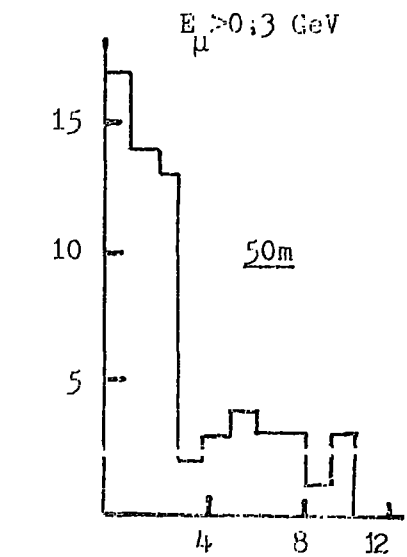


30cm Lead

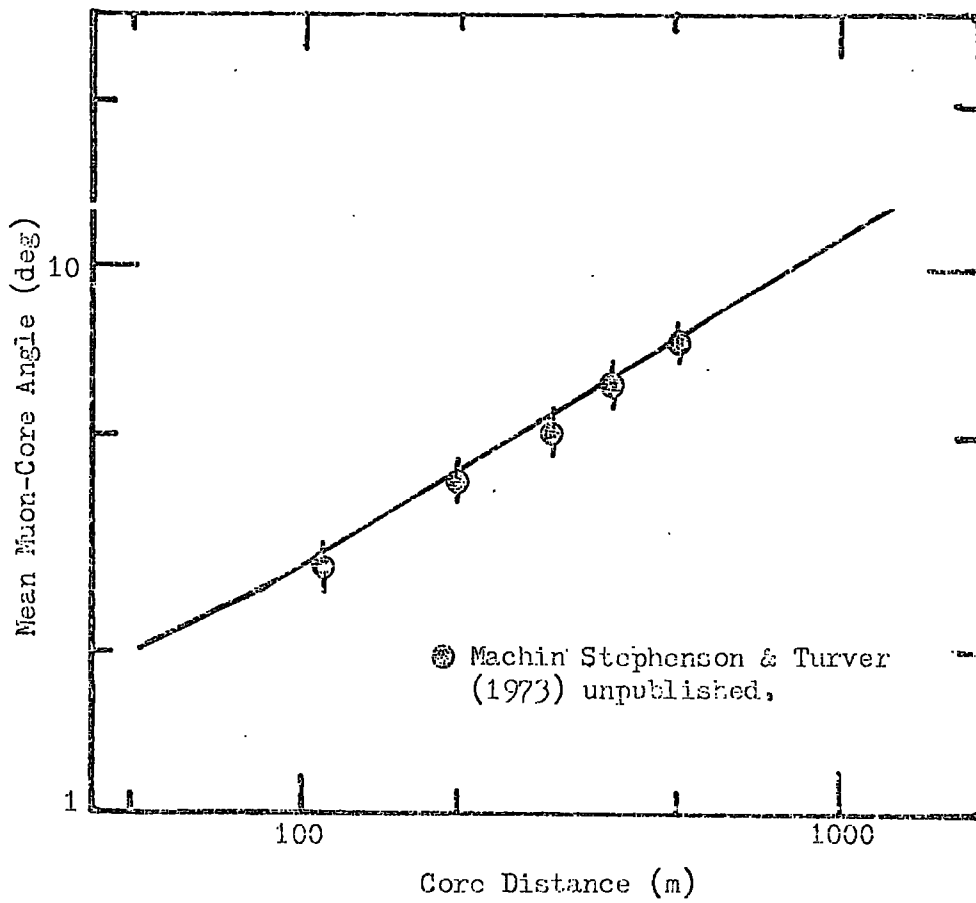
-5 0 5 10 15 20

Angle (deg)

CORE DISTANCE (m)	ABSORBER THICKNESS (cmPb)	MEAN ANGLE (deg)	MEDIAN ANGLE (deg)	STANDARD DEVIATION (deg)	A _{20-80%} (deg)
50	30	1.41 (9 ± 3.4%)	0.67 (14 ± 5%)	3.0 (13 ± 5)	3.2 (25 ± 9)
100	30	2.35 (21 ± 8%)	1.45 (10% ± 2.6%)	3.9 (22% ± 8%)	4.5 (10% ± 2.6%)
200	30	3.3 (18 ± 7%)	2.5 (32% ± 12%)	3.4 (13% ± 5%)	4.3 (25% ± 9.5%)
300	30	4.4 (15 ± 6%)	3.5 (24% ± 9%)	4.8 (15 ± 6%)	6.7 (21 ± 8%)
500	0	10.1 (16% ± 7%)	7.3 (18% ± 7%)	9.0 (32 ± 12%)	12.7 (32 ± 12%)
700	0	14.7 (16% ± 6%)	9.8 (23% ± 8.6%)	13.0 (48 ± 18%)	27.4 (72 ± 27)



Height of Origin (Km)

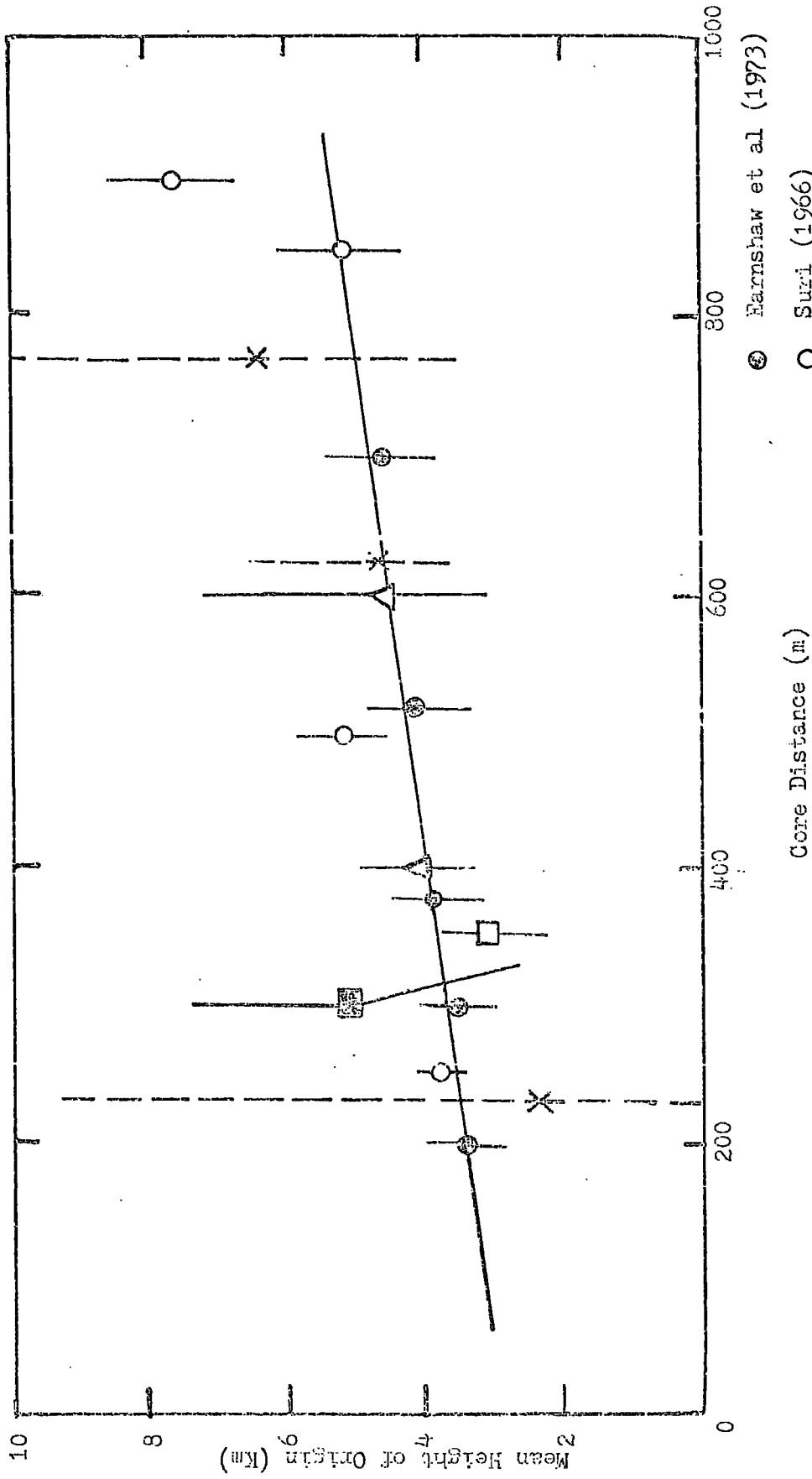


(1962). The work was summarised by Earnshaw et al and adjusted to a common observational level (sea level) and a common muon energy threshold (0.3GeV) and is reviewed in chapter two. The results and the expectation from the simulation data (vertical shower initiated by 10^{18} eV Proton) are reproduced in Figure 3-7.

3-4 Temporal Characteristics.

If effects arising from the detector (e.g. bandwidth limitations and non perfect timing) are ignored then the typical timing information portrayed in Figure 3-2 indicates the origin of the signal recorded in a fast timing detector. The pulse profiles to be expected at various core distances for an ideal scintillation detector beneath 15cm of lead (giving an energy threshold of 0.3GeV) are shown in Figure 3-8. Such profiles are normally represented as rise times between two predetermined points but these measurements are often complicated by the definition of the reference zero time. For this series of simulations the zero time was defined as 'the time at which a spherical wave with height of origin 30Km and travelling at the velocity of light passed through the detector'. The positions of other zero times which were used in the earlier work are also shown on Figure 3-2.

The fluctuations introduced by sampling the showers with a detector of finite size ($30m^2$) were studied and are illustrated in Figure 3-9. In this case muons were repeatedly propagated from the same average 10^{18} eV shower and the data are appropriate to a core distance of 500m. A summary of the fluctuations (expressed as relative standard deviation) to be expected for muons with energy in excess of various thresholds and at different core distances is given in Table 3-3.



Core Distance (m)

● Earnshaw et al (1973)

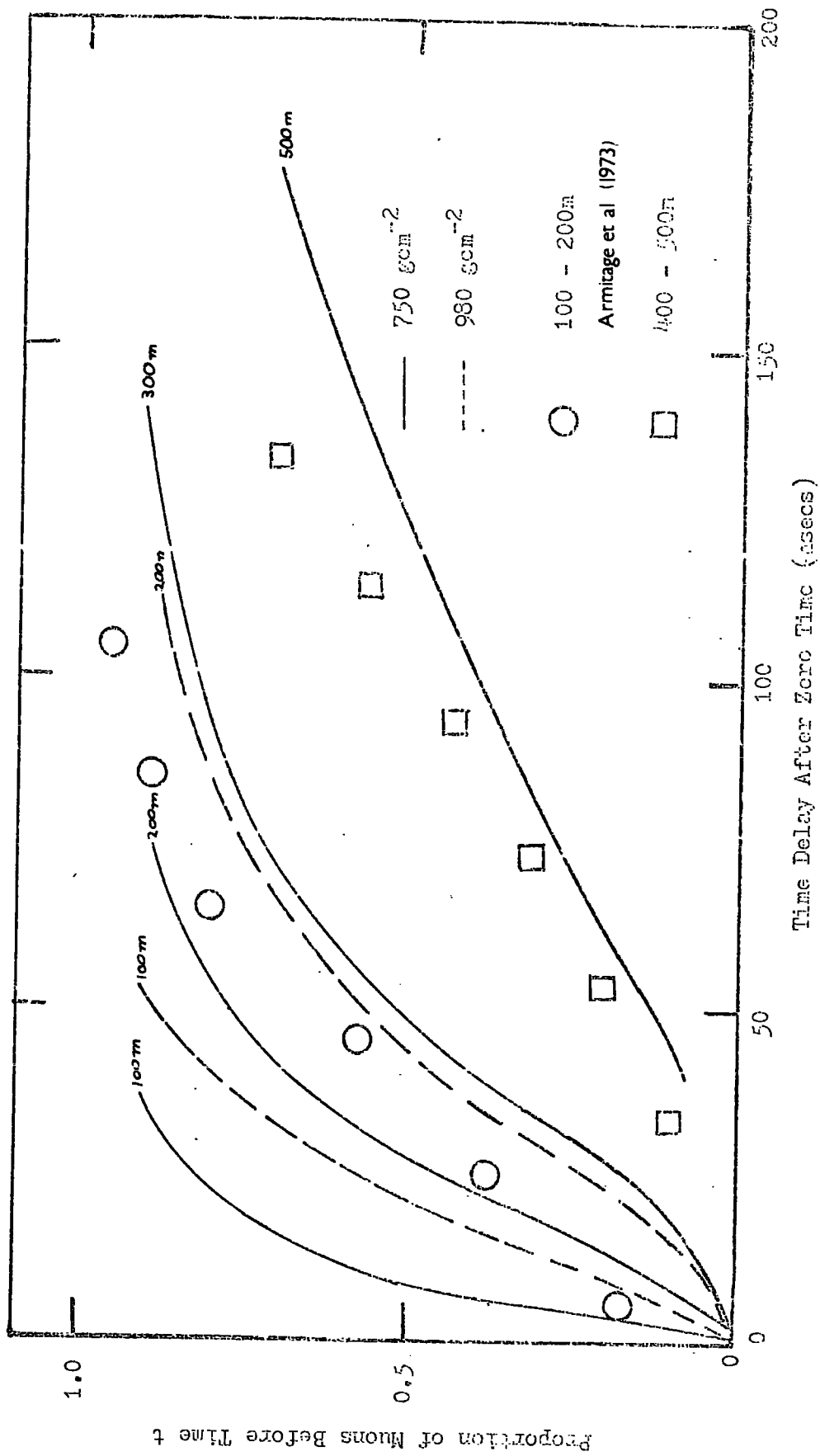
○ Suri (1966)

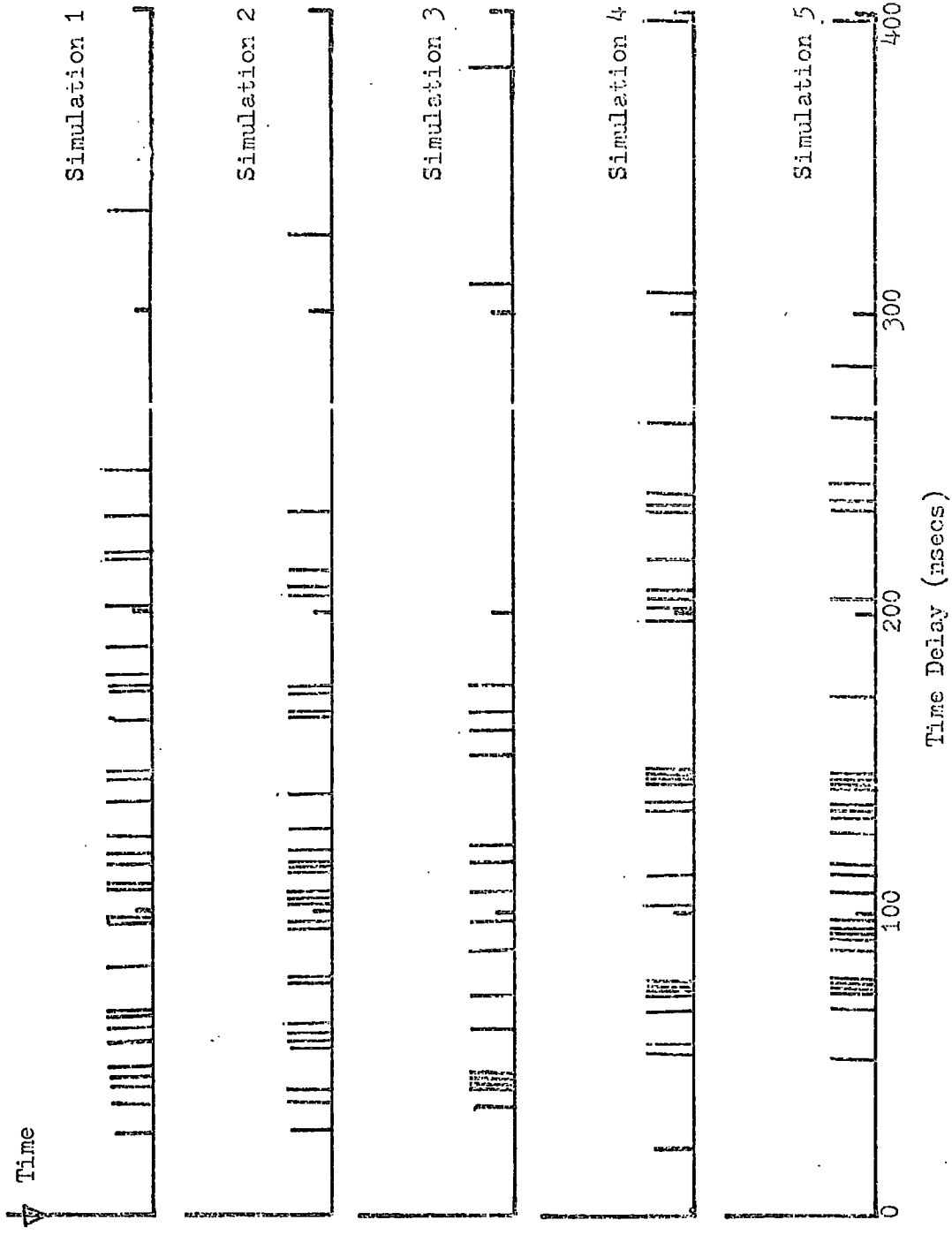
△ Baxter (1967)

□ de Beer et al (1962)

■ Earnshaw et al (1973)

× Linsley & Scarsi (1962)



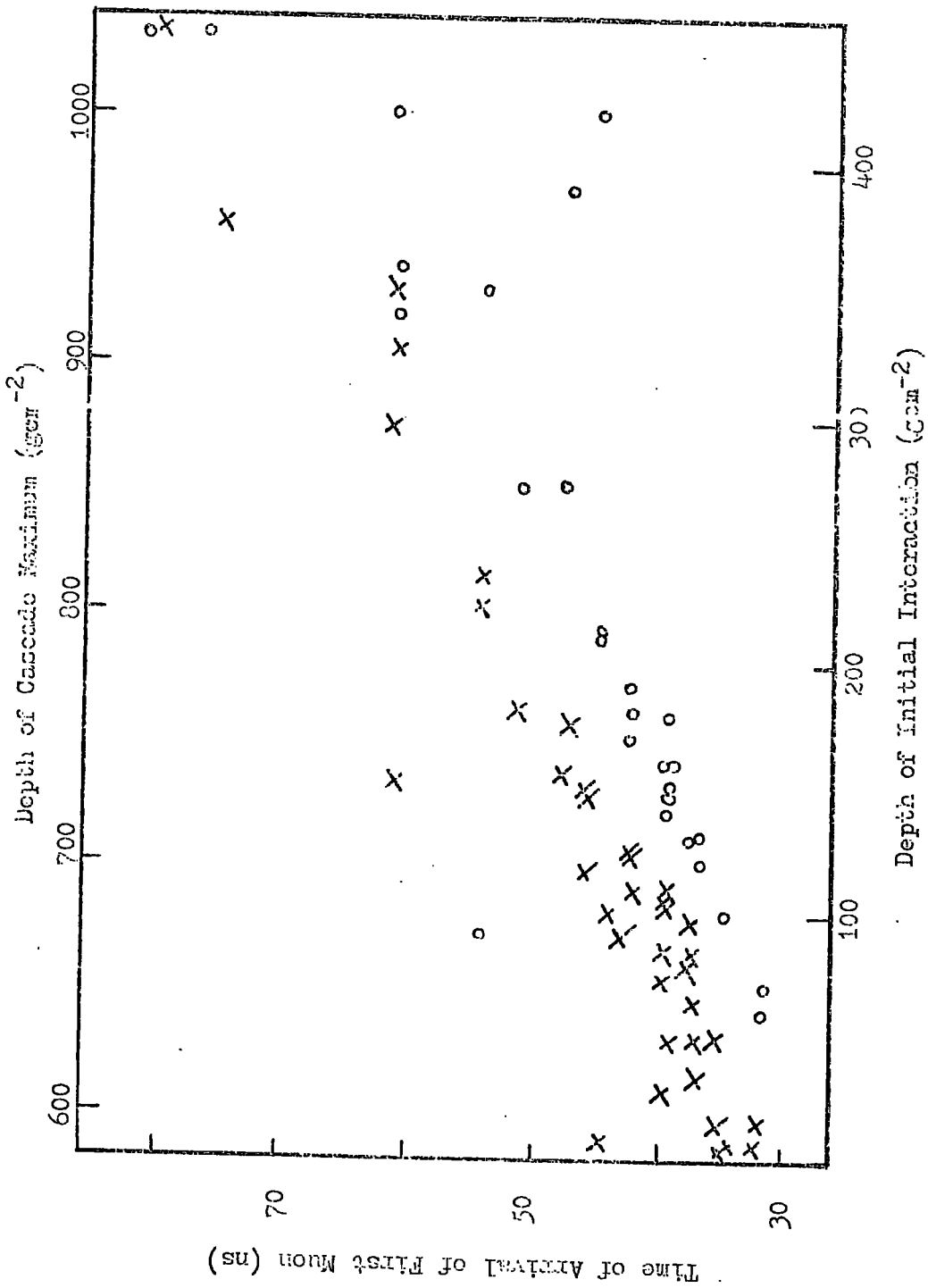


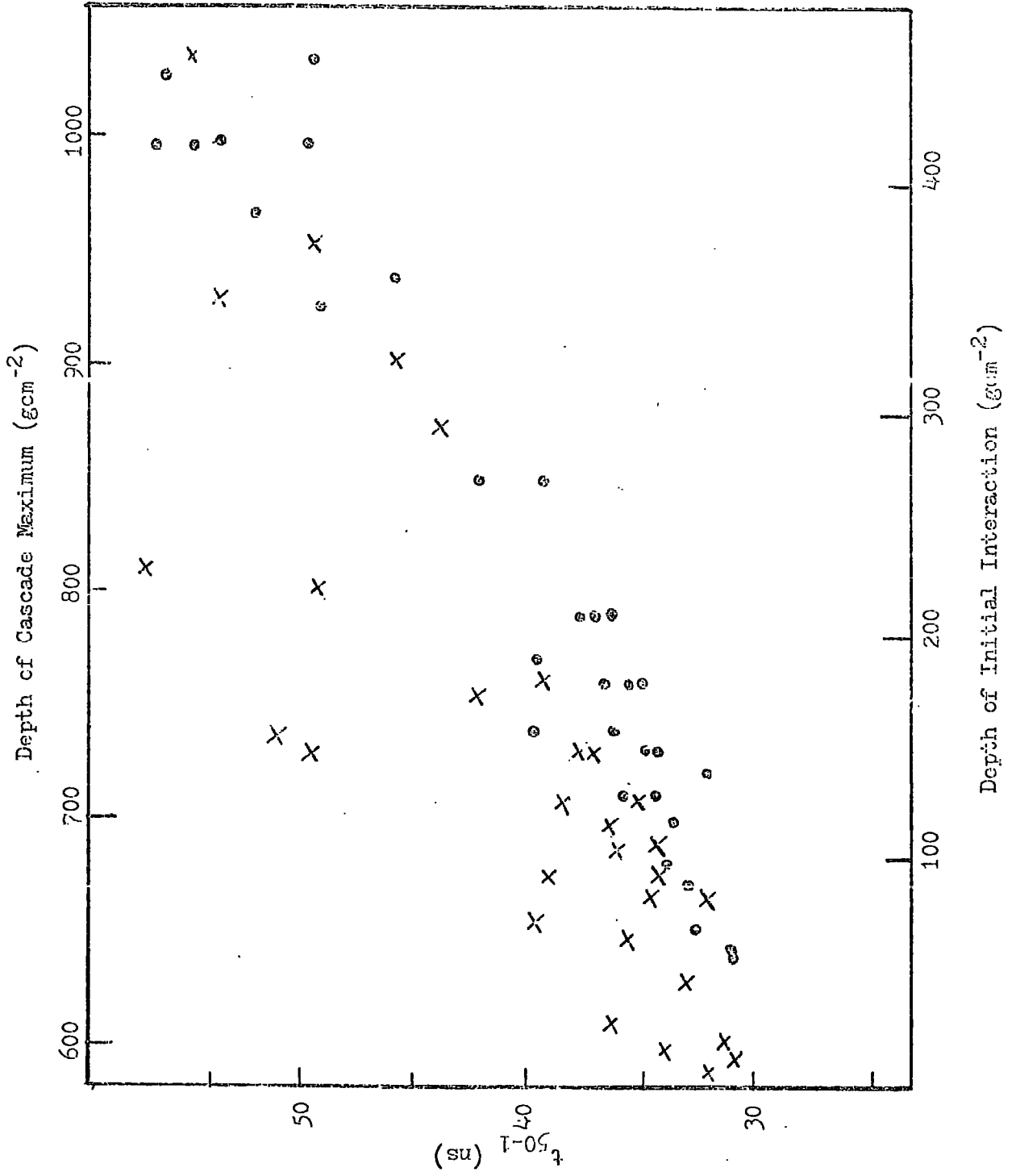
CORE DISTANCE AND AREA OF DETECTOR	Energy Threshold $E > 0$		Energy Threshold $E > 0.3 \text{ GeV}$		Energy Threshold $E > 1 \text{ GeV}$	
	$t_{20-80\%}^{\mu}$ (ns)	$t_{20-70\%}^{\mu}$ (ns)	$t_{20-80\%}^{\mu}$ (ns)	$t_{20-70\%}^{\mu}$ (ns)	$t_{20-80\%}^{\mu}$ (ns)	$t_{20-70\%}^{\mu}$ (ns)
50m (1m ²)	8.9 (40 ₋₁₅ %)	5.2 (27 ₋₁₁ %)	8.4 (36 ₋₁₄ %)	4.2 (20 ₋₈ %)	4.8 (22 ₋₈ %)	3.3 (37 ₋₁₄ %)
100m (3m ²)	24.7 (12 _{-4.5} %)	15.2 (12 _{-4.5} %)	19.6 (19 ₋₇ %)	12.5 (14 ₋₅ %)	12.1 (13 ₋₅ %)	6.5 (16 ₋₆ %)
200m (8m ²)	50.1 (20 ₋₇ %)	31 (25 ₋₁₀ %)	41.3 (25 ₋₉ %)	29.7 (25 ₋₉ %)	22.8 (10 ₋₄ %)	19.1 (11 ₋₄ %)
300m (20m ²)	102 (15 _{-5.5} %)	65 (4.5 _{-1.7} %)	68 (12 _{-4.5} %)	52 (14 _{-5.3} %)	38 (10 ₋₄ %)	29 (16 ₋₆ %)
500m (30m ²)	194 (27 ₋₁₀ %)	130 (15 _{-5.6} %)	130 (12 _{-4.5} %)	113 (9 _{-3.4} %)	82 (43 ₋₁₆ %)	53 (32 ₋₁₂ %)
700m (30. m ²)	248 (40 ₋₁₅ %)	196 (15 _{-5.6} %)	173 (10 ₋₄ %)	159 (13 ₋₅ %)	72 (41 ₋₁₆ %)	42 (55 ₋₂₁ %)

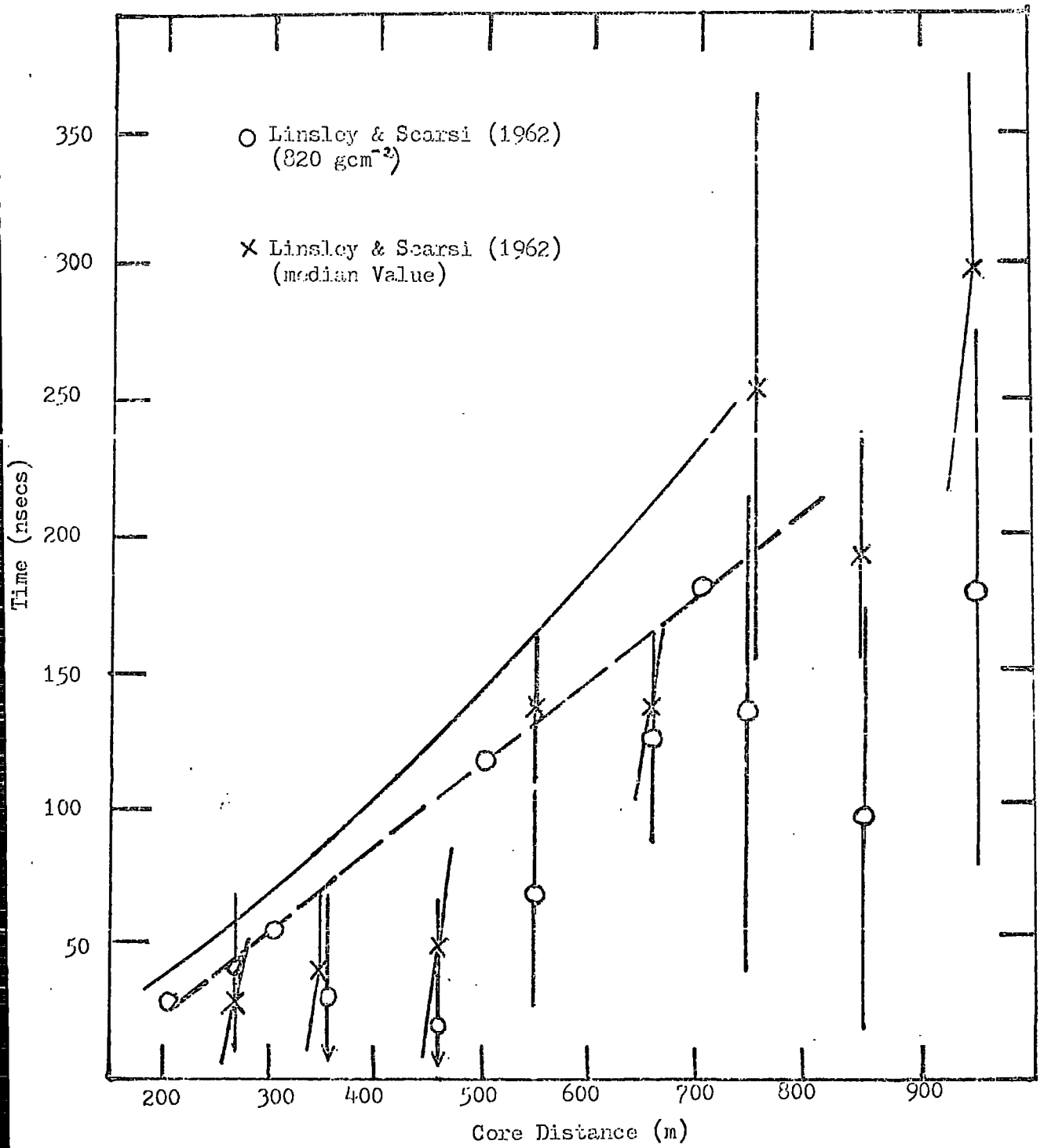
Correlations between the parameters displayed in Figures 3-2 and 3-9 and longitudinal cascade development details were considered. Figure 3-10 plots the arrival time of the first muon at 500m (t_i) and the depth of first interaction (λ_i) for a proton primary induced shower. Also shown is the correlation with depth of cascade maximum development t_{\max} (no allowance being made here for the sampling effects of a detector of prescribed area). The quantity t_i is of fundamental importance and dominates the radius of curvature measurements (e.g. Suri [1966] and Baxter [1967]). A further measurable quantity is t_{50-1} , the time of arrival of 50% of the muons after the first. Figure 3-11 shows the correlation of this quantity with λ_i and t_{\max} .

3-4.1 Comparison of Simulation Data with Experiment.

Due to the small amount of experimental data available it is not easy to compare the spatial angles simulation data with experiment. However, comparisons can be drawn with several sets of temporal data, most measurements having been made with shielded scintillation detectors. The earliest measurements were made by Linsley and Scarsi (1962) (at the Volcano Ranch Array) who studied the arrival times of single muons (of energy greater than 100MeV) with $4m^2$ detectors. Figure 3-12 compares their results with the simulations. (N.B. No allowance is made for the demand that a single muon be incident on the detectors or corrections for altitude effects). Further measurements, again on specific particles, were made at Haverah Park by Armitage et al (1973) which is presented in a similar manner in Figure 3-8.







3-5 Sensitivity of the Simulations to the Parameters of Showers and Shower Models.

The simulations described above are dependent on several basic but important assumptions, principally the atomic mass number of the primary particle, the properties and nature of the nuclear interactions and decay processes occurring in the cascade and finally the muons' propagation through the atmosphere. This section presents brief descriptions of the effects of changes in the assumptions and Chapter Five presents a preliminary report of investigations involving a different model for the nuclear cascade.

3-5.1 Sensitivity to Changes in the Propagation Model.

The results obtained from the full simulation procedure were compared with those obtained from a far simpler type of routine. The simplified program assumed that the sole cause of temporal and spatial effects in muons was the transverse momentum of the particles. If the comparisons had proved satisfactory a great many showers could have been simulated for very detailed study with different assumptions about the high energy interactions for a relatively small amount of machine time.

Typical spatial and temporal parameters for both assumptions are tabulated in Table 3-4. The muons considered were all in excess of 1GeV, an energy for which the detailed propagation may be expected to vary least from the simple model. The satisfactory correlation in Table 3-4 indicates the validity of predictions of the spatial and temporal characteristics of the energetic muons in showers derived from the various models for high energy nuclear interactions. The lateral distributions for muons of energy greater than 300MeV for

	CORE DISTANCE 100m				CORE DISTANCE 500m			
	Time for % (nsecs)			Median Core Angle (deg)	Time for % (nsecs)			Median Core Angle (deg)
	20%	50%	90%		20%	50%	90%	
Simple Propagation	2.3	5.0	18.5	1.7	6.	96	208	6.4
Detailed Propagation	2.5	10.0	20.0	1.45	56	84	176	6.0

both the simple and rigorous treatments are compared in Figure 3-13.

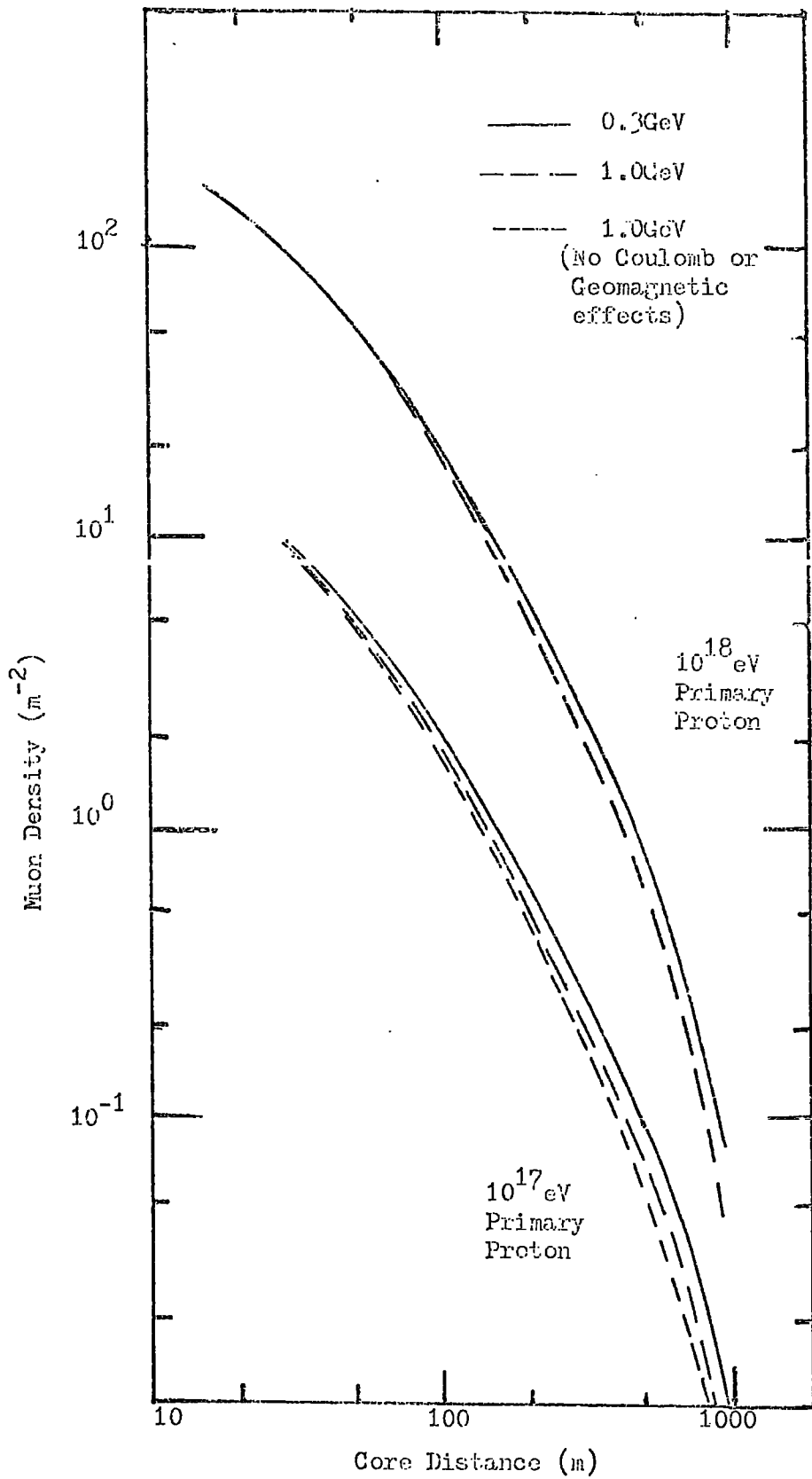
3-5.2 Sensitivity to the Model of High Energy Interactions.

Using the simple treatment of muon propagation for those muons generated from different models of the nuclear cascade described by Dixon et al (1974) comparisons were made for the spatial and temporal characteristics, typical data being shown in Table 3-5. It is evident that at large core distances small differences exist between all models used, excluding simple scaling with proton showers and, given a large amount of experimental data, the differences may be detectable. In the case of the simple scaling model for interactions very marked differences exist and are detected experimentally with relative ease. These differences are, however, removed if a heavy primary is assumed and an increased inelastic cross section for p-p collisions.

3-5.3 Sensitivity to the Atomic Mass Number of the Primary Particles.

Dixon and Turver (1974) confirmed that the most likely method to yield data on the nature of the primary particles in the energy ranges of interest to this work should rely on detecting the large fluctuations in longitudinal development which would exist in showers initiated by primary protons. Consideration of the spatial and temporal characteristics of the muon components in individual large showers would reflect the depth of maximum cascade development and, hopefully, the deeper developing proton induced showers will be revealed.

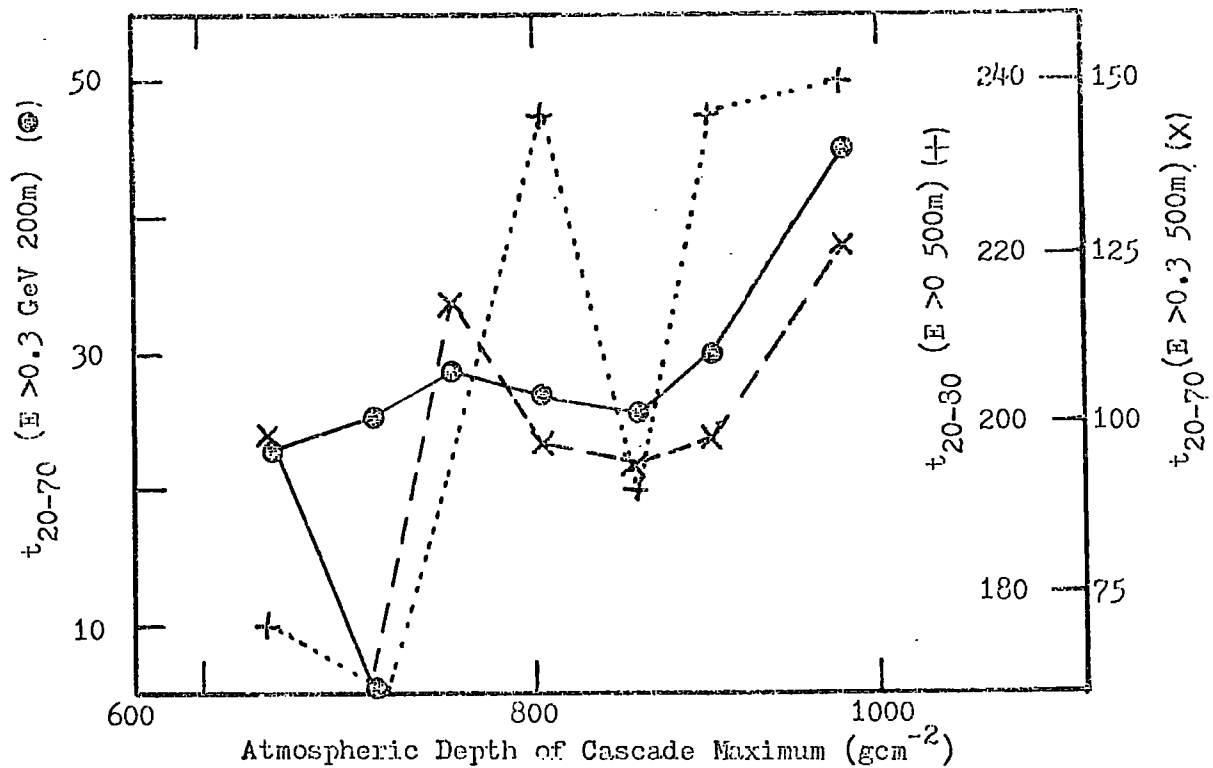
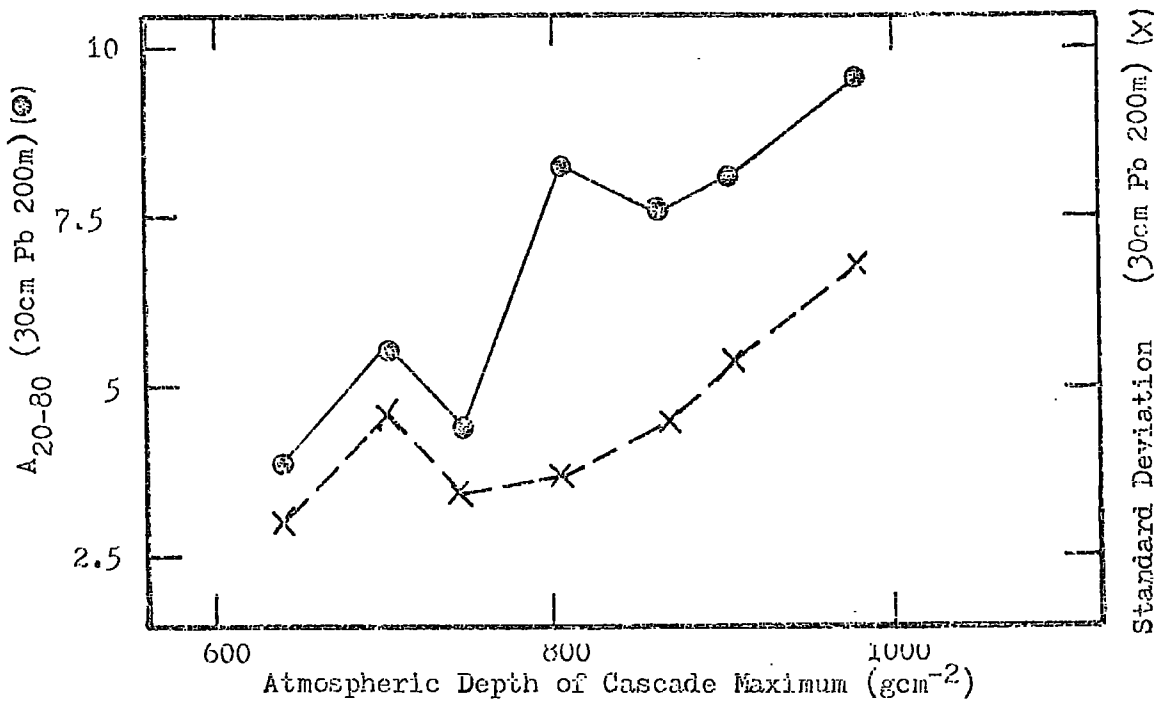
Those muons of energy greater than 0.3GeV at a core distance of 200 and 500 metres in 10^{18} eV showers with maximum development in the range 600. - 1000 gcm^{-2} were considered. The data are based on



PRIMARY PARTICLE	HIGH ENERGY INTERACTIONS MODEL	CORE DISTANCE LOOM										CORE DISTANCE - 500m					
		Time for indicated % (nsecs)					Median Core Angle (deg)	Time for indicated % (nsecs)					Median Core Angle (deg)				
		t _{10%}	t _{20%}	t _{50%}	t _{70%}	t _{80%}		t _{90%}	t _{10%}	t _{20%}	t _{50%}	t _{70%}		t _{80%}	t _{90%}		
Proton	Normal	1.9	2.5	4.3	5.6	10	14	1.50	42	55	86	120	138	160	5.7		
Proton	Increasing cross section	1.6	2.1	3.6	5.7	7.5	10	1.20	44	52	80	105	130	160	5.3		
Proton	Enhanced Multiplicity	1.4	1.8	3.2	5.5	7	12	1.10	38	45	68	97	120	200	4.6		
Proton	Scaling Model	3.0	3.8	6.7	9.2	11.1	12.5	2.33	66	80	130	260	330	430	8.5		
Iron Nucleus	Normal	1.7	2.2	4.2	6.7	8.3	13	1.47	44	52	80	130	180	225	5.3		
Iron Nucleus	Scaling, Increasing cross section.	1.9	2.5	5.5	7.0	12.0	15	1.95	45	55	80	110	138	-	5.3		

individual simulations for the propagation of muons in a range of showers with increasing depths of maximum, representing possible measurements in individual showers with differing depths of maximum. It should be noted that the showers were selected for their depth of maximum only and no attempt was made to ensure that they were 'typical'. The data is shown in Figures 3-14 and 3-15 being spatial and temporal respectively. It will be noticed that some of the measurable parameters indicate stronger dependence on depths of maximum than others (e.g. $t_{20.30}$) but are subject to larger fluctuation.

The simple model was also used to investigate the properties of iron nucleus initiated showers and results are summarized in Table 3-5. It can be seen that the spread in proton shower data derived from the different interaction models is comparable with the differences in the average characteristics of proton and iron showers. Therefore, until a more detailed understanding of the interactions in the nuclear cascade is available it is unlikely that the iron nucleus primaries will be differentiated from others on the basis of average characteristics. On the basis of these data the experiment to be described in Chapter Four was designed and construction commenced in January 1975.



Chapter Four.

The Experiment.

4-1 Introduction.

As a development of the work of Earnshaw et al (1973), Machin (1973) and Pickersgill (1973) which was reviewed in Chapter Two and in view of the encouraging predictions of subsequent computer simulations, it was decided to construct an experiment specifically to measure the spatial details of the muons in showers. The termination of the Mark II Spectrograph programme (and simultaneously the Durnam Nuclear Active Particle Spectrograph which has been described, Hook [1972]) made available some 18000 flash tubes. These have been redeployed at Haverah Park to form the new experiment comprising two large area shielded muon detectors.

The larger of the two new detectors is located on the site of the Magnet Spectrograph in the centre of the air shower array and the other approximately 250m away in a newly commissioned experimental area. This latter site also accommodates a complimentary muon detector employing liquid scintillation counters (operated by the University of Nottingham Group). These two detectors are fully integrated and use the same shielding material.

Previous experience of the use of flash tube detectors in air shower measurements suggested a photographic data recording system which would be quick and easy to assemble and, once commissioned, would require a minimum of maintenance ensuring great reliability over long periods of recording.

4-2 The Requirements of the Measurement.

Earnshaw et al (1973) attempted, by experiment and simulation, to study the mean heights of production of muons in various momentum and distance bands in large air showers. Using the data from the Haverah Park Spectrograph they investigated the charge ratio distortion caused by geomagnetic effects and the lateral and angular scatter of muons with respect to the shower core location and direction. Due to the small sensitive area of the Spectrograph it was necessary for the results to be averaged over many showers; the average characteristics of the EAS muons so observed agreed with model predictions. It was not possible, however, to obtain estimates of the atomic mass number of the primaries from the measurements.

More general and complex simulations (discussed in Chapter Three) have shown that the spatial properties (and inferred heights of origin) contain information on cascade development. The simulations also indicate a sensitivity to the mass of the primary particle in that early and late developing showers which are to be expected if, and only if, there exist primary protons should show detectable differences in muon heights of origin. These new simulation results allied with the simplicity of the trigonometrical method (described in Chapter Two) have rendered viable an experiment based upon two large area detectors with the aim of studying the muon component of individual large showers.

The two detectors (a detailed description of which follows) have been designed on the basis of simulation results and are of sufficient area to enable 15 - 30 muons to be studied in a shower of primary energy $> 10^{17}$ eV. The core direction resolution available from the main array, the trade off between the detector sensitive area and particle track resolution (governed by the number of flash tubes

available) indicated a designed maximum measurement error of 0.5° in the muon directions. It is hoped that this figure can be bettered by using improved analysis techniques should the need arise.

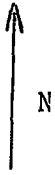
Past experience and a study of the University of Leeds Air Shower analyses indicate that several useful events per day may be expected. Facilities are available for the detectors to operate in conjunction with the University of Durham Čerenkov light detecting array and thus be able to extend the study of showers to those of lower energy ($\approx 10^{16}$ eV). Experience during 1974-75 and 1975-76 winters show that several useful events per hour are likely in this mode of operation.

4-3 The Haverah Park Experimental Array.

The Haverah Park Air Shower Array is described in detail by Tennent (1967) and Andrews (1970) and only a brief description will be presented here. The array is located at a latitude of $53^\circ 58.2' N$ longitude $1^\circ 38.1' W$ and at a mean altitude of 220m equivalent to an atmospheric depth of 1016 gm cm^{-2} . A plan of the array is presented in Figure 4-1.

The principal method of shower detection relies on recording the Čerenkov light emitted when the shower particles pass through clear water. The individual detectors consist of galvanised steel tanks each with a surface area of 2.3 m^2 and filled to a depth of 1.2m and lined internally with sheets of white plastic material (Darvic) to scatter and diffuse the light. A small fraction of the light (0.05%) is recorded by a 5 inch photomultiplier in optical contact with the water. Detailed descriptions of the tanks and their performance have been discussed by Turver (1963).

Each of the main detector sites shown in Figure 4-1 consists of



oc

oc

oc

oc

oc

oc

t

oc

oc

t



oc



oc



○ 2Km Array

□ 500m Array

□ Central Detector

○ 150m Array

oc Night Sky Cerenkov Array

m Muon Spatial Angle Detectors

t Muon Timing Detectors

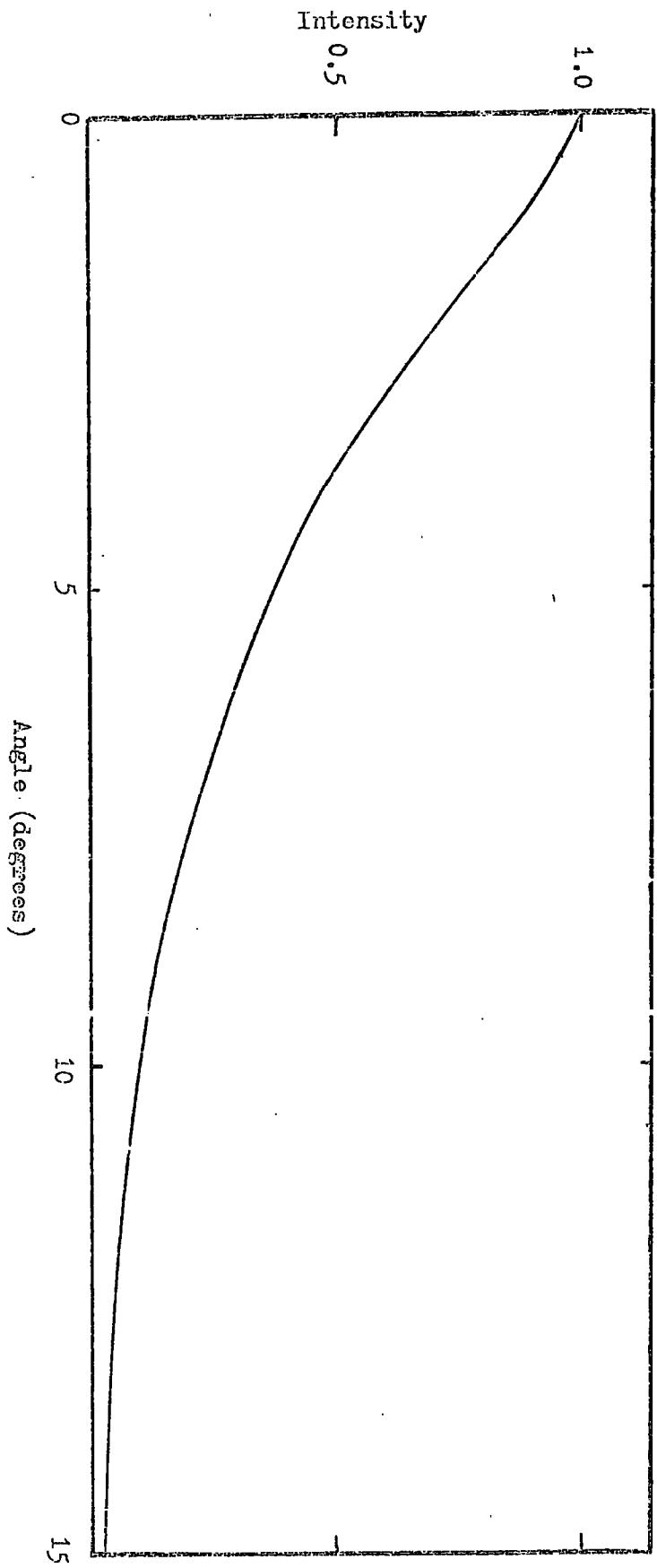
an assembly of tanks. The output from the individual tanks is passed to an adding unit before transmission and/or recording. Large area detectors (out to distances of 500m) are linked to the array centre by cables for all recording. An air shower is recorded when the ten particle level in the centre detector and two of the 500m detectors is exceeded simultaneously. This triggers the recording systems of the array and subsidiary experiments.

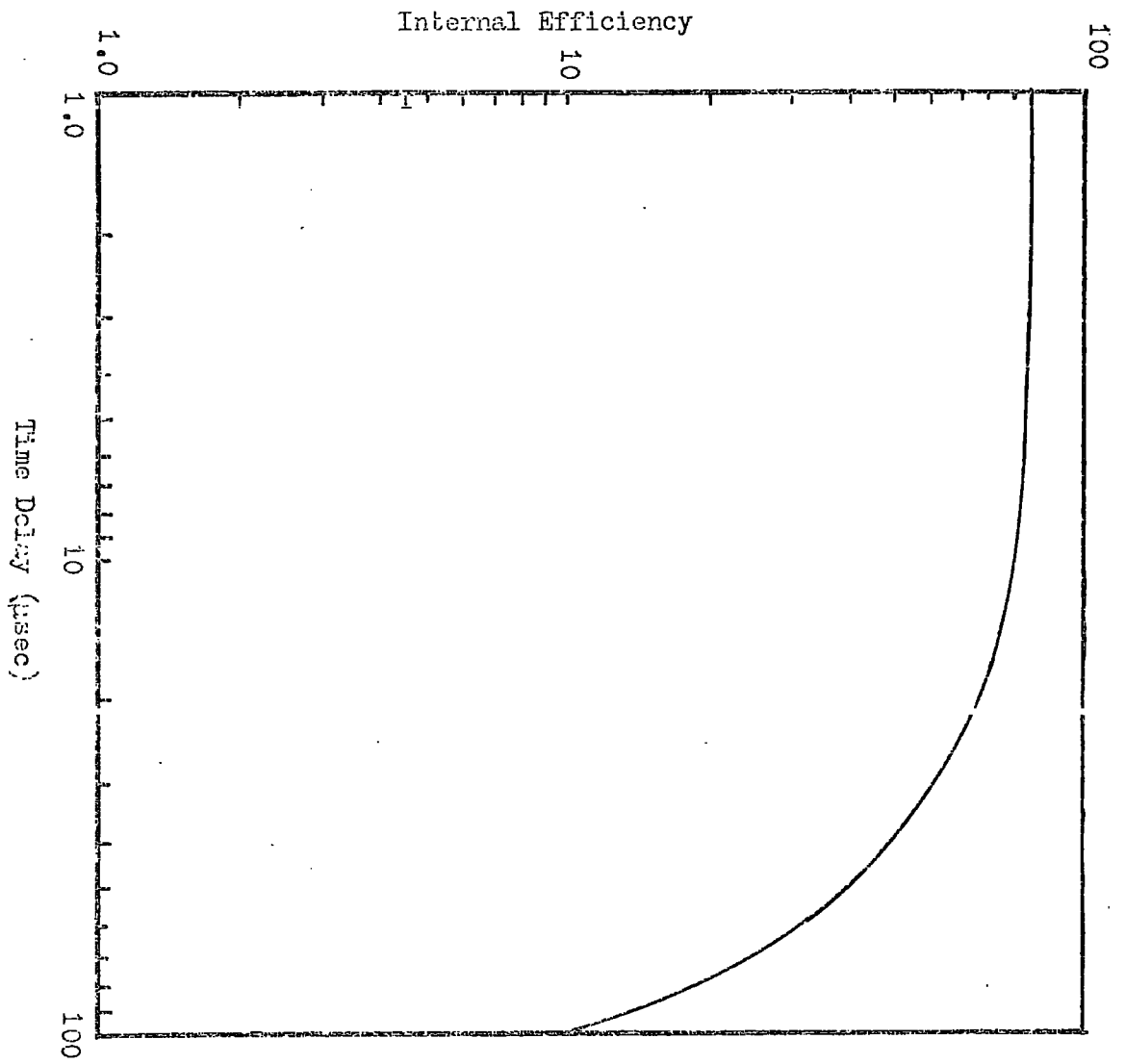
In addition to the particle detector array several subsidiary experiments exist. During the winter months an array of eight Night Sky Air Čerenkov detectors is operated. The detectors are located at the positions shown in Figure 4-1. Currently being commissioned is another array of small (1.25m^2) closely spaced water detectors within the 500m array to study the regions close to the shower cores. The muon component of EAS, the topic of this thesis, is extensively studied and two new experiments are at present nearing completion.

4-4 The Instrument.

4-4.1 The Neon Flash Tube Detector.

The neon flash tube detector was introduced by Conversi and Gozzini (1955) and has since become popular in cosmic ray studies due to its versatility and long life. It consists of a flat ended sealed glass tube filled with an inert gas mixture. To form a useful large area detector an array of tubes is placed between sheet metal electrodes and, when an external trigger detector records the passage of a charged particle, a high voltage pulse is applied to the plates. The tubes through which the particles passed give a flash of light which can easily be recorded on film. Many theories of flash tube operation





have been put forward. A comprehensive survey has been given by Breare (1973).

Two important constraints have to be born in mind when designing flash tube arrays. Firstly, work by Coxell et al (1961) showed that the intensity of the emitted light declined rapidly with polar angle (Figure 4-2) leading, for small camera flash tube distances, to difficulties in photographing the peripheral tubes of an array. The large voltage pulse necessary to trigger the tubes inevitably creates electronic noise to the detriment of other equipment. Fortunately the tubes have a 'long' memory and, as figure 4-3 shows, high efficiencies are maintained up to 20 μ s after the passage of a particle. Thus, with a suitable pause before pulsing, interference with other equipment can be eliminated.

4-4.2 Flash Tube Mountings and Common Constructional Details.

Previous experience with both the Mk.I and Mk.II Spectrographs at Haverah Park led to a simple, cheap, accurate and reliable system for supporting flash tubes. Dural bars (Durals) are milled with a series of constant and parallel pitch slots across their length. (Exact details can be found in Pickersgill [1973]). The durals are then mounted at the front and rear of each flash tube tray and carefully aligned to ensure that the front and rear slots correspond. This alignment was achieved by using perspex cylinders of the same diameter as the tubes with the centre of one face clearly marked. A cathetometer and series of plumb lines were then used to position the durals within the trays giving the desired tube position offsets. Simulations by Bull et al (1962) showed that no discernible difference in measurement accuracy existed between random and regular arrays of

tubes; a simple half pitch stagger was adopted for all the new trays.

The weight of the glass tubes cause considerable distortion and sag along the length of the durals. This problem is easily overcome by mounting vertical 6mm perspex strips along the front and back of the tray at frequent intervals. The durals are then bolted to the perspex and as this operation is performed under controlled workshop conditions during the construction and alignment stage the exact dural location is assured.

The engineering facilities at Haverah Park are very limited so it was decided to perform all tray construction and setting up in Durham and, where possible, to transport these intact. This was not possible with the trays of Detector B, so they were designed to be dismantled; exact reconstruction being ensured by key slots on all major joints. The deployment of the trays in the two muon detectors is detailed in the relevant sections. As the trays are not directly interdependent in contrast with earlier applications of neon flash tubes in a spectrograph, the exact relationships and positions to each other is not of vital importance. A simple measurement technique was employed giving colinearity of tubes between detectors to much better than 1%.

4-4.3 Detector A.

a) General Details.

The larger detector is located at the approximate centre of the main particle detector array on the site originally occupied by the solid iron Magnet Spectrographs. Only the magnet iron remains of the original configuration of the spectrographs; it now shields and gives a 1GeV threshold to two of the original flash tube trays which have

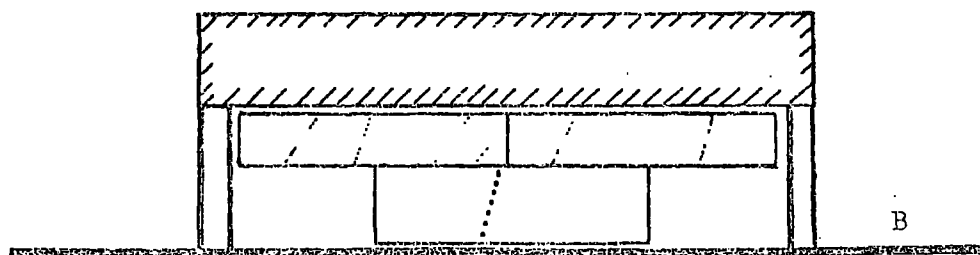
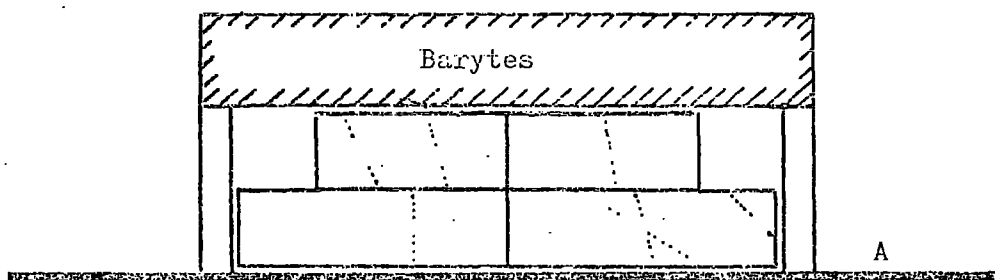
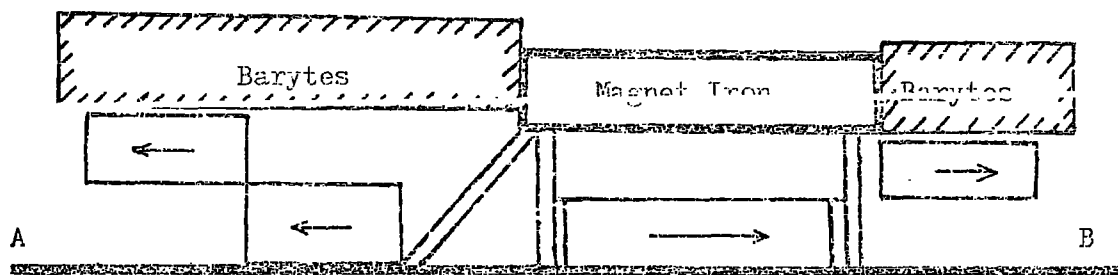
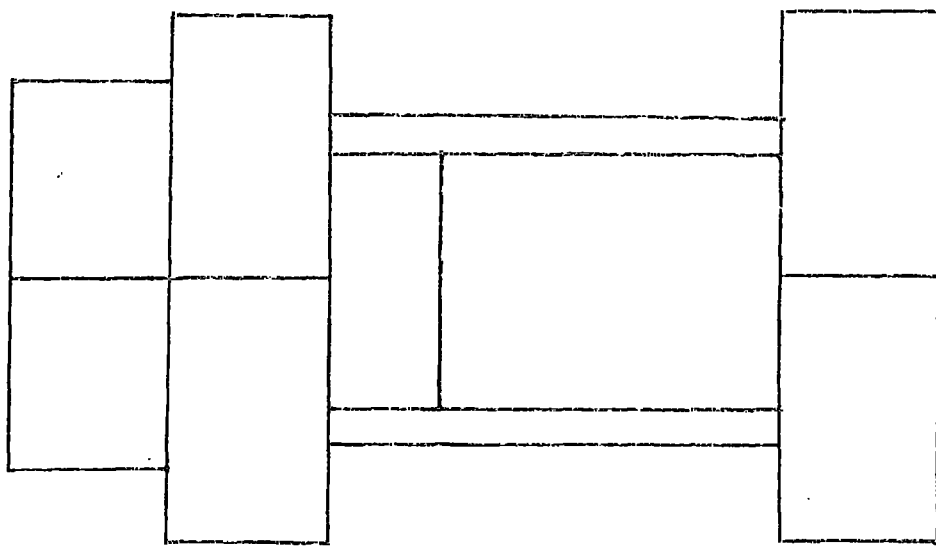
been relocated with their tubes perpendicular to each other. The remainder of the original flash tubes have been redeployed in six new trays each of area slightly less than 2.4m^2 giving a total area of 16.7m^2 which is shielded by 0.53m of new barytes concrete.

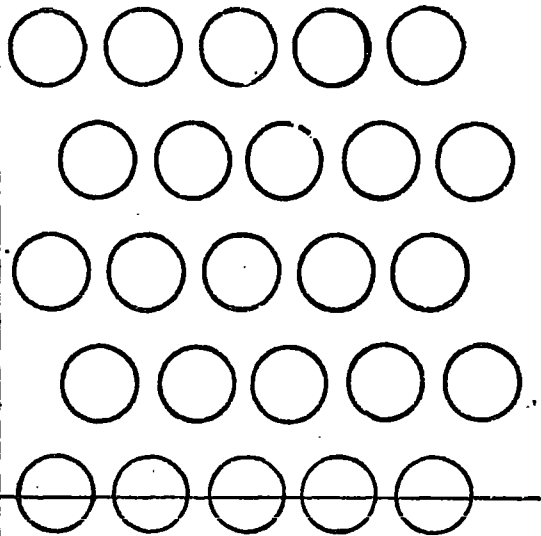
b) Mechanical Details.

To economise on time and labour the two large flash tube trays (approx 2m square) designated A1 and B1 on the Mk.II Spectrograph (described by Machin [1973] and Pickersgill [1973]) were relocated with their tubes perpendicular to each other one above the other beneath the degaussed magnet. The central hole in the magnet plates has been filled with sufficient lead to give the same approximate thickness (500 gmcm^{-2}) and thus energy threshold. The remaining six trays are located underneath two substantial steel 'tables' supporting the Barytes bricks as shown in Figure 4-4.

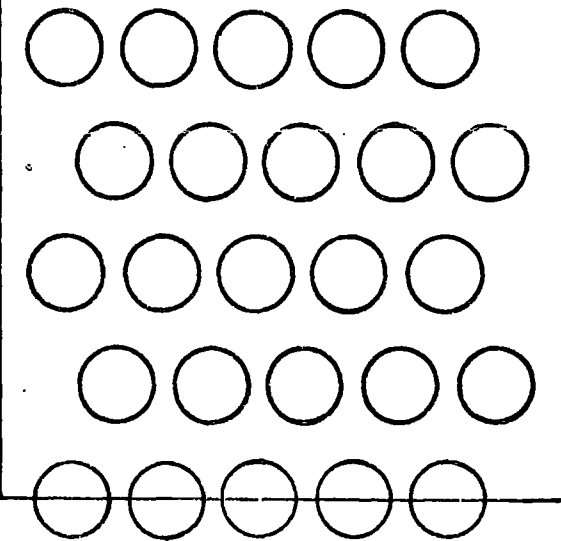
These six trays are of similar basic mechanical design with variations where appropriate to allow for different tube sizes. Each tray is divided into two banks of tubes spaced by an air gap to give the desired angular resolution of particle track delineation. This gap is so adjusted to correspond to an exact number of tubes (7 on trays containing 1.7cm diameter tubes; 13 on 0.7cm tube trays). A flash tube bank consists of five layers of durals with one layer of flash tubes per dural. To prevent inter-tube contamination by photoionisation the large tubes are either painted black or enclosed in polythene sleeves; the small tubes are alternatively painted black and white and the electrodes covered by a non-reflecting black paint.

On studying Figure 4-4 it will be noticed that the 1.7cm diameter tubes are all located at one end of the detector in four trays of two different sizes. The larger two trays are mounted on





$\frac{1}{7}$ or $0\frac{1}{7}$ cm



the floor with the smaller pair of trays located on two steel frames near the edge of the absorber at such a height that the rear trays can be viewed through the legs of the frames. Several constraints dictated the upper trays being smaller, the most important being the number of flash tubes available (approximately 3500) and the necessity to move them to their final positions after loading with flash tubes. The two trays containing 0.7cm tubes are mounted on frames to enable the lower sub-magnet tray to be photographed.

4-4.4 Detector B.

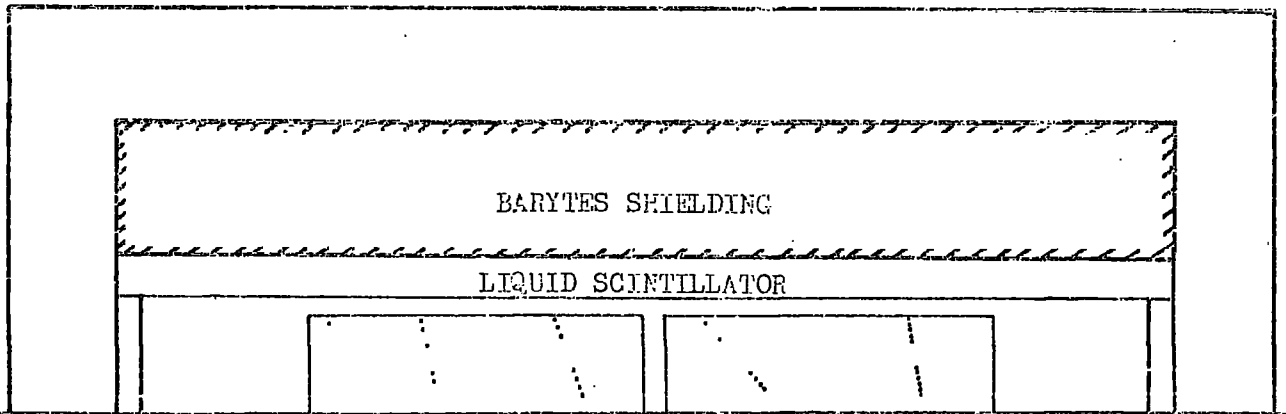
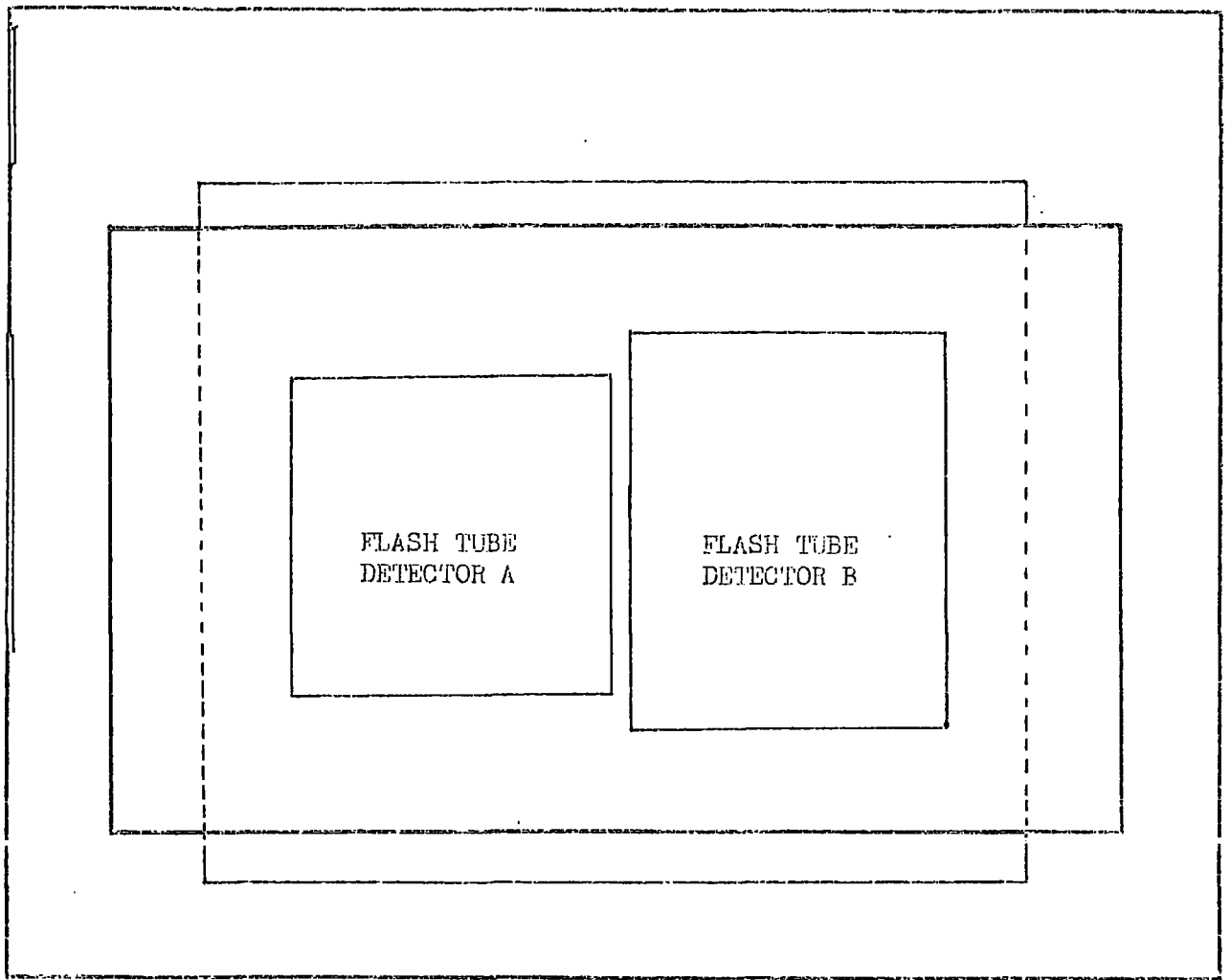
a) General Details.

This detector is located 250m from and 7.86m above the array centre in a South Easterly direction. The instrument is positioned below an array of liquid scintillation counters. The scintillators are covered with 76cm of Barytes concrete absorber with contamination of the detector extremities being reduced by the overhang of the Barytes on all sides.

b) Mechanical Details.

The thickness of the shielding material, the space requirements of the optical recording system, and the limited headroom of the experimental area caused a compromise to be made between keeping the height of the flash tube array as small as possible whilst spacing the flash tubes to enable the desired 0.5° angular resolution to be obtained. With these constraints the following design evolved.

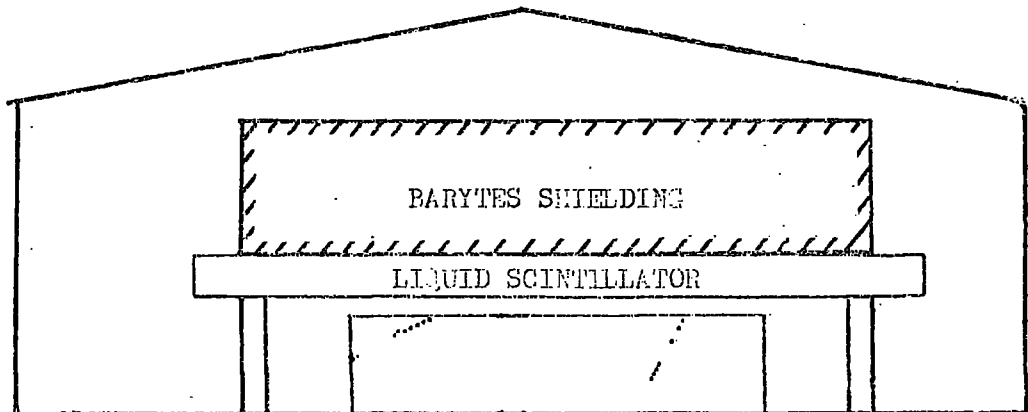
The detector consists of two floor standing trays giving a total sensitive area of 9m^2 involving 6400 black or sleeved 1.7cm flash tubes (the flash tube lengths are either 2.0 or 2.5m). To compensate for the modest area of the detector it was decided to give



DETECTOR A

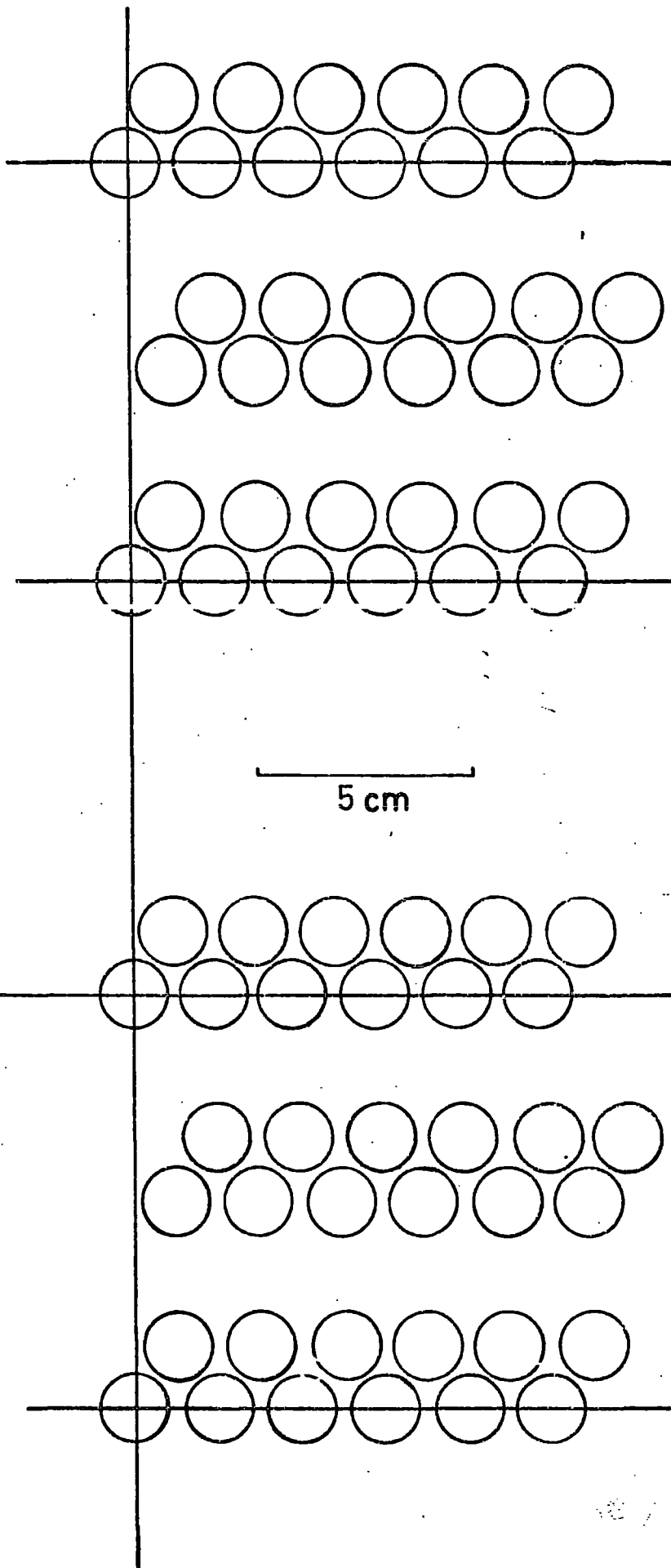
DETECTOR B

1 in



BARYTES SHIELDING

LIQUID SCINTILLATOR



the detector the capability of viewing in two perpendicular planes. Useful measurements may then be made in EAS falling with their cores in a 360° range in azimuth. Each viewing plane has a depth of twelve tubes which are split into two banks of six with a centre separation of 30cm. Three layers of tubes in each bank are mounted on durals as previously described and the other three layers rest on top of these in the gaps between tubes.

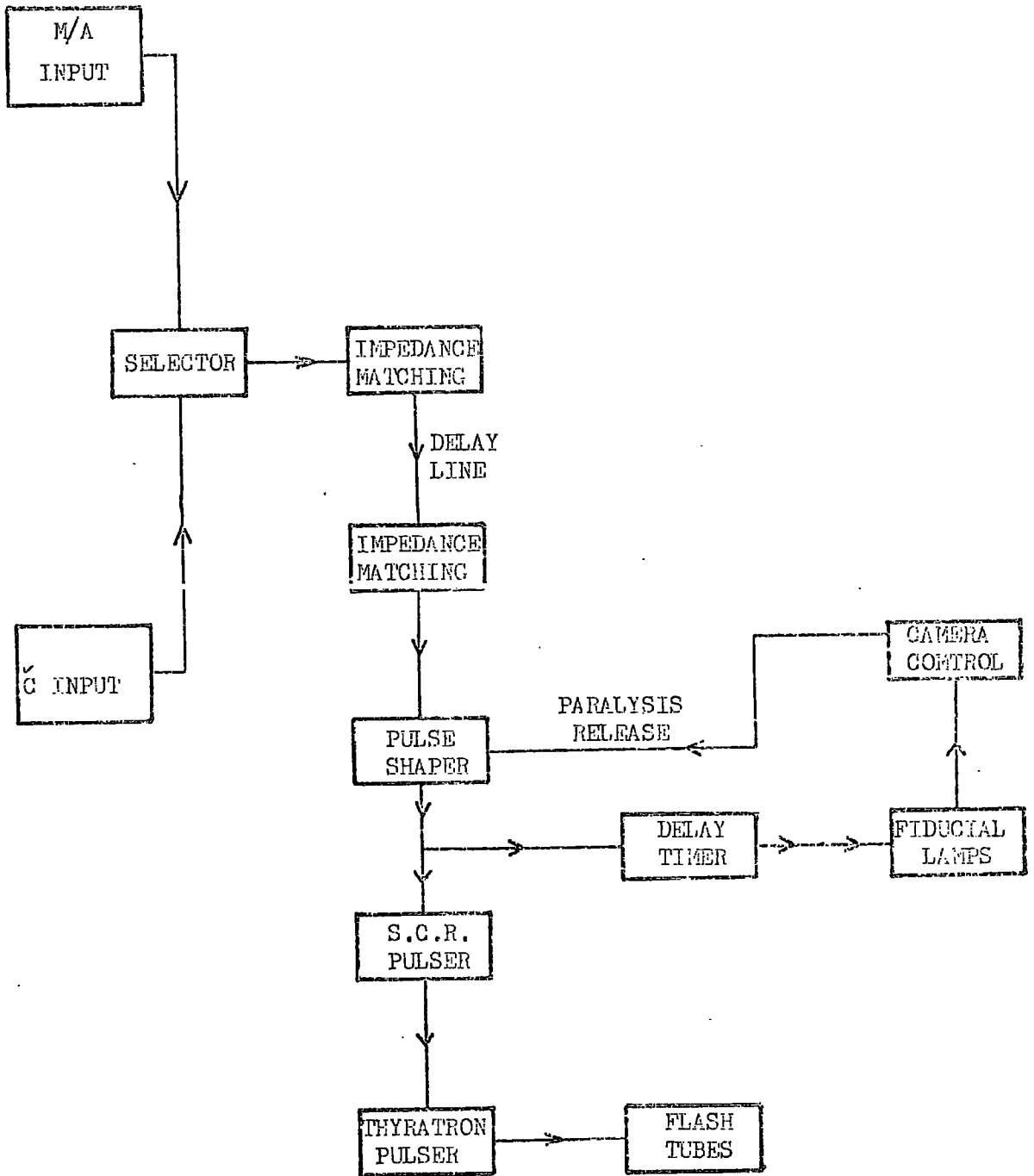
4-5. Electronics and Pulsing System:

a) Low Voltage System.

The instruments are controlled by a simple circuit which is responsible for the correct sequencing of the EHT pulsers, fiducial markers and advancing the cameras. On receipt of a trigger signal from either the particle detecting array or the Air Cerenkov System ($5\mu\text{s}$ and $1.7\mu\text{s}$ respectively after the centre deep water detector responds to the 10 particle threshold) a pause of approximately $12\mu\text{s}$ (obtained by passing a signal down a passive delay line) occurs to allow the other equipment in the vicinity liable to interference to record. A $20\mu\text{s}$ long high voltage pulse is then applied to the flash tube electrodes via the thyratrons. Simultaneously a paralysis state is entered for about 4 seconds to prevent spurious operation of the fiducial markers, camera advance, and multiple pulsing. On termination of the paralysis the fiducial markers flash and the cameras advance, resetting the entire system to await the next event.

b) High Voltage System.

The EHT pulse is switched through thyratrons, a system which, although antiquated, was used with great reliability and effect on both the Mk.I and Mk.II Haverah Park Spectrographs. This slow system



causes the minimum electronic disturbance to other equipment. To prevent spurious triggering from both electronic noise and mechanical shock a system of D.C. biasing evolved in addition to the paralysis system described above. The thyatron grids are maintained at a constant D.C. level of -75 volts and are A.C. coupled to a thyristor circuit which switches some 150 volts on command from the control electronics to fire the valve.

4-6 The Optics and Photographic Recording System.

A photographic recording system has been chosen in accordance with previous experience in EAS measurements at Haverah Park and Durham. Although it is quite possible to digitize the neon flash tube (see e.g. Breare [1973]) the technique involves large scale electronics (with associated pick-up problems), time and expense (particularly in view of the number of tubes involved) and is not proven in handling the multiple track response typical in EAS. Problems may also arise in the subsequent event reconstruction and analysis, especially with the inevitable spurious discharges and crossing particle tracks.

A system of three cameras, each fitted with a 100mm F1.9 lens has been adopted to record all data. One camera is employed with detector B and two with detector A. To bring the tube images to the cameras and to ensure that all tubes fit on a 25mm² frame a path length of approximately 10m is necessary and due to the sizes of the huts a complex system of mirrors is required

Due to the short light pulse from the tubes (20µs) a fast recording film is essential. Unfortunately this also entails a large grain size, thus reducing resolution. This is particularly

important with the small (7mm diameter) tubes since, with the chosen path length, they present an image diameter of 0.09mm and a centre to centre separation of 0.13mm at the focal plane of the camera. Previous experience with the Mk.II Spectrograph has shown that Ilford HP4 film has a resolving power of ≈ 40 lines mm^{-1} approximately $\frac{1}{4}$ the size of a small tube at the path lengths used (Machin [1973]). Care when processing the film should result in acceptable data from the present system.

To identify each event a six digit number is projected on to each frame after the tubes have flashed. This number is advanced every 30 seconds by a master clock and is used to relate measurements to data for the other experiments.

4-7 Extraction of Data for Analysis.

A straight-forward and reliable system of data retrieval was developed for the Magnet Spectrograph film records. Similar techniques are to be employed with the new instruments.

The developed film negatives are first scanned by eye and the index numbers of those events showing particle tracks noted. These events are selected for analysis and the shower analysis from either the deep water detectors or the Air Cerenkov array noted. Core distance, primary energy estimate and shower directions are recorded for those showers possessing a full and reliable analysis.

The chosen muon detector records are printed on to a large format whose size corresponds exactly to a transparent overlay showing all the tube positions. This overlay is prepared from photographs taken on fine grain film exposed via the recording cameras under carefully controlled lighting conditions. Spuriously flashing tubes

are noted to avoid confusion. Using the overlay, the identity of flashed tubes may be established and the tube coordinates recovered for analysis.

Machin (1973) developed a program to analyze the particle tracks in the Mk.II spectrograph. A development of this is to be used with the new experiment. The program relies on finding the maximum path length within the flashed tubes and the modus operandi is briefly described below.

a) The top and bottom flashed tubes in a potential track are used to define a line.

b) Any non-flashed tubes traversed by this line are located and the coordinates of the nearest gap found.

c) A least squares fit is then made to all flashed tubes or gaps.

d) The line thus found is then rotated and shifted laterally through small increments over a limited range and the resulting path length calculated. The trial giving maximum path length is then deemed to be best.

e) A path is then ascribed a form of $y = x \tan \theta + c$ and the muon's projected zenith angle determined.

f) The projected zenith angle thus determined is normalised to give the muon angle with respect to the shower core direction.

The analysis procedure outlined above is repeated for all the particles recorded in the instrument and the information on each muon stored for further study.

Chapter Five.

Recent Computer Simulations and an Outline of Likely Running Conditions for the New Experiment.

5-1 Introduction.

During the construction of the new instruments work was recommenced to extend the computer simulations described in Chapter Three. A different model for the nucleon cascade was investigated, the new simulations used Feynman Scaling in place of the C.K.P. momentum distribution to describe the production of secondary pions which, in turn decay to muons. Similar techniques to those described in Chapter Three were used to calculate the muon component's spatial and temporal properties. Preliminary results of the new simulations are presented in this chapter and their relevance to the new experiment is discussed.

In recent months the likely operational conditions for the new experiment have become clear and are described together with possible methods to further update the simulations, both to resemble more closely the experimental arrangements and to investigate different models for the nucleon cascade of Extensive Air Showers.

5-2 The Recent Simulations.

Using the simulation routine described in section 3-2 further calculations were made to investigate the spatial and temporal characteristics of muons in Extensive Air Showers initiated by primary particles (both protons and iron nuclei) of energy 10^{18} eV. As before the effects of Coulomb and Geomagnetic scattering were included in the simulations. To assist with other parallel studies

(and economise on computer time) a few temporary changes were made to the areas and locations of the hypothetical detectors employed in the simulations. The most significant being a relocation of the inner detectors at different core distances (90, 158, 280, 500m) and a change of assumed detector area to 30m^2 in each case.

The recent simulations are based upon scaling for the pion momentum distribution (in place of the earlier C. K. P. distribution) and uses the data of Bøggild et al (1971) employing a scaling function of the form:-

$$F(x, P_t) \propto \frac{\exp(-\frac{|x|}{0.2}) \exp(-\frac{P_t}{0.205}) P_t^{1.47}}{1 + \exp(\frac{|x| - 0.62}{0.065})} \quad (1)$$

The interaction of the primary and secondary particles is based upon the proton - air mean free paths reflecting the increase in proton - proton mean free paths observed in accelerator data. This was extended to EAS energies following a suggestion of Formanek and Franek (1975) to give a plausible expression for the proton - air inelastic cross-section with the form:-

$$\sigma_{in}(p\text{-air}) = 226.9 + 14.9 \log_{10} E + 1.997 (\log_{10} E)^2 \text{ mb} \quad (2)$$

A consequence of this expression is a reduction in the mean free path of proton - air collisions by some 30% to a value of approximately 58gcm^{-2} at energies of 10^{17}eV .

Heavy primaries ($A = 56$) were treated as described in Dixon Waddington and Turver (1974) except that the proportion of nucleons interacting in the fragmenting of a heavy nucleus is now based upon

data of Tomazewski and Wdowczyk (1975).

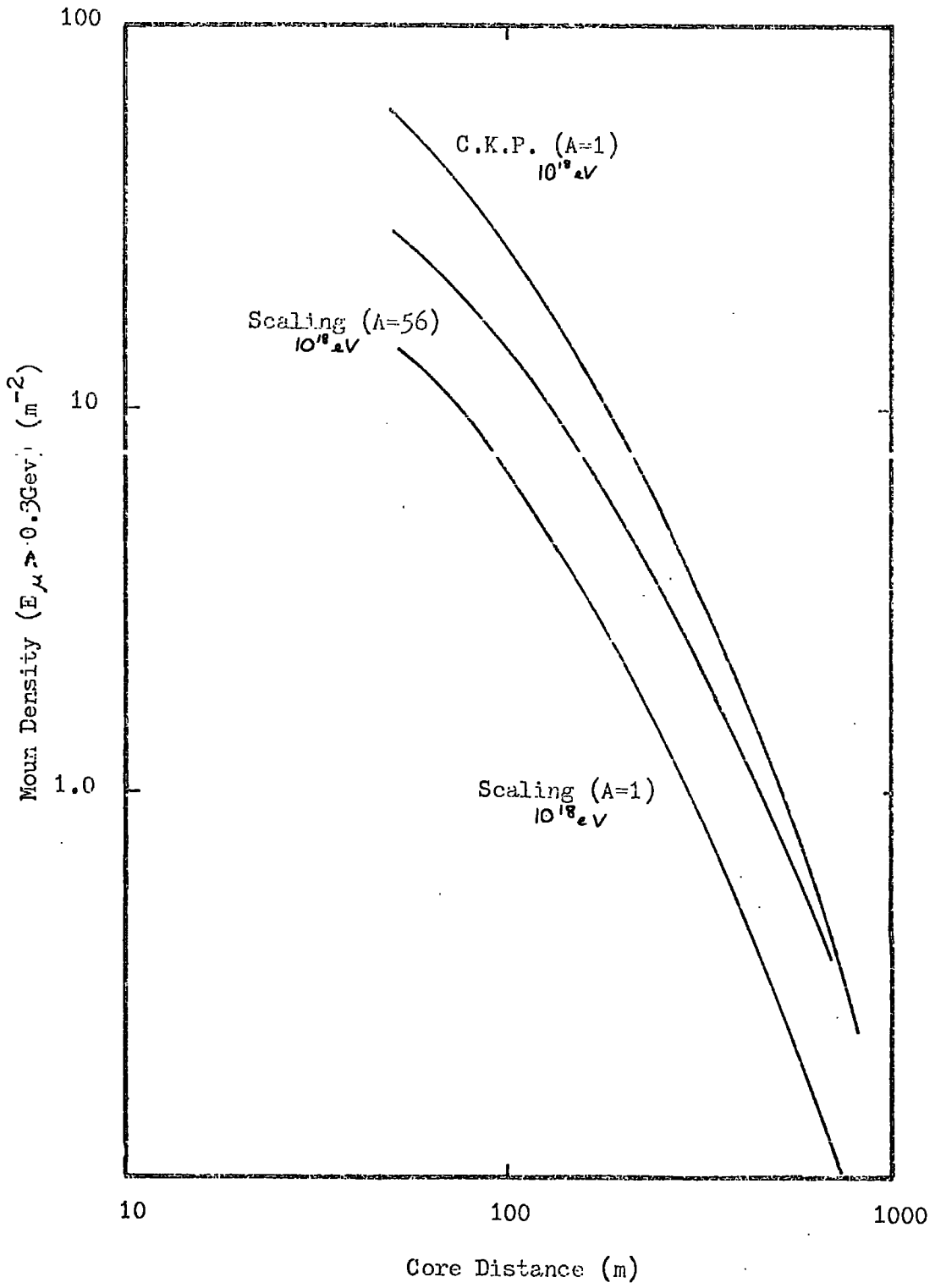
The results of these preliminary simulations have shown several interesting differences to the earlier work. One of the most striking is the reduction in the numbers of muons produced (see figure 5-1). The lateral distribution of scaling muons is reduced by a factor of approximately 3 in comparison with that generated from the pionization simulations. Assumption of a heavy primary ($A = 56$) causes an increase in the muon numbers towards the values predicted by proton initiated pionization model simulations. More detailed results of the simulations are presented in the following sections.

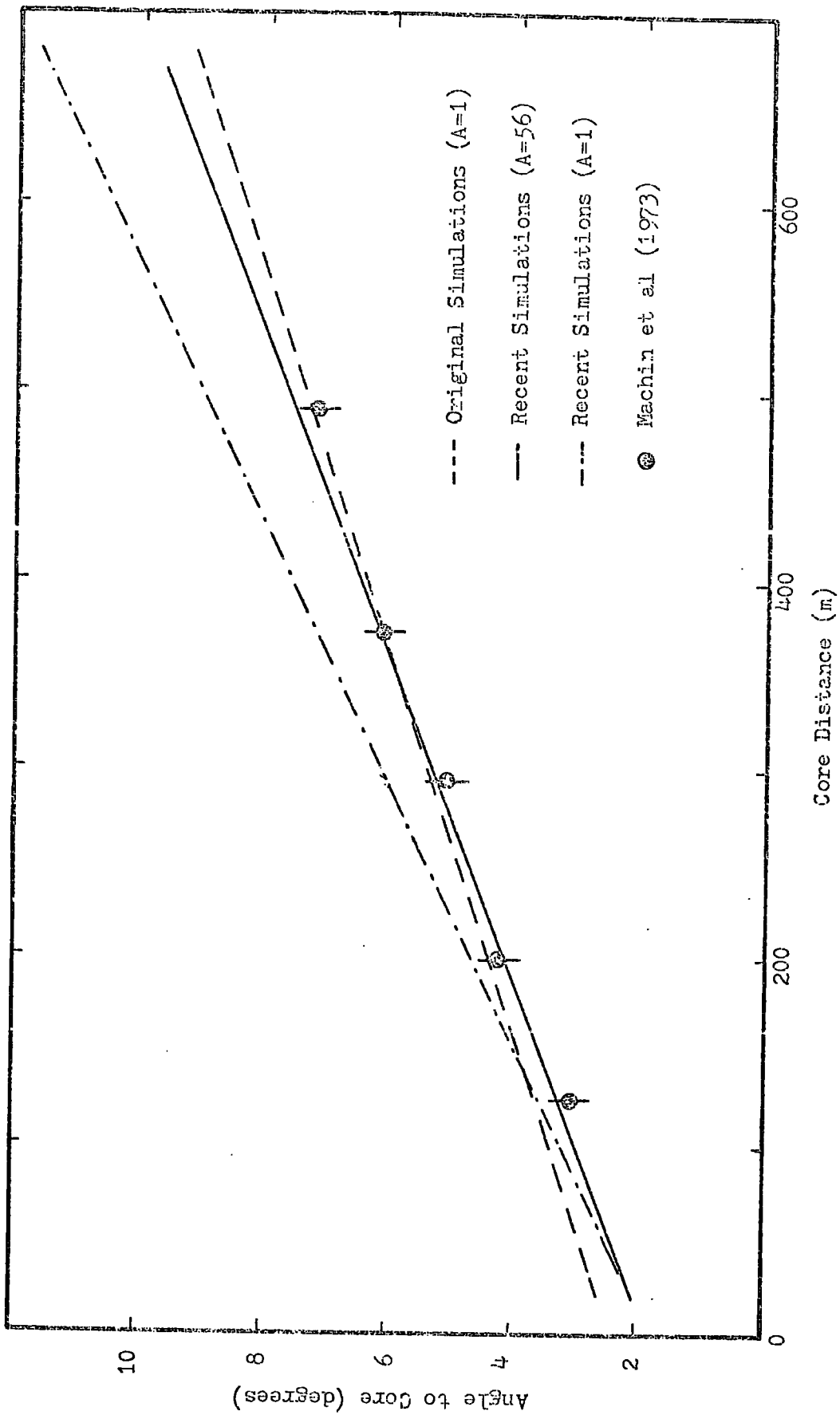
5-3 The Spatial Characteristics of Muons in EAS as Indicated by the New Simulations.

For direct comparison with the new experiment all simulation results presented here are those predicted to be observed beneath the equivalent of 15cm of lead shielding.

Figure 5-2 shows that the predicted dependence of angle to core on core distance for average proton (both scaling and C.K.P. showers) and iron nuclei induced showers; also shown are the unpublished experimental points of Machin et al (1973). It can be seen that good agreement with the experimental data exists for the original proton simulations and the new iron nuclei induced showers. The recent simulations of proton induced showers show some divergence from the other simulation results and the experimental data, particularly at the larger core distances.

The sensitivity of the new simulation results to the depth of maximum (and hence the mass of the primary particle) was investigated at various core distances for both proton and iron nucleus induced



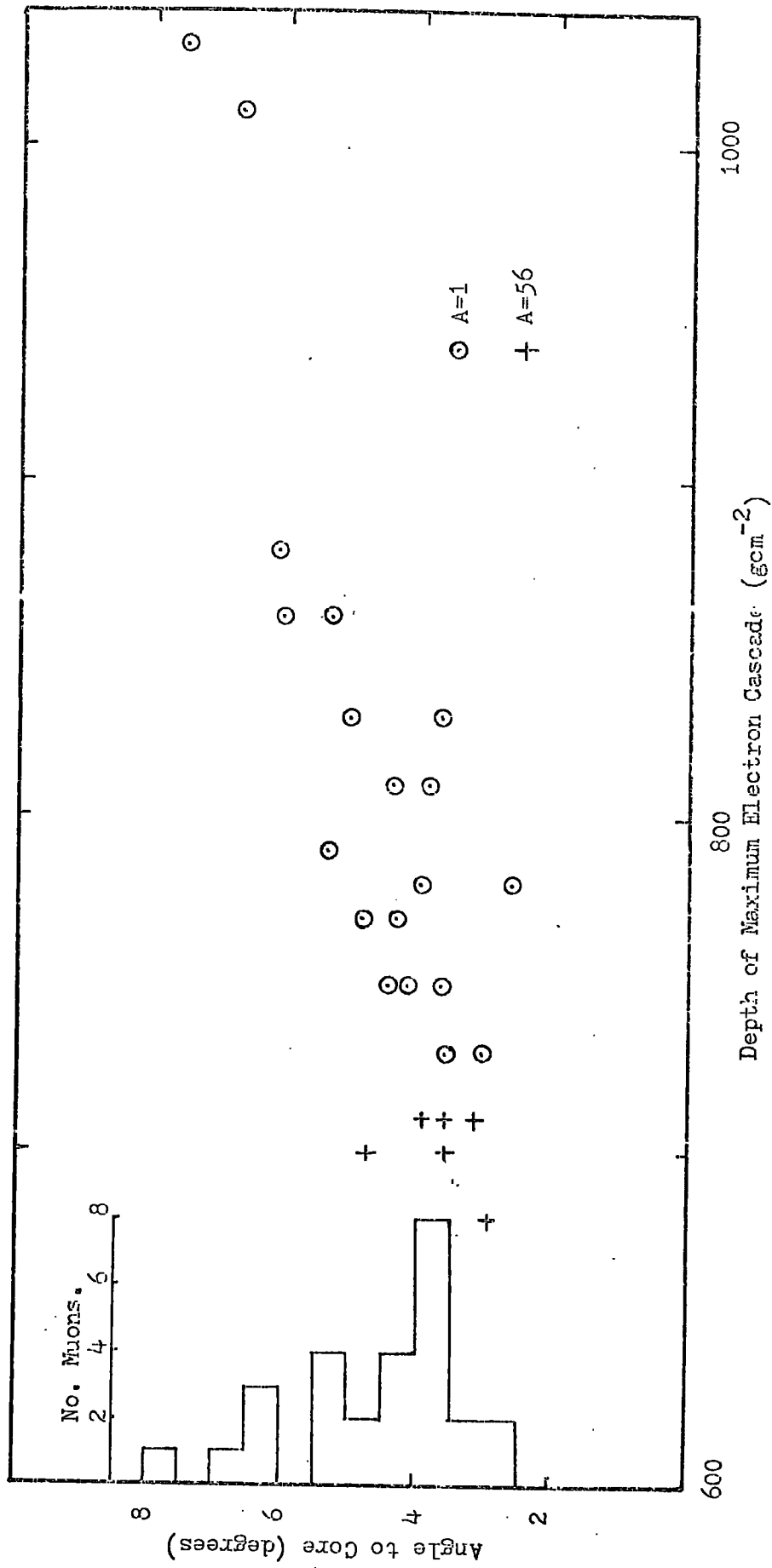


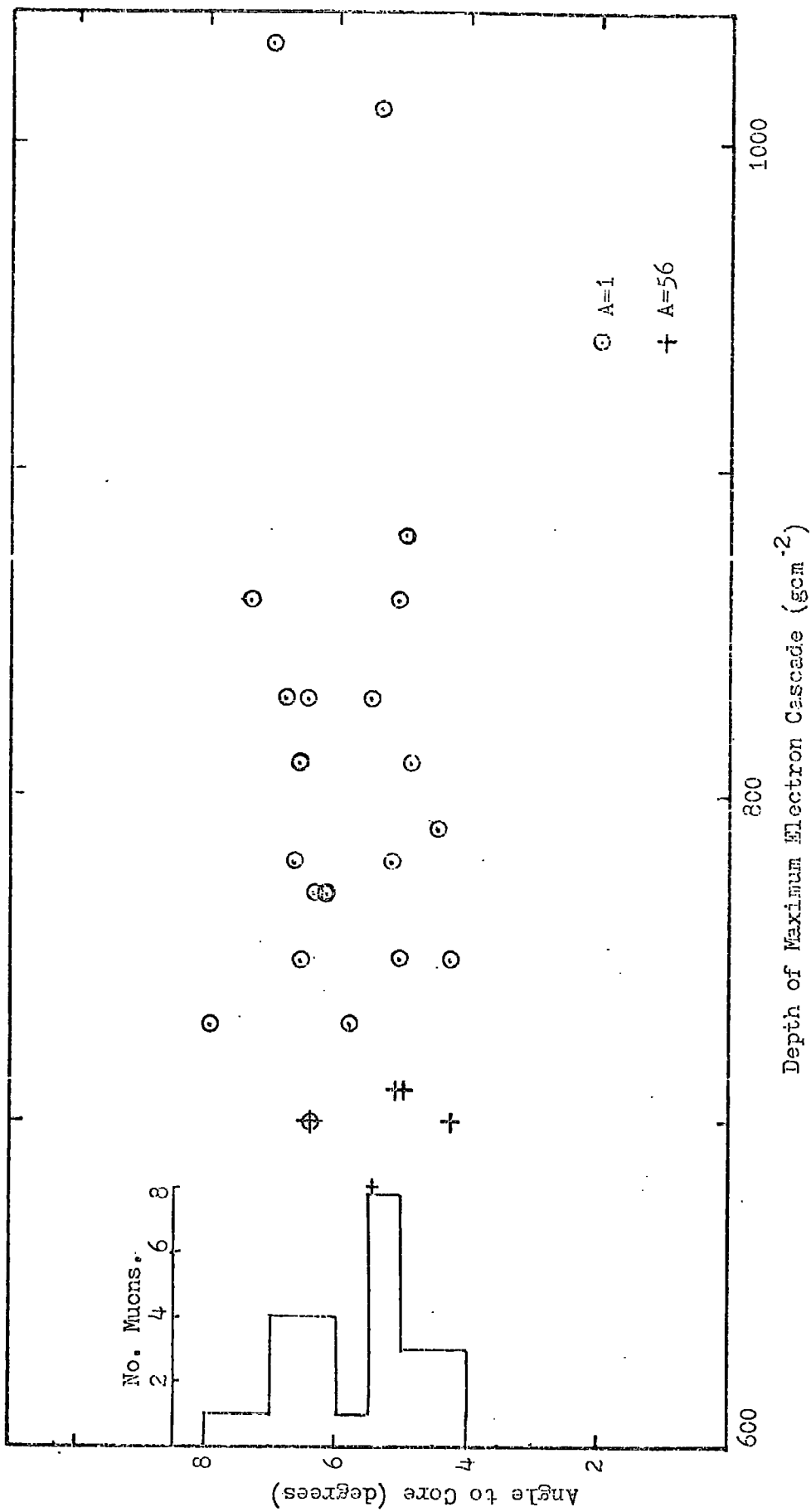
showers (see Figures 5-3, 5-4, and 5-5). At the smaller core distances (<400m) some correlation between the mean angle of the muons and the depth of cascade maximum is evident. The earlier developing cascades due to iron primaries agree with the trends established by early developing proton showers but their small angles to the core and their similarity to the proton showers could make experimental identification difficult without a large number of carefully measured and analysed events. With core distances in excess of 400m the correlation between the core/muon angle and the depth of cascade maximum fades (see Figure 5-5) and the wide angular spread would make experimental identification of the primary mass difficult. The standard deviation of the muon angles measured in the hypothetical detectors was also investigated and the results (at the same core distances as the 'pure' angle data) are shown in Figure 5-6. Again there is less sensitivity to depth of maximum than was suggested by the earlier calculation results.

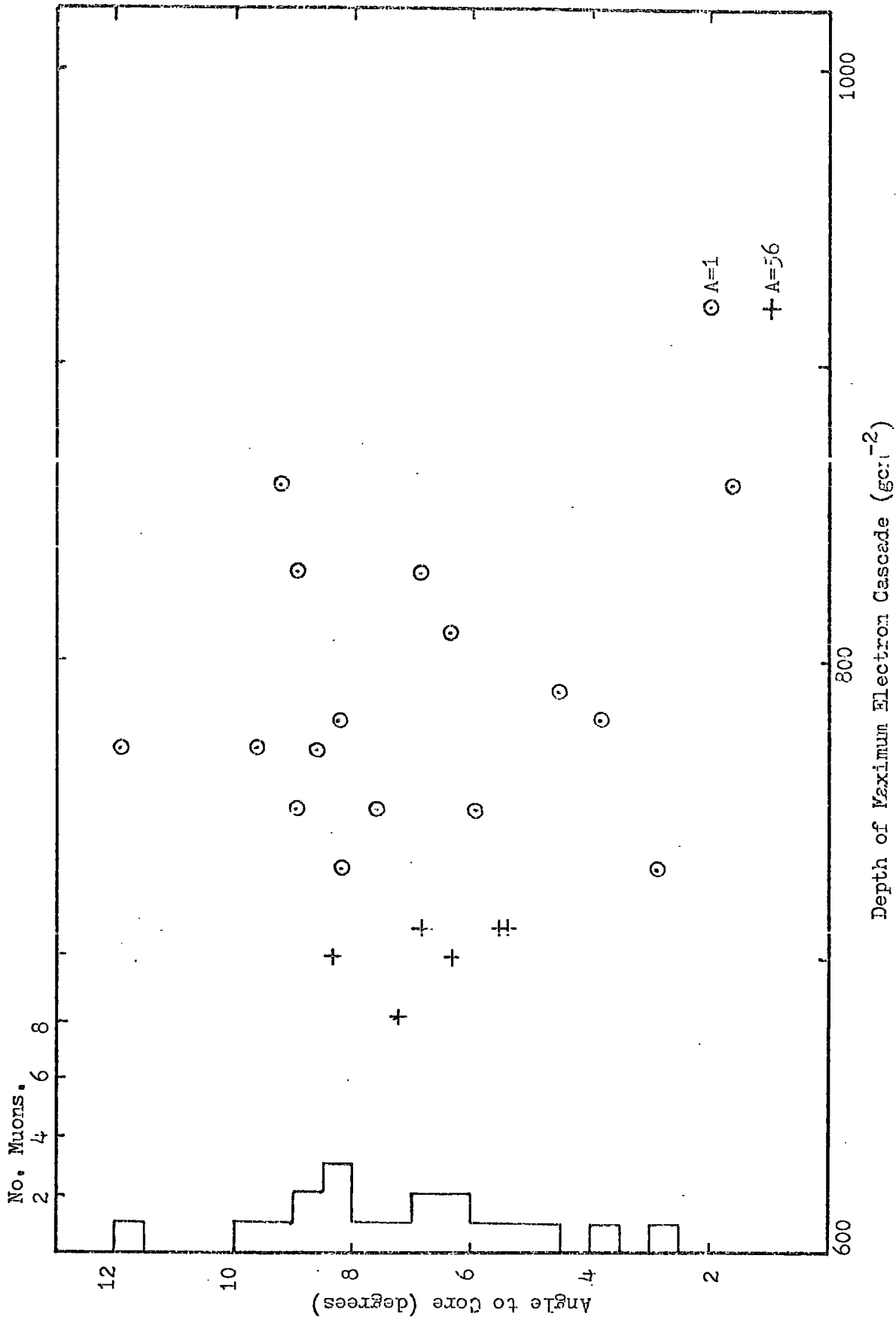
To conclude, the preliminary investigations into the muon spatial properties have shown a reduction in particle numbers and some decrease in sensitivity to primary mass (particularly at larger core distances) for proton showers in comparison to previous simulations and the sparse experimental data available. The simulations of heavy nuclear induced showers appear more promising and there is some agreement with available experimental data for average spatial characteristics.

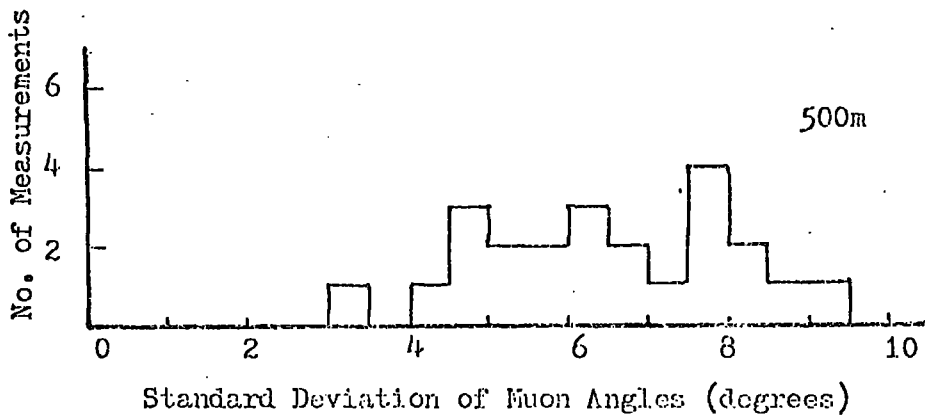
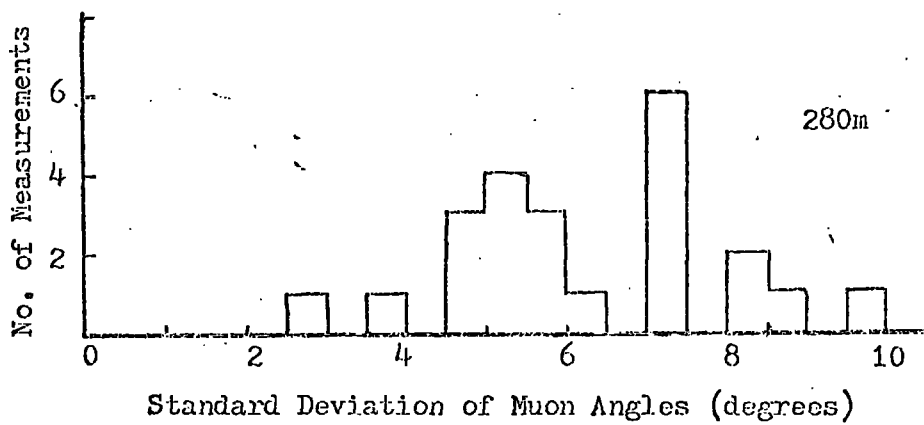
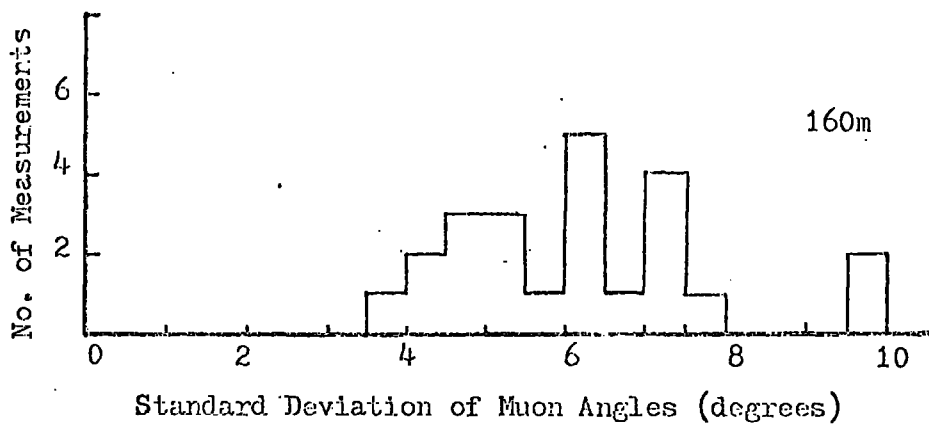
5-4 The Temporal Effects According to the New Simulations.

The temporal properties of muons in EAS are of considerable interest owing to the close proximity of the scintillation detectors









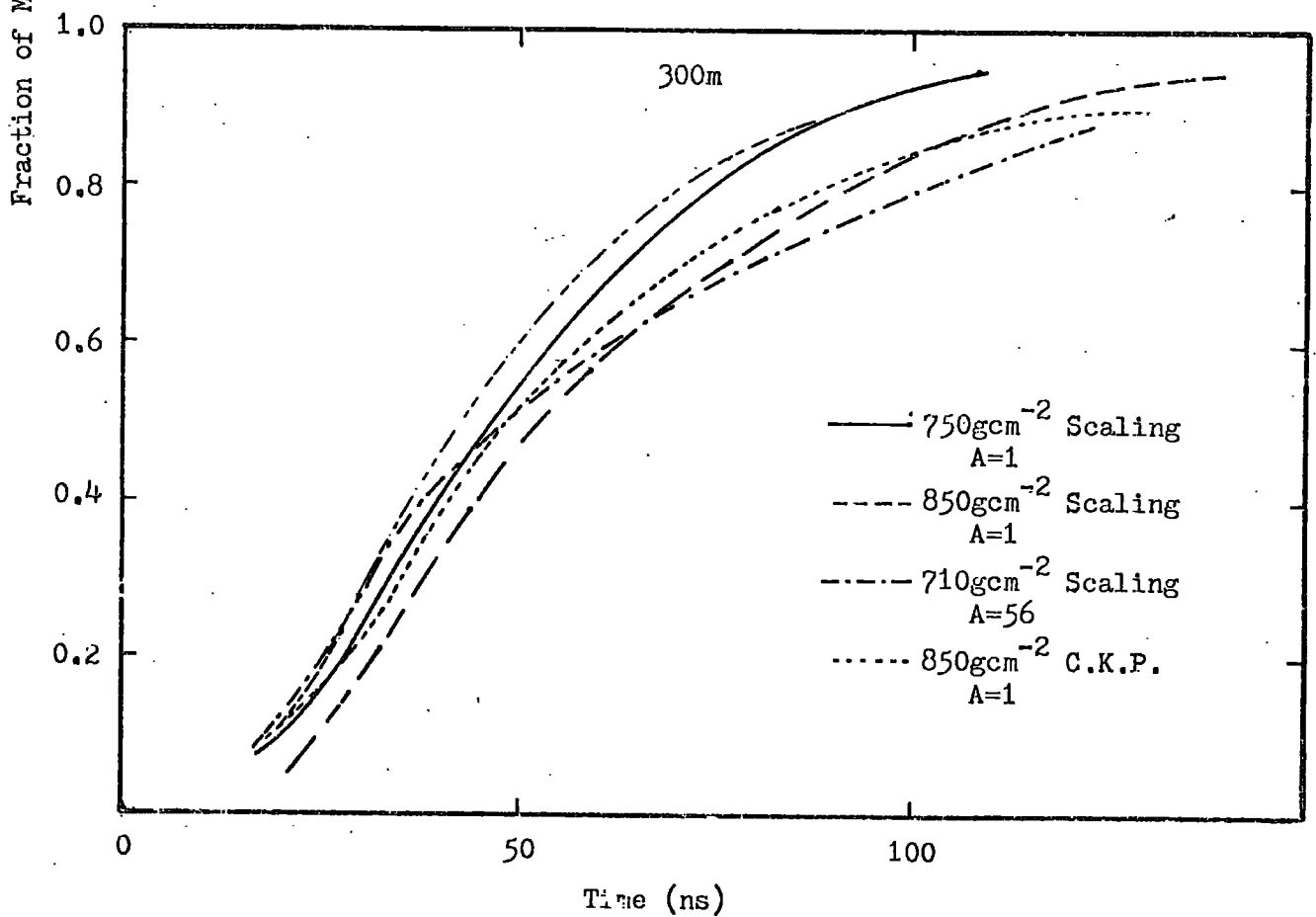
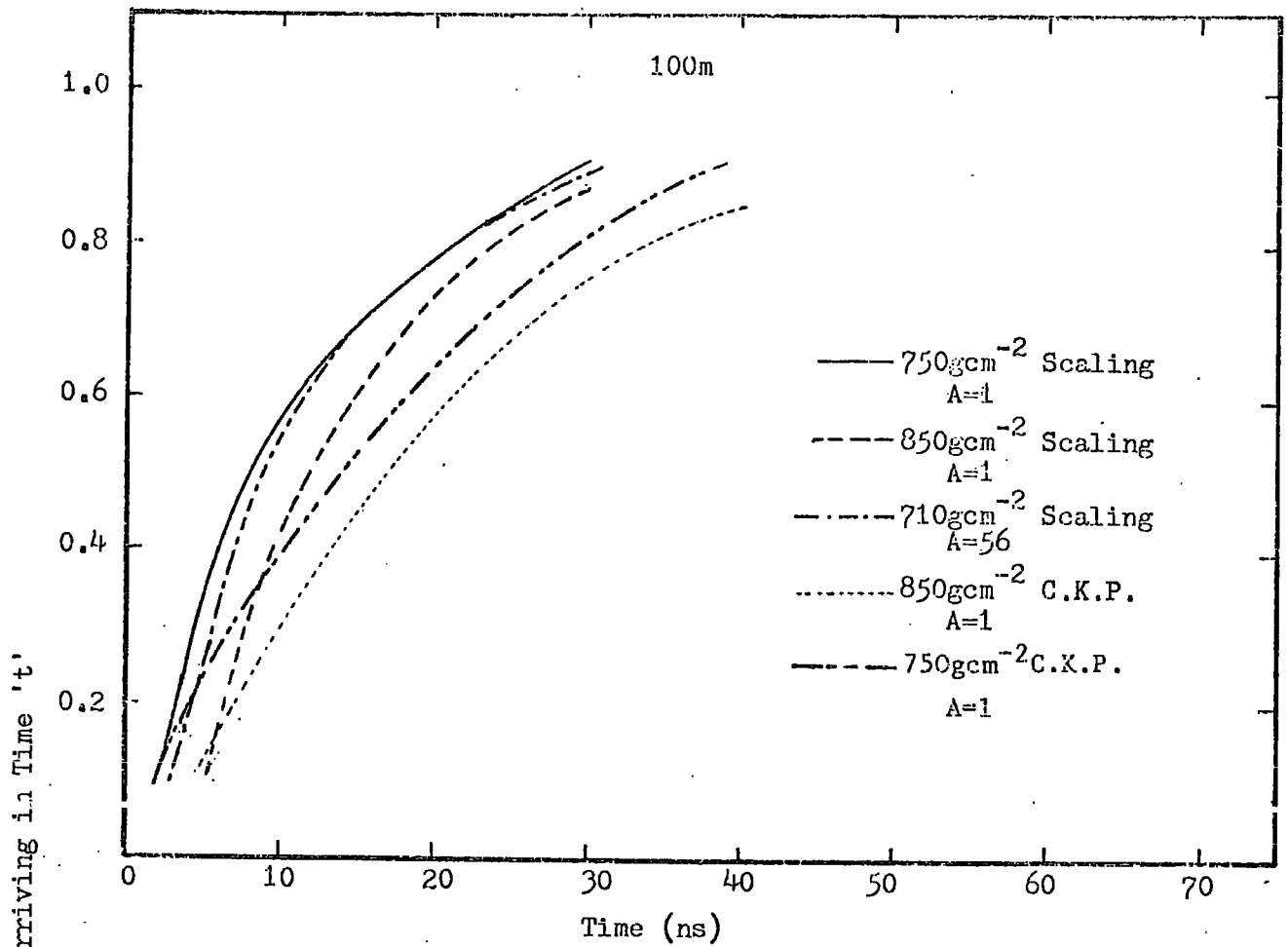
operated by the University of Nottingham to the spatial angle detector B. Temporal details have thus been included in the recent simulations and will also be included in the final revised form of the program (to be described later).

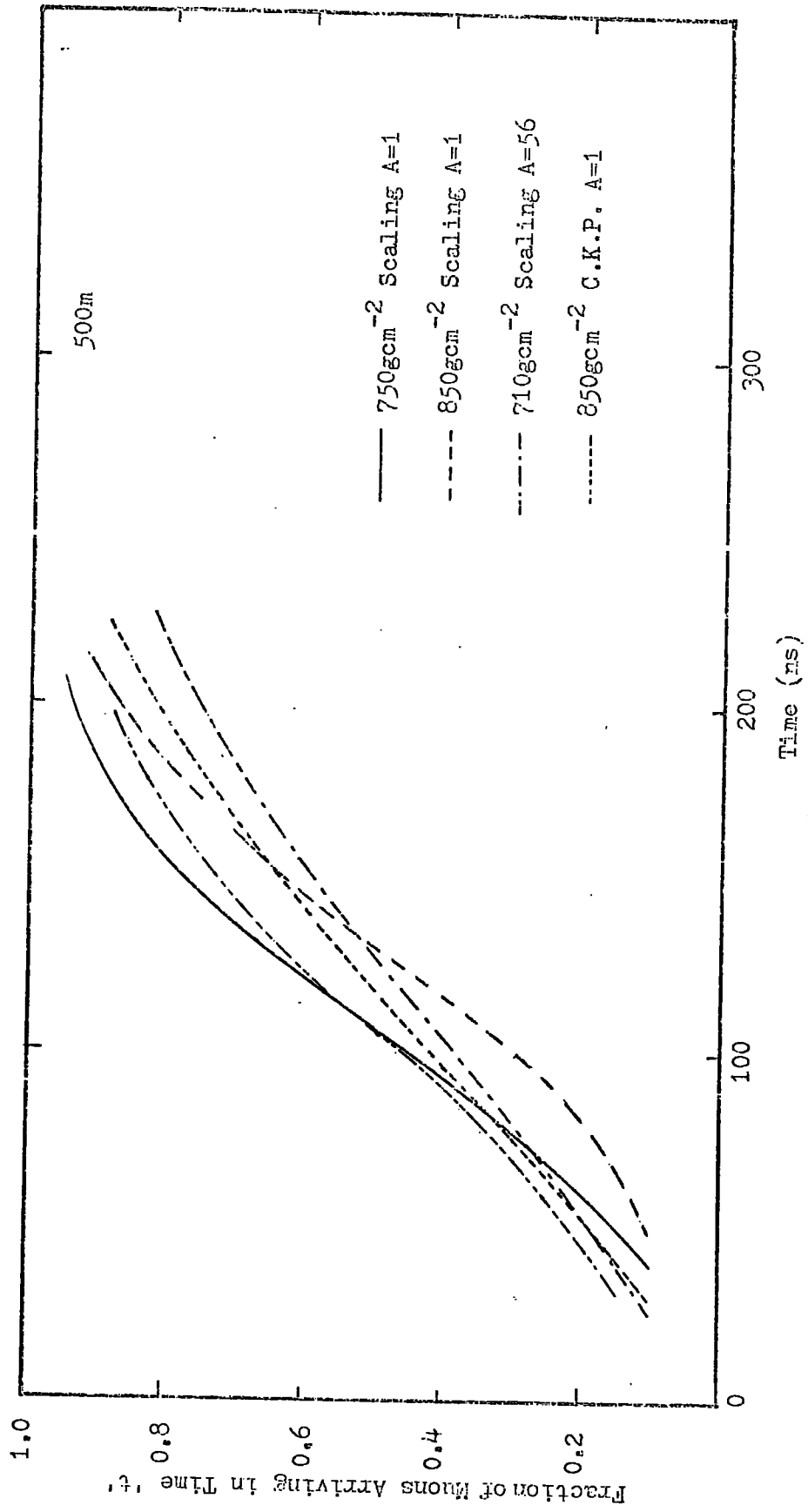
Predicted pulse profiles expected for ideal detectors at various core distances were investigated for proton and heavy particle induced showers and are shown in Figures 5-7 and 5-8. Also shown are profiles from C.K.P. proton initiated showers. In the regions close to the core substantial differences in the signal rise times exist between the scaling and pionization simulations, but with core distances in excess of 300m the differences between the models and ordinary particles become smaller.

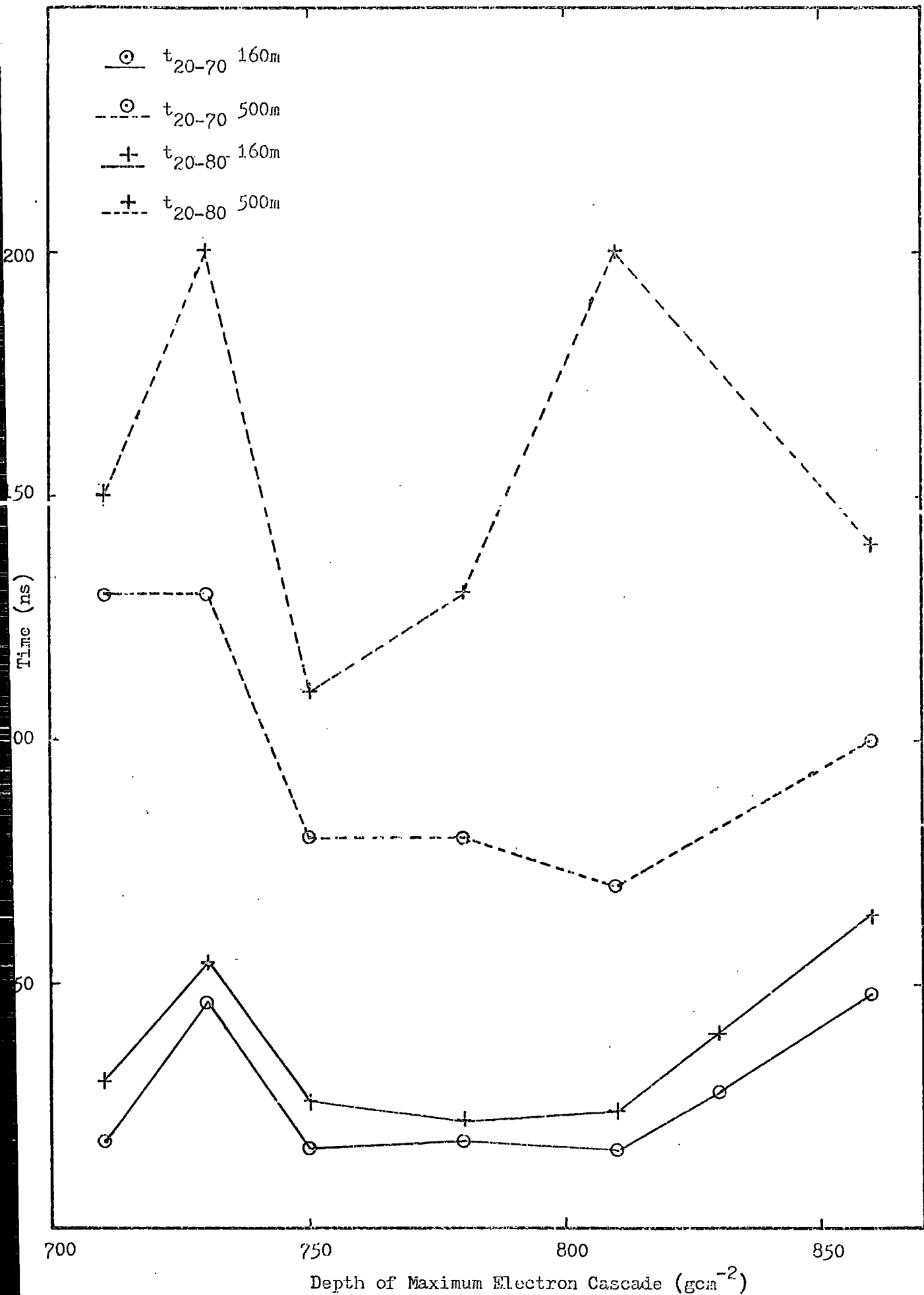
Other aspects of the temporal characteristics were investigated to seek out other measurable parameters of the temporal characteristics which relate more directly to the depth of maximum electron cascade. Figure 5-9 shows the relationship of t_{20-70} and t_{20-80} to the depth of cascade maximum. At small core distances it is possible to identify the later developing showers but saturation effects tend to dominate the earlier events masking the heavier nuclei. Further from the core ($> 500m$) fluctuations start to appear (arising mainly from the small samples of particles). It should be noted that the showers selected for this illustration were chosen solely for their depth of maxima and are thus liable to sampling fluctuations.

5-5 Implications of the Recent Simulations for the New Experiment.

The preliminary results from the new simulations have shown several interesting differences from the earlier simulation work.







Proton induced showers show an appreciable divergence from the pionization models, both in lateral distribution and in their relationships to the depth of maximum cascade development. These new predictions for proton primaries also show differences from the sparse experimental data available. Showers induced by heavy particles show closer agreement with experimental data, particularly the unpublished angular results obtained by Machin et al. (The predictions of the pionization models for proton initiated showers has similar success in explaining these data). Further work (both simulation and experimental) may indicate that a pionization model offers the best description of proton showers and a scaling form for showers induced by heavy nuclei. If this were to be the case several potentially awkward consequences could arise in the present work which have arisen in earlier experiments.

The new experiment was designed on the basis of the pionization simulations of proton showers to measure three parameters viz:- the lateral distribution of muons, the mean angles of the muons to the core direction and the spread of these angles, each of these measurements to be made at two separate locations. The accuracy of measurement of the shower parameters by the main array dictated an angular resolution of $<0.5^\circ$ for all measurements of angles.

The changes in the lateral distribution of muons predicted by the new simulations would reduce the numbers of particles recorded by the detectors particularly those generated by 'scaling protons'. Heavy nucleus initiated showers resemble the pionization results and thus should be more easily measured in both detectors simultaneously. The reduced area of detector B may well preclude the observation of useful numbers of particles from 'scaling proton' showers landing in

the northern regions of the array whereas both pionization showers and scaling heavy nuclei initiated showers produce sufficient particles to enable full studies to be made.

The consequences for angular measurements of the recent simulations pose less of a problem as the smallest muon core angle predicted is of the order of two degrees. Difficulties in distinguishing between proton and heavier nuclei initiated showers may however arise due to the close similarity between the muon component's spatial properties in the different cascade models. To resolve between the showers initiated by different primary particles it may prove necessary to explore means of optimising the angular resolution of the new experiment. It would also be necessary to obtain a corresponding improvement in shower parameters (core location and shower arrival direction). In this context it is fortunate that the Night Sky Optical Čerenkov Array will be operational for periods during the running of the experiment. Combining the accurate arrival direction from the night sky Čerenkov data with the particle detector array analyses would probably yield the necessary improvement. Similar precautions may have to be used in the investigation of the spread in muon angles in each detector.

5-6 An Outline of Likely Running Conditions for the New
Experiment.

Both of the new detectors will be fully operational by the onset of winter 1976/77. Initially, to test the operation of the system and its effects (if any) on the surrounding equipment the detectors will be triggered solely on the 500m coincidence signal from the particle detecting array.



During the initial 'running in' stage the data recording, extraction and analysis techniques will be developed with a view to making operation of the system an easy routine, thus minimising human and other error sources. Simultaneously, the resolution limits of the system will be explored and the maximum effective core distances and zenith angle at which showers may usefully be recorded will be determined. Once the operational procedures have been determined it should be possible to accelerate the extraction and analysis of data considerably and it is therefore important to use only those showers which are known to be capable of a full and accurate analysis in the early running periods of the experiment.

As soon as the entire system is operating correctly the triggering requirements will be changed to include the trigger employed by the Night Sky Cerenkov Array which will be available on clear moonless nights throughout the winter months. A full description of the array and its capabilities is given by Wellby (1976) and only a brief description of the data available from it will be given here.

For large events ($> 10^{18}$ eV) the array records about 7 detector responses and much data is available on the shower. Used in conjunction with the particle detecting array improved accuracy in shower parameters is possible (core location to a few meters and shower direction to a fraction of a degree). Due to the limited running hours of the optical array (restricted by the moon and bad weather) and the relative scarcity of high energy events only a few useful events are likely in this mode but the precision to which they could be observed would compensate for their scarcity.

The optical array also records a large number ($\approx 15 \text{ hour}^{-1}$) of small 4 fold (the four inner detectors only [see Figure 4-1])

coincidences. These are due to showers created by primary particles of about 3×10^{16} eV and the showers are about 10 times smaller than those usually observed by the particle array. They usually land with their cores within 70m of the array centre and are, in general, within $30 - 35^\circ$ of the zenith. At present these showers are not capable of an accurate and full analysis of the type described above, but, in the forthcoming winter it is intended to install large area flux collectors at the 500m stations in the hope of detecting signals from these small showers and to render a full and accurate analysis possible. Due to the small size of the showers it may only be possible to make useful measurements with muon detector A. The proximity to the shower core could lead to saturation in the majority of the lightly shielded regions of the detector with high energy electrons. In this case it may prove necessary to record only on the two crossed flash tube trays beneath the old spectrograph magnet (threshold 1GeV).

5-7 Future Work and Prospects.

Several areas of related future work are clear, perhaps the most important being the modification of the simulation routines to resemble the experimental facilities (and hence assist in the analysis of data). For each future shower simulation two detectors resembling the experimental arrangements as closely as possible should be considered at appropriate relative positions. The routine should take into account the area, alignment, resolution and efficiency of the detectors and all the modes of analysis described in section 3-3 should be investigated. The muon timing information should be retained and a representation of the non ideal detector response incorporated. The temporal details should be fully integrated with the spatial

results to ensure the optimum analysis of the results from detector B. The simulations as a whole should be expanded to take a fuller account of various representations of the nuclear interactions occurring in the cascade. The muon propagation program as it stands is expensive on computer time (a typical 'run' at 10^{18} eV takes in the order of 600 seconds of processor time on an I.B.M. 370/168) and ways must be investigated of speeding up it's operation thus enabling more simulations to be made. Should it prove possible to make useful observations of muons in showers initiated by 10^{18} eV primaries the simulations should be extended to lower energies.

On the experimental side, as well as investigating the muon spatial properties in large numbers of showers which are of importance in the choice of model, individual showers will be thoroughly studied using all the facilities available at Haverah Park to identify and measure fluctuations and hence investigate the nature of the primary particles in the energy range from 10^{16} - 10^{18} eV.

With the wide ranging experimental facilities now becoming available at Haverah Park backed by rigorous and thorough simulations, the future for the determination of the primary particle atomic mass number would appear to be both very promising and exciting, although the difficulty of the task must not be underestimated.

References.

Note; The abbreviation PICCR represents The Proceedings of the International Conference on Cosmic Rays.

- Andrews D. (1970) Ph.D. Thesis University of Leeds.
- Armitage M.L., Blake P.R. & Nash W.F. (1973) PICCR Denver 4 2545-50.
- Barsanti G. et al (1956) Proc. of the CERN Symposium 2 56-60.
- Baxter A.J. (1967) Ph.D. Thesis University of Leeds.
- Bergeson et al (1975) PICCR Munich. 8 3059-64.
- de Beer J.F. (1960) Ph.D. Thesis University of Potchefstroom.
- de Beer J.F., Crawshaw T.E. & Parkham A.G. (1962) Phil. Mag. 7 499-514.
- de Beer L.F., Holyoak B., Wdowczyk J. & Wolfendale A.W. (1966) Proc. Phys. Soc. 89 567-585.
- de Beer J.F., de Villiers E.J., Reincke J.P.L. & Venter F.A. (1970) Acta. Phys. Hung. 29 657-660.
- Bennett S. & Greisen K. (1961) Phys. Rev. 124 1982-1987.
- Bøggild H. et al (1971) Nuc. Phys. B27.1.
- Breare J.M. (1974) Cosmic Rays at Ground Level Inst. Phys.
- Bull R.M., Coates D.W., Nash W.F. & Rastin B.C. (1962) del Nuovo Cimento Vol. 23 39-51
- Clark G., Earl J., Kraushaur W., Linsley J., Rossi B. & Sherb F. (1958) Supp. Nuovo Cimento 3 628-652.
- Cocconi G., Koester L.J. & Perkins D.H. (1961) Lawrence Radiation Lab. High Energy Physics Study Seminars 28 (2) UCID-1444, 1.
- Conversi M., Gianolli G. & Spillantini P. (1972) Nuovo Cimento Lett. 6 339-40.
- Conversi M. & Gozzini A. (1955) Nuovo Cimento 2 189-91.

- Dixon H.E. (1974) Ph.D. Thesis University of Durham.
- Dixon H.E. et al (1974a) Proc. Roy. Soc. 339 133 - 55.
- Dixon H.E. & Turver K.E. (1974) Proc. Roy. Soc. 339 171 - 95.
- Dixon H.E., Turver K.E. & Waddington G.J. (1974b) Proc. Roy. Soc. 339 157-70
- Earnshaw J.C. (1968) Ph.D. Thesis University of Durham.
- Earnshaw J.C., Machin A.C., Pickersgill D.R. & Turver K.E. (1973)
J. Phys. A. 6 1244-1261.
- Earnshaw J.C., Maslin G.C. & Turver K.E. (1968) Can. J. Phys 46 5115-118.
- Earnshaw J.C., Orford K.J., Rochester G.D., Samogi A.J. & Turver K.E.
(1967) Proc. Phys. Soc. 90 91-108.
- Formanek & Franek (1975) Rutherford Lab. Preprint RL -74-156.T101.
- Greisen K (1966a) PICCR London. 2 609.
- Greisen K. (1966b) Phys. Rev. Lett. 16 748-50.
- Hess V.F. (1912) Physics 2 13 1084.
- Hillas A.M. (1966) PICCR London. 2 758 - 61
- Hillas A.M. Hollows J.D., Hunter H.W. & Marsden D.J. (1970) Acta.
Phys. Hung. 29 533-538.
- Hillas A.M., Hollows J.D., Hunter H.W. & Marsden D.J. (1971) PICCR Hobart. 103
- Hollows J.F. (1969) Ph.D. Thesis University of Leeds.
- Jelley J.V. et al (1965) Nature 205 327-9.
- Khristiansen G.B. (1957) ZETF 34 956-61.
- Kamiya Y., Sugisaka S., Uenco H., Kato S. & Sekido Y. (1962)
J. Phys. Soc. Japan 17 A- III 315-8.
- Lapikens J., Watson A.A., Wild P. & Wilson J.G. (1973) PICCR Denver. 4 2581
- Lillicrap S.C., Wills R.D. & Turver K.E. (1963) Proc. Phys. Soc. 82 95-106
- Linsley J. & Scarsi L. (1962) Phys. Rev. Lett. 9 123-5.
- Linsley J. & Scarsi L. (1962) Phys. Rev. 128 2384-92.
- Machin A.C. (1973) Ph.D. Thesis University of Durham.

- Machin A.C., Orford K.J., Pickersgill D.R. & Turver K.E. (1970) Acta. Phys. Hung. 29 579-584.
- Oren Y. (1959) Bull. Res. Council of Israel. 8 103-12.
- Orford K.J., Turver K.E. & Walton A.B. (1968) Can. J. Phys. 46 S 119-22.
- Orford K.J. & Turver K.E. (1970) Acta. Phys. Hung. 29 585-92.
- Pickersgill D.R. (1973) Ph.D. Thesis University of Durham.
- Somogi A.J. (1966) Ann. Physik 17 221-231.
- Sreekantan B.V. (1972) Space Science Reviews 14 103.
- Suri A.N. (1966) Ph.D. Thesis University of Leeds.
- Tennent R.M. (1967) Proc. Phys. Soc. 92, 622-631
- Tomazewski A. & Wdowczyk J. (1975) PICCR Munich. 8 2899 - 2904.
- Turver K.E. (1963) Ph.D. Thesis University of Leeds.
- Turver K.E. (1975) PICCR Munich. 8 2851 - 2857.
- Walton A.B. (1966) M.Sc. Thesis University of Durham.
- Watson A.A. & Wilson J.G. (1974) J. Phys. A. 11 99-1212
- Wellby D.W. (1976) Ph.D. Thesis University of Durham (to be published).
- Wilson J.G. (1970) PIACCR Bolivia II 393-426.

Further References

- Coxell, H., Meyer, M.A., Scull, P.S., and Wolfendale, A.W. (1961), Nuovo Cim. Supp. 21, 7-20.
- Galbraith, W. and Jelley, J.V. (1953), Nature 171, 349.
- Hook, J.R. (1972), Ph.D. Thesis, University of Durham.

Acknowledgements.

I am indebted to Professor A. W. Wolfendale and Dr. K. E. Turver for making this study possible. Dr. K. E. Turver is also thanked for his continual encouragement, advice and guidance.

I am also very grateful to those many members of the technical staff of the Physics Department of the University of Durham for their invaluable advice and assistance on countless occasions. Particularly Mr. W. Leslie, Mr. P. Cottle, Mr. H. Davison and Mr. A. Turnbull for their help in construction work. The Science Research Council is thanked for financial assistance in the construction of the new experiment.

Finally for their encouragement and assistance in preparing and typing this thesis, my parents are sincerely thanked.

